UCLA/PPG--1325

DE91 002992

DISCLAIMER

This report was prepared as an account of work sponsored by an agency of the United States Government. Neither the United States Government nor any agency thereof, nor any of their employees, makes any warranty, express or implied, or assumes any legal liability or responsibility for the accuracy, completeness, or usefulness of any information, apparatus, product, or process disclosed, or represents that its use would not infringe privately owned rights. Reference herein to any specific commercial product, process, or service by trade name, trademark, manufacturer, or otherwise does not necessarily constitute or imply its endorsement, recommendation, or favoring by the United States Government or any agency thereof. The views and opinions of authors expressed herein do not necessarily state or reflect those of the United States Government or any agency thereof.

PISCES Program
Plasma-Surface Interactions Research
Progress Report for 1989-1990

Edited by Y.Hirooka

UCLA PPG#1325 September, 1990

This report has been contributed by

The PISCES-team at UCLA:

Research Staff	Support Staff	Graduate Student
R.W.Conn	T.Sketchley	G.Tynan
Y.Hirooka	G.Gunner	R.Lehmer
L.Schmitz	L.Chousal	Y.Ra
R.Doerner	P.Luong	P.Chia
G.Chevalier	M.C.Srinivasan	
M.Khandagle		

The PMI-theory group at UCLA: A.Grossman

The tokamak laboratory at UCLA: R.J.Taylor and P.Pribyl

Sandia National Laboratories, Livermore: R.Causey and K.L.Wilson

Idaho National Engineering Laboratory: G.Smolik and D.Holland

Visiting scientists to UCLA: T.Shoji from Plasma Science Center, Nagoya Univ.
A.Sagara from NIFS, Nagoya
T.Sogabe and T.Matsuda from Toyo Tanso Inc.Ltd.
A.Pospieszczyk from KFA, Jülich.

MASTER

DISCLAIMER

This report was prepared as an account of work sponsored by an agency of the United States Government. Neither the United States Government nor any agency thereof, nor any of their employees, makes any warranty, express or implied, or assumes any legal liability or responsibility for the accuracy, completeness, or usefulness of any information, apparatus, product, or process disclosed, or represents that its use would not infringe privately owned rights. Reference herein to any specific commercial product, process, or service by trade name, trademark, manufacturer, or otherwise, does not necessarily constitute or imply its endorsement, recommendation. or favoring by the United States Government or any agency thereof. The views and opinions of authors expressed herein do not necessarily state or reflect those of the United States Government or any agency thereof.

PREFACE

Since 1984, the PISCES-team has been working on a wide range of PMI issues including: materials erosion-redeposition and control-tranport in edge plasmas. These long-term research objectives are currently recognized as the most critical issues concerning the divertor design of the International Thermonuclear Experimental Reactor (ITER). With the hope of contributing to the ITER activity, the PISCES-team has conducted PMI-experiments with a balanced emphasis on both materials and plasma issues.

Concerning materials issues for ITER, the PISCES-team has collaborated with a Japanese industry to develop a new material for plasma-facing components. As a result, bulk-boronized graphite has been developed and tested systematically at UCLA and many other institutions in the U.S. The plasma erosion of this boronized graphite has been found to be less than that for ordinary graphites by a factor of 3. This material is presently planned for use in the Tokamak de Varennes in Canada later this year.

In the area of edge-plasma physics research, the PISCES-team has conducted intensive research on the gaseous target as divertor concept for ITER and has provided very encouraging experimental proof of this concept. The data indicate that the heat flux associated with the plasma flow to a target plate can be reduced by 3 orders of magnitude, yet the back flow of the neutral gas into the upstream plasma is not significant due to the plasma plugging effect. This result has generated considerable interest in the re-entrant divertor concept within the ITER community.

These ITER-related data and other work by the PISCES-team were presented at the 9th International Conference on Plasma-Surface Interactions in Controlled Fusion Devices at Bournemouth this year. Overall, this past year has been the most productive one for the PISCES-team. This report provides a brief summary of research projects in the PISCES-program at UCLA.

Yoshi Hirooka
Editor, Program Manager and
Principal Investigator

Robert W.Conn
Director, IPFR and
Principal Investigator

TABLE OF CONTENTS

Page

PISCES-Program

1. Major Objectives of the PISCES-Program i
2. The PISCES Program at UCLA ii
3. Highlights in the Program History (84-90) iii
4. PISCES collaboration in 1989-1990 iv
5. List of Publications v

PISCES Facilities

1. PISCES-A Facility 2
2. PISCES-B Facility 4
3. PISCES-C Facility 7
4. Fast Scanning Probes 9
5. Spectroscopic Diagnostics 12
6. PISCES Laboratory Data Acquisition System 14
7. SEM & EDX Facilities 16
8. Vacuum Outgassing Facility 19

PISCES Experiments - Materials Physics

1. Evaluation of Bulk-Boronized Graphites 22
2. Chemical Sputtering of C-C Composites 34
3. D-Retention in Redeposited Carbon 36
4. TEXTOR-Exposed Graphite 38
5. Oxygen Plasma Reactions with Graphite 40

PISCES Experiments - Edge-Plasma Physics

1. Gaseous Divertor Simulation 43
2. Experimental Proof of RF-limiter 48
3. H-Mode Transition by DC-Biasing 52
4. Edge-Plasma Physics Experiments in the CCT-Tokamak 56
5. He-Spectroscopy for Edge-Plasma Diagnosis 61

PISCES-Program

MAJOR OBJECTIVES OF THE PISCES-PROGRAM

(1) To understand materials behavior subject to high-flux, continuous plasma bombardment in fusion devices.

(2) To evaluate and develop new materials for use as plasma-facing components in fusion devices.

(3) To understand the atomic physics associated with the transport of impurities in the edge-plasma.

(4) To understand the behavior of the edge-plasma which interacts with surface components.

(5) To develop innovative techniques to modify and control the edge-plasma characteristics.

(6) To collaborate with national and international groups to conduct PSI-experiments in the areas where PISCES can play an unique role.

THE PISCES PROGRAM AT UCLA

Funding Agency: U.S. Department of Energy, Office of Fusion Energy

Faculty Staff: Prof. R.W.Conn (Principal Investigator)
Director, IPFR

Research Staff: (1) Surface and Materials Physics:

Dr. Y.Hirooka (Principal Investigator)
Principal Scientist, IPFR

Dr. M.Khandagle
Postdoctral fellow, IPFR

(2) Plasma Spectroscopy:

Dr. G.Chevalier
Postdoctral fellow, IPFR

(3) Edge-Plasma Physics:

Dr. L.Schmitz
Senior Scientist, IPFR

Dr. R.Doerner
Staff Scientist, IPFR

Senior Support Staff: (1) Computing: M.C.Srinivasan

(2) Mechanical: T.Sketchley
L.Chousal

(3) Electrical: G.Gunner
P.Loung

Graduate Students: R.Lehmer, Y.Ra
C.Ping, G.Tynan

HIGHLIGHTS IN THE PROGRAM HISTORY(84-90)

1984 - PISCES-program funded by DOE-OFE.
* PISCES-A facility in operation.

1985 - First experimental demonstration of the redeposition effects in PISCES-A.
* AES-SIMS surface analysis station constructed.

1986 - Pump limiter simulation experiments in PISCES-A.
* Optical diagnostics established for plasma spectroscopy.

1987 - First off-line hydrogen plasma pumping experiments in PISCES-A.
- First off-line biased limiter (**E** x **B**) experiments in PISCES-A.
* Fast reciprocating Langmuir probe developed.
* PISCES-B design started.

1988 - Graphite radiation enhanced sublimation experiments in PISCES-A.
- CCT experiments started in collaboration with Tokamak Lab., UCLA.
- Collaboration with China, SWIP on Omegatron development.
- Collaboration with KFA on plasma spectroscopy.
* SEM-EDX installed (TRW).
* PISCES-B plasma source in operation.

1989 - First boronized graphite erosion experiments in PISCES-B.
- First biased divertor channel experiments in PISCES-A.
- Gaseous divertor experiments in PISCES-A.
- Collaboration with Japan, IPP Nagoya on the RF-limiter.
- Collaboration with the NET-team, Garching the materials erosion.
* PISCES-B with in-situ AES-SIMS completed.

1990 - Systematic evaluation bulk-boronized graphites with Toyo Tanso, SNLs, NEL.
- Collaboration with Japan, NIFS on C-C composites for LHS.
- Collaboration with KFA on He-beam diagnostics
- TEXTOR graphite tiles analysis work started.

PISCES COLLABORATION IN 1989-1990

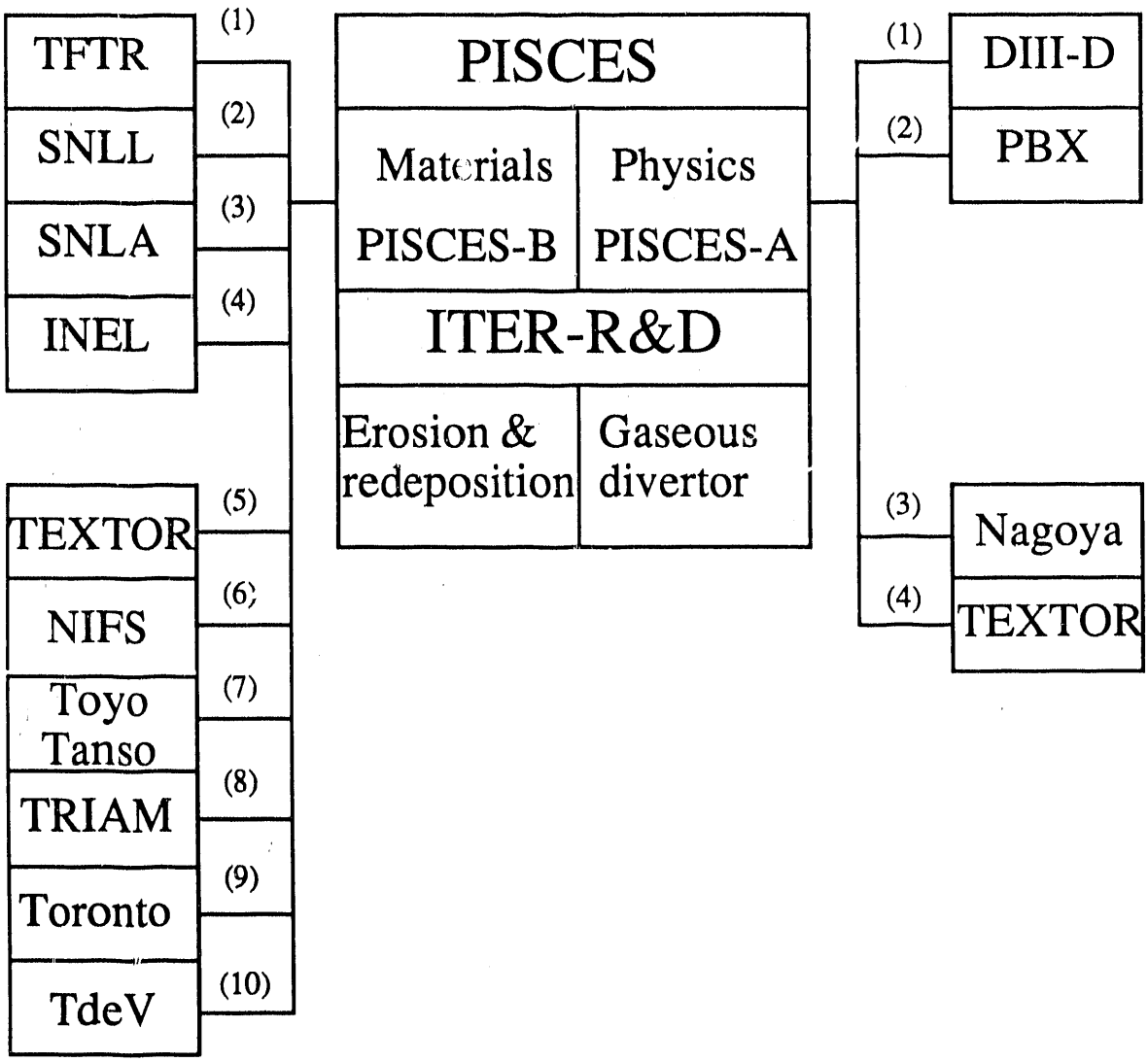

Materials collaboration:

(1) DT-Materials Physics Meeting,
(2) Boronized graphite: T-inventory,
(3) Boronized graphite: thermal shock
(4) Boronized graphite: Steam oxidation
(5) TEXTOR graphite tile analysis
(6) C-C composites for LHS
(7) Boronized and titanized graphite
(8) Redeposition experiment
(9) High fluence D-implantation
(10) Boronized graphite limiter exps. in TdeV

Plasma physics collaboration:

(1) Biased divertor
(2) Biased divertor
(3) RF limiter
(4) RF limiter
He radiation spectroscopy

PUBLICATIONS FROM THE PISCES-TEAM

(1) "Plasma surface interaction experimental facility (PISCES) for materials and edge physics studies"
D.M.Goebel, G.Campbell and R.W.Conn
J.Nucl.Mater. 121(1984)277.

(2) "Observation of enhanced particle removal rates in pump limiter simulation experiments"
D.M.Goebel and R.W.Conn
J.Nucl.Mater. 129&129(1984)249.

(3) "Large area lunthanum hexaboride electron emitter"
D.M.Goebel,Y.Hirooka and T.A.Sketchley
Rev.Sci.Instrum. 56(1985)1717.

(4) "Large area lanthanum molybdenum electron emitters"
D.M.Goebel, Y.Hirooka and G.A.Campbell
Rev.Sci.Instrum. 56(1985)1888.

(5) "Quasi-thermodynamic prediction of hydrogen reemission behavior from titanium films"
Y.Hirooka, D.M.Goebel and R.W.Conn
J.Nucl.Mater. 135(1985)82.

(6) "Materials erosion and redeposition studies at the PISCES facility - net erosion under redeposition"
Y.Hirooka, D.M.Goebel, R.W.Conn, W.K.Leung and G.A.Campbell
J.Nucl.Mater. 141-143(1986)193.

(7) "Erosion and redeposition experiments in the PISCES facility"
D.M.Goebel, Y.Hirooka, R.W.Conn, W.K.Leung, G.A.Campbell, J.Bohdansky, K.L.Wilson, W.Bauer, R.A.Causey, A.E.Pontau, A.R.Krauss, D.M.Gruen and M.H.Mendelsohn
J.Nucl.Mater. 145-147(1987)61.

(8) "High plasma-flux elevated temperature sputtering of Cu-Li alloys"
A.R.Krauss, D.M.Gruen, M.H.Mendelsohn, R.W.Conn, D.M.Goebel, Y.Hirooka and W.K.Leung
J.Nucl.Mater. 145-147(1987)401.

(9) "Materials surface modification by plasma bombardment under simultaneous erosion and redeposition conditions"
Y.Hirooka, D.M.Goebel, R.W.Conn, G.A.Campbell, W.K.Leung, K.L.Wilson, R.A.Causey, M.H.Morse and J.Bohdansky
Nucl. Instr. & Methods-B 23(1987)458.

(10) "Behavior of graphite under heat load and in contact with a hydrogen plasma"
J.Bohdandsky, C.D.Croessmann, J.Linke, J.M.McDonald, D.H.Morse, A.E.Pontau, R.D.Watson and J.B.Whitley , D.M.Goebel, Y.Hirooka, K.Leung, R.W.Conn, J.Roth, W.Ottenberger and H.E.Kotzlowsky
Nucl.Instr. & Methods-B 23(1987)527.

(11) "Temperature and composition dependence of the high flux plasma sputtering yield of Cu-Li binary alloys"
A.R.Krauss, M.H.Mendelsohn, D.M.Gruen, R.W.Conn, D.M.Goebel,Y.Hirooka, W.K.Leung and J.Bohdansky
Nucl.Instr. &Methods-B 23(1987)511.

(12) "Hydrogen pumping and release by graphite under high flux plasma bombardment"
Y. Hirooka, W. K. Leung, R. W. Conn, D. M. Goebel, B. LaBombard and R. E. Nygren
J. Vac. Sci. & Technol.-A 6(1988)2965.

(13) "Erosion of graphite by high flux hydrogen plasma bombardment"
D. M. Goebel, J. Bohdansky, R. W. Conn, Y. Hirooka, B. LaBombard, W. K. Leung, R. E. Nygren, J. Roth and G. R. Tynan
Nuclear Fusion 28(1988)1041.

(14)"Deuterium pumping and erosion behavior of selected graphite materials under high flux plasma bombardment in PISCES-A"
Y.Hirooka, R.W.Conn, D.M.Goebel, B.LaBombard, W.K.Leung, R.E.Nygren and Y.Ra
J.Nucl. Mater. 163-165(1988).

(15) "Erosion and Redeposition Behavior of selected NET-candidates under high-flux plasma bombardment in PISCES-A"
E.Franconi, Y.Hirooka, R.W.Conn, B.LaBombard, W.K.Leung and R.E.Nygren
J.Nucl.Mater 163-165(1989).

(16) "Presheath profiles in simulated tokamak edge plasmas"
B.LaBombard, R.W.Conn, Y.Hirooka, R.Lehmer, W.K.Leung, R.E.Nygren, Y.Ra, G.Tynan
J.Nucl.Mater. 162-164 (1989)314.

(17) "Erosion and redeposition of graphite by hydrogen plasmas"
D.M.Goebel, J. Bohdansky, R.W. Conn, Y. Hirooka, B. LaBombard,W. K. Leung, R. E. Nygren and G.R.Tynan
Fusion Technol. 15(1989)102.

(18) "An in-situ spectroscopic erosion yield measurement and its applicationas to sputtering and surface morphology alterations"
W.K.Leung, Y.Hirooka, R.W.Conn, D.M.Goebel, B.LaBombard and R.E.Nygren
J.Vac. Sci. & Technol.-A. 7(1989)21.

(19) "In-situ spectroscopic measurements of erosion behavior of TFTR-redeposited carbon materials under high-flux plasma bombardment in PISCES-A"
Y.Hirooka, A.Pospieszczyk, R.W.Conn, B.LaBombard, B.Mills, R.E.Nygren
Presented at 35th National Symposium of American Vacuum Society, Atlanta, 1988
J.Vac. Sci. & Technol.-A 7(1989)1070.

(20) "Hydrogen isotope trapping on graphite collectors during an isotope exchange experiment in the Tokamak Fusion Test Reactor"
S.J.Kilpatrick, R.E.Nygren, W.R.Wampler, M.Ulrickson, H.F.Dylla, D.M.Manos, A.T. Ramsey, and Y.Hirooka
J.Vac.Sci. & Technol.-A 7(1989)1087.

(21) "Spectroscopic studies of carbon impurities in PISCES-A"
Y.Ra, A.Pospieszczyk, Y.Hirooka, W.K.Leung, R.W.Conn
J.Vac.Sci.& Technol.-A8(1990)1783.

(22) "A new plasma-surface interactions research facility: PISCES-B and first materials erosion experiments on bulk-boronized graphite"
Y.Hirooka, R.W.Conn, T.Sketchley, W.K.Leung, R.Doerner, J.Elvurm, G.Gunner, M.Khandagel, R.Lehmer, P.Luong, Y.Ra, L.Schmitz and G.Tynan
J.Vac.Sci.&Technol.-A8 (1990)1790.

(23) "Radiation-enhanced sublimation of graphite in PISCES-experiments"
R.Nygren, J.Bohdansky, A.Pospieszczyk, R.Lehmer, Y.Ra, R.W.Conn, R.Doerner, Y.Hirooka, W.K.Leung, and L.Schmitz
J.Vac.Sci.&Technol.-A8 (1990)1778.

(24) "An electrostatic barrier scrape-off Layer for control of core plasma effluxes in tokamaks,"
B. LaBombard, R.W. Conn, G. Tynan,
To be published in Plasma Physics and Controlled Fusion (1989).

(25) "An Omegatron mass-spectrometer for plasma ion species analysis"
E.Y.Wang, L.Schmitz, Y.Ra, B.Labombard, R.W.Conn
To be publshed in Rev.Sci.Instr.

(26) "Bulk-boronized graphites for plasma-facing components in ITER"
Y.Hirooka, R.W.Conn, R.Causey, D.Croessmann, R.Doerner, D.Holland, M.Khandagle, T.Matsuda, G.Smolik, T.Sogabe, J.Whitely, K.Wilson
Paper presented at the 9th PSI-conf. at Bounemouth, UK, May, 1990.
To be published in J.Nucl.Mater. (UCLA-Report#UCLA-PPG-1312).

(27) "Interactions of bulk-boronized graphites with deuterium plasmas in PISCES-B"
Y.Hirooka, R.W.Conn, M.Khandagle, G.Chevalier, T.Sogabe, T.Matsuda, H.Ogura, H.Toyoda, H.Sugai
Paper presented at the 5th Carbon Workshop at KFA, May, 1990.
To be published in Fusion Technol. (UCLA-Report#UCLA-PPG-1313).

(28) "Evaluation of bulk-boronized graphite as a plasma-facing material in fusion devices"
Y.Hirooka, R.W.Conn, T.Sogabe, T.Matusda, H.Ogura
Paper to be presented at the Int.Symp. on Carbon, Tsukuba, Nov. 1990.

(29) "Experimental simulation of the gaseous divertor concept in PISCES-A"
L.Schmitz, R.Lehmer, G.Chevalier, G.Tynan, P.Chia, R.Doerner, R.W.Conn
Paper presented at the 9th PSI-conf. at Bounemouth, UK, May, 1990.
To be published in J.Nucl.Mater.

(30) "Materials analysis of TEXTOR limiter tiles"
R.Doerner, B.Mills, E.Wallura, D.S.Walsh, G.Chevalier, R.W.Conn, K.H.Dipple, B.L.Doyle, H.G.Esser, K.H.Finken, D.Gray, Y.Hirooka, K.Koizlik, A.Miyahara, R.A.Moyer, J.G.Watkins, J.Winter
Paper presented at the 9th PSI-conf. at Bounemouth, UK, May, 1990.
To be published in J.Nucl.Mater.

(31) "Performance of boron/carbon first wall materials under fusion relevant conditions"
J.Linke, H.Bolt, R.Doerner, H.Grübmeier, Y.Hirooka, H.Hoven, C.Mingam, H.Schlze, M.Seki, E.Wallura, T.Weber, J.Winter
Paper presented at the 9th PSI-conf. at Bounemouth, UK, May, 1990.
To be published in J.Nucl.Mater.

(32) "Experimental proof of a novel RF limiter concept in PISCES-A"
T.Shoji, A.Grossman, R.Conn, Y.Hirooka, R.Lehmer, W.Leung, L.Schmitz, and G.Tynan
Paper presented at the 9th PSI-conf. at Bounemouth, UK, May, 1990.
To be published in J.Nucl.Mater.

(33) "Chemical erosion of selected carbon-carbon composites under high-flux hydrogen plasma bombardment in PISCES-B'
A.Sagara, Y.Hirooka, R.W.Conn, A.Miyahara, G.Chevalier, R.Doerner, M.Khandagle and N.Noda
Paper to be presented at 16th SOFT conf.

(34) "Hydrogen and deuterium plasma interactions with brazed first wall elements"
I.Smid, E.Wallura, J.Winter, H.Nickel, R.Doerner, Y.Hirooka, R.W.Conn, W.Jager, M.Grasserbauer, E.Kny, N.Rehis
Paper to be presented at 16th SOFT conf.

(35) "Applications of SiC and B4C coat-mix material: a new candidate for plasma-facing components"
C.Mingam, R.W.Conn, F.Dias, R.Doerner, Y.Hirooka, J.Linke, H.Nickel
Paper to be presented at 16th SOFT conf.

PISCES-Facilities

PISCES-A: A Versatile Facility for Plasma Edge Physics Studies

The PISCES-A facility[1] (Fig. 1) has been extensively used for Plasma-Materials Interaction studies and is currently devoted to boundary layer physics experiments, edge plasma turbulence and transport studies, biased limiter and divertor simulation experiments, and the testing of novel divertor and edge management concepts. The plasma source consists of a hot LaB_6 cathode with an annular, water-cooled copper anode and attached drifttube. The vacuum system includes four turbo-molecular pumps with a pumping speed of 1500 l/s each. The main diagnostics include: (1) motor-driven water-cooled Langmuir probes; (2) a fast scanning probe capable of measuring radial density, floating and plasma potential, as well as flow velocity and Mach number profiles; (3) a 1.3 m Czerny-Turner monochromator with OMA system; (4) a fast reciprocating probe for density and potential fluctuation measurements; (5) several baratron and ionization gauges for neutral pressure measurements; (6) a CID camera; (7) an IR surface temperature monitor. A CAMAC crate with slow and fast data loggers and a Micro Vax computer system is used for data acquisition and processing.

Differential pumping is employed to achieve a neutral gas pressure of 2×10^{-4} - 10^{-2} torr in the plasma source, while keeping the main chamber pressure between 6×10^{-5} and 2×10^{-3} torr. Plasma is produced in H_2, D_2, He, and Ar gas. Plasma densities of 10^{11} - 3×10^{12} cm^{-3} in hydrogen and helium, and up to 3×10^{13} cm^{-3} in argon have been achieved. The electron temperature is in the range of 3 - 30 eV.

Presently, the PISCES-A plasma source is converted for higher density hydrogen operation in order to study plasma plugging effects in the gaseous divertor simulation experiment (described in detail in a separate section). Pulsed operation will enable us to operate at a discharge current as high as 250 A. The differential pumping capability is increased by installing a second turbumolecular pump at the plasma source. This allows plasma production at higher neutral pressure while maintaining high electron temperature and ionization efficiency. The diagnostic systems are modified for pulsed plasma data acquisition.

The plasma diameter can be adjusted beween 3 and 10 cm by three independent magnet coils located in the source region. The main chamber magnetic field (variable between 100 and 1800 gauss) is produced by four water-cooled coils.

The PISCES-A chamber provides good diagnostic access. The fast scanning probe system has been extensively used for 2-D and 3-D mapping of plasma density and potential profiles during biased limiter and divertor simulation experiments and tests of magnetized probe theory and presheath measurements.

[1]D. M. Goebel, G. Campbell, R. W. Conn, J. Nucl. Mater. **121** (1984) 277

Fig. 1

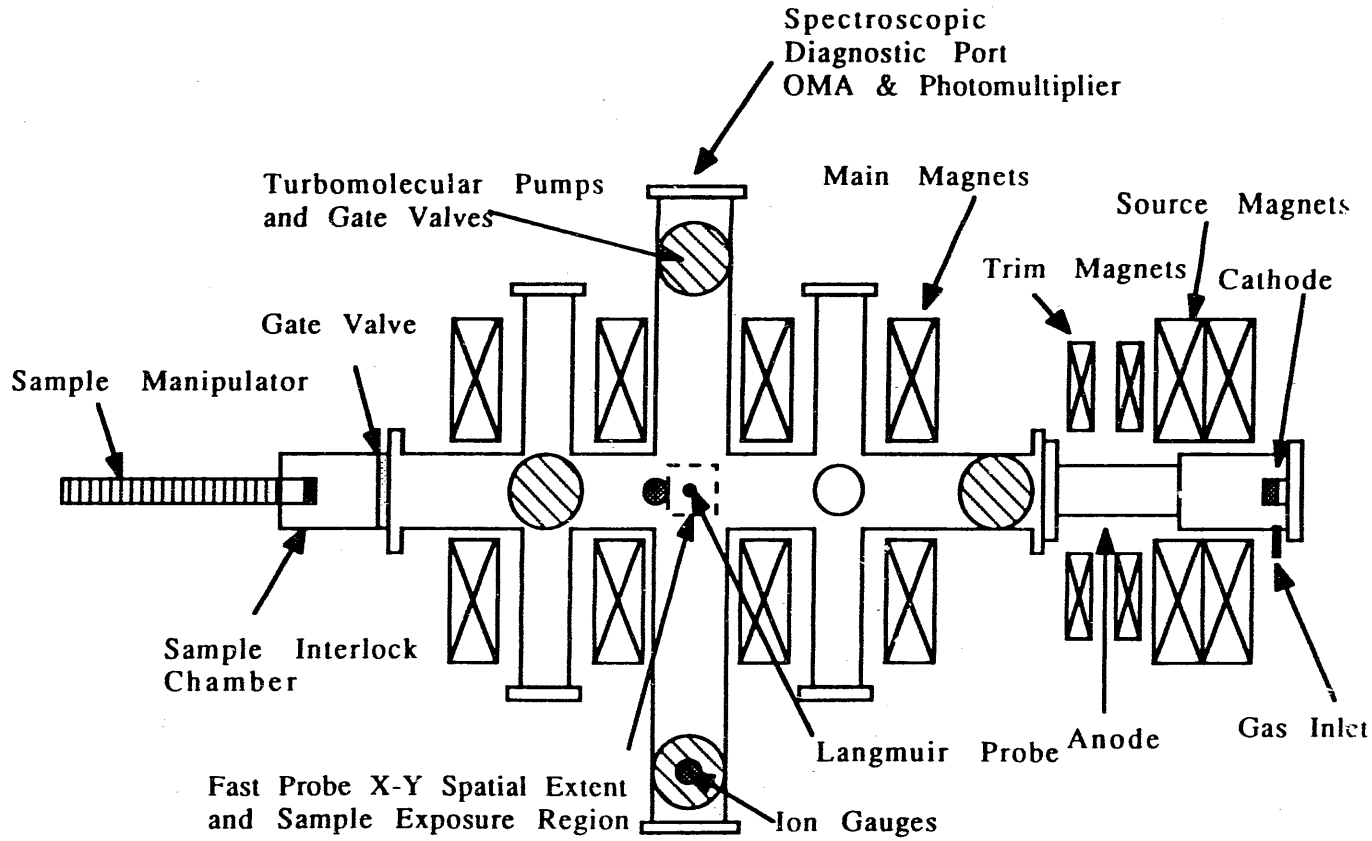
Spectroscopic
Diagnostic Port
OMA & Photomultiplier
Turbomolecular Pumps
and Gate Valves
Main Magnets
Source Magnets
Trim Magnets
Cathode
Gate Valve
Sample Manipulator
Sample Interlock
Chamber
Langmuir Probe
Anode
Gas Inlet
Fast Probe X-Y Spatial Extent
and Sample Exposure Region
Ion Gauges

PISCES-B: Fully Diagnosed Plasma-Surface Interaction Experiments [1]

A new plasma-surface interactions experimental research facility: PISCES-B has been constructed and operating at UCLA since 1989. A schematic diagram of the facility is shown in Fig. 1. The PISCES-B facility is specially designed fully diagnosed plasma-surface interaction experiments. For this purpose, the following features are given: (1) the vacuum system is pumped by two turbo-molecular pumps with the effective pumping speeds of 5000 l/s and 1000 /s; (2) the main vacuum chamber has 10 line-of-site ports focusing at the sample surface; (3) a differentially pumped residual gas analyzer (RGA) to monitor gaseous plasma-surface interactions products (the minimum detectable partial pressure of 10^{-14} torr); (4) a temperature-controlled (RT-1800°C) sample probe; (5) In-situ surface analysis diagnostics including: Auger Electron Spectroscopy (AES), X-ray induced Photoelectron Spectroscopy (XPS) and Secondary Ion Mass Spectrometry (SIMS); (6) a 1.3 m monochromator coupled with an optical multi channel analyzer (OMA) for the in-situ spectroscopic detection of plasma-surface interactions products; (7) a swing-linear sample manipulator to transport the sample between the main chamber and the in-situ surface analysis station (8) an ultra-violet (UV) spectrometer; (9) scanning Langmuir (single and double) probes, the data from which are processed by a MicroVax computer.

The PISCES-B facility has been successful in generating steady-state plasmas of hydrogen, deuterium, helium and argon. The plasma densities of 10^{11} -10^{13} cm^{-3} and electron temperatures of 3 - 50 eV have been achieved as shown in Fig. 2. The plasma operation space is found to be wider than the PISCES-A-facility, which is presumably owing to the large pumping speed of the turbo molecular pump to control the neutral particle density. In fact, the neutral pressure of the plasma working gas in the main chamber can be as high as 10^{-3} torr (divertor mode) and as low as 10^{-5} torr (limiter mode). The ion bombardment energy to the material sample is controlled by applying a DC-bias in the range from the floating potential to about 500 V. The magnetic field is variable between 100 to 1000 gauss in the sample region. These plasma bombardment conditions allow us to simulate plasma-surface interactions in tokamaks such as ITER. Important PSI-related parameters are listed in table 1.

---

[1] Y.Hirooka et.al. J.Vac.Sci. & Technol. A8, 1790 (1990).

Fig. 1

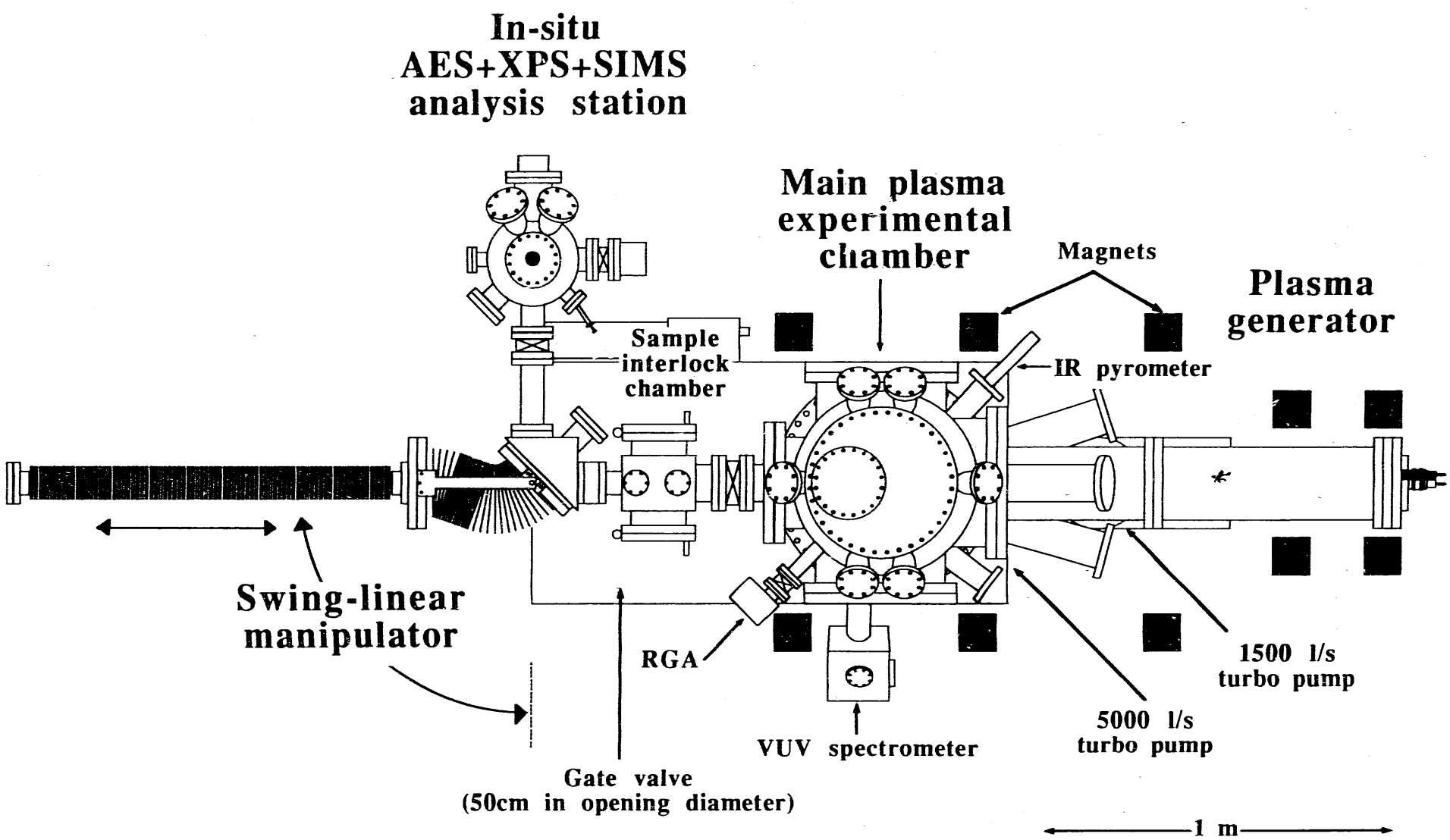
In-situ
AES+XPS+SIMS
analysis station
Main plasma
experimental
chamber
Magnets
Plasma
generator
Sample
interlock
chamber
IR pyrometer
Swing-linear
manipulator
RGA
VUV spectrometer
1500 l/s
turbo pump
5000 l/s
turbo pump
Gate valve
(50cm in opening diameter)
1 m

Table PSI-parameters in PISCES-A, PISCES-B and ITER

PSI-parameters	PISCES-A	PISCES-B	ITER
Plasma species	H, D, He Ar, N	H, D, He Ar, N	D, T, He
Pulse duration (s)	Continuous	Continuous	200 or longer
Plasma density (cm^{-3})	10^{11} - 10^{13}	10^{11} - 10^{13}	$\approx 10^{10}$ for first wall $\approx 10^{14}$ for divertor
Electron temperature (eV)	3-30	3-50	$\approx$ 100
Ion bombading flux (ions s^{-1} cm^{-2})	10^{17} - 10^{18}	10^{17} - 10^{19}	$\approx 10^{15}$ for first wall $\approx 10^{19}$ for divertor
Target area (cm^2)	50-100	50-700	
Ionization mean free path for carbon redeposition (cm)	down to 1	down to 0.5	down to 0.1
Ion bombarding energy (eV)	10 - 500 (dc bias)	10 - 500 (dc bias)	$\approx$ 300 - 500
Base pressure (Torr)	10^{-6}	10^{-8}	$\approx 10^{-8}$
Neutral pressure (Torr)	10^{-4} - 10^{-5}	10^{-5} - 10^{-3}	$\approx 10^{-5}$ for first wall $\approx 10^{-3}$ for divertor

PISCES-C: A New RF Plasma Source for Plasma Chemistry Research[1]

A new RF plasma source (which may be referred to as PISCES-C), has been developed for the genration of chemically reactive plasmas, which is not possible in PISCES A & B for the contamination of the electrode. This source is designed to study the interaction of fusion reactor materials such as graphite with chemically reactive plasmas such as oxygen. A schematic diagram of PISCES-C is shown in Fig. 1. The system is pumped by a diffusion pump and a base pressure of the order of 10^{-6} torr is attained. The plasma is generated by a Nagoya type III antenna surrounding a 30 cm long pyrex glass tube attached to a 1.5m long stainless steel cylindrical chamber. The RF source has a frequency of 13.56 MHz with a maximum power of 1.5 kW. The impedance is matched using two vacuum capacitors. A pair of Helmholtz coils produce the magnetic field up to 1 kGauss in the main chamber so that the plasma generated in the pyrex glass tube can be confined. A Langmuir probe is built to measure plasma parameters. Material samples can be inserted in the main chamber. Optical emission spectroscopy is currently the main diagnostic method for plasma-material interaction experiments.

Radial density profiles of argon and oxygen plasmas are shown in Fig. 2. The oxygen plasma with a density of 10^{12} cm^{-3} and an electron temperature of 10 eV is obtained with a power of 600 W and a pressure of $4X10^{-4}$ torr. The density of argon plasma is found about 3 times higher than that of oxygen plasma. The plasma is produced both capacitively and inductively. Negative biasing of the end plate increases plasma current and a dark space begines to develop below - 300 V. A resonance has been found at a magnetic field of 100G at the source region. It is not clear if this is due to the magnetic field effect or due to the resonance with the plasma wave like Trievelpeice Gould mode. The change of plasma color is observed (for an argon plasma, the color changes from pink (Ar I) to blue (Ar II)) near the end of the source region where a relatively strong magnetic mirror effect exists. This indicates that the magnetic mirror effect helps making intense plasmas.

---

[1] Y.Ra et.al., paper to be presented at the 37th National Symposium of AVS, 1990.

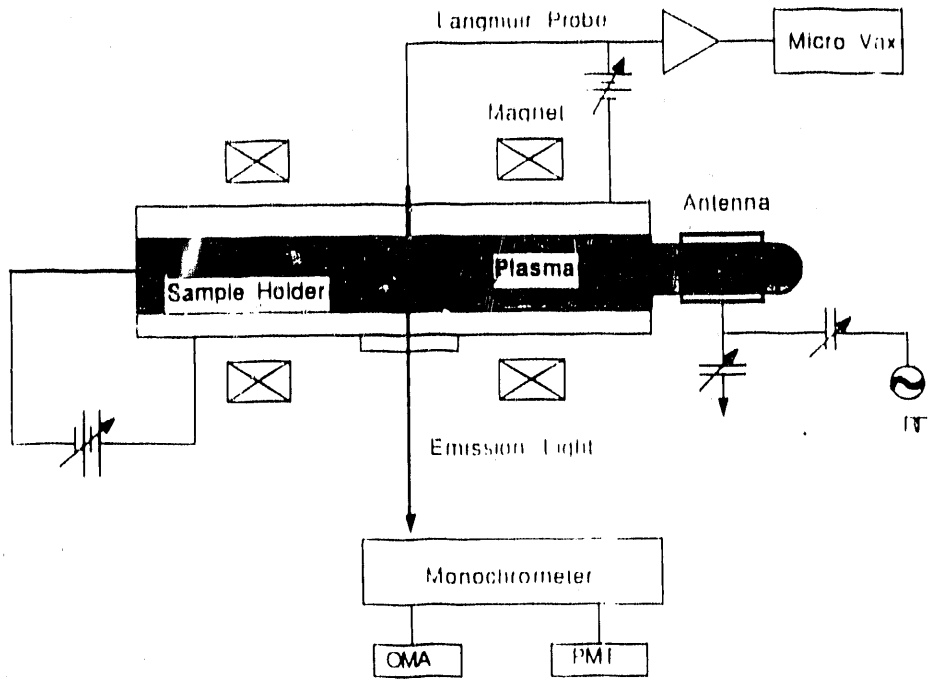

Fig. 1. The Schematic diagram of an RF plasma source.

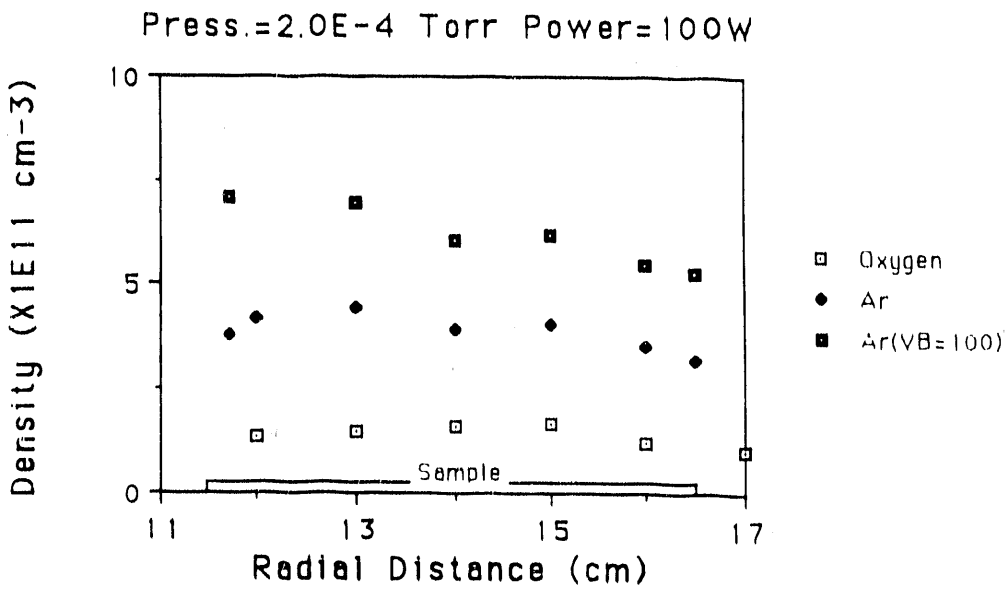

Fig. 2. Radial density profiles of an argon and an oxygen plasmas.

Fast Scanning Probes as Diagnostics for Steady-State Plasmas[1]

The fast scanning probe developed by the PISCES-team uses a pneumatic cylinder to drive a combination emissive and mach probe tip across the plasma column. This allows for single scan or shot profiles of the space or floating potential, density, and parallel mach number. Profiles of the space and floating potentials under identical plasma conditions can be obtained by using successive shots of the fast probe. To record the floating potential profile, the emissive probe tip is left cold. To record the space potential profile, the probe is resistively heated so that it will thermionically emit electrons into the plasma.

The fast probe actuator (figure 1) has a 15cm stroke and the total round trip time for the probe is 300msec. The probe is constructed of an alumina shaft with six holes for wires to pass through. The tip (figure 2) is made up of five electrical probes: a loop of thoriated tungsten wire for the emissive probe, and two pairs of unidirectional probes. Each pair of unidirectional probes has one tip that faces towards the source ("upstream") and the other faces away from the source ("downstream"). One pair has tips larger than the ion Larmor radius and is referred to as a magnetized mach probe, while the other pair is smaller than the ion Larmor radius and has been used to study ion flow in plasma wakes. The parallel mach number is computed from the ratio of the currents collected by the upstream and downstream magnetized probes. Density profiles are computed from the average of the current collected by the two probes.

The fast probe diagnostic was first built for the PISCES-A facility and has been used for virtually all the edge-plasma physics experiments including: presheath profile measurements in front of material samples, the modification of the potential profiles and scrape-off layer lengths in biased scrape-off layer simulation experiments, ion flows in the wakes of probes in the plasma, modification of density profiles in RF limiter/divertor simulation experiments.

Recently, a fast scanning double probe has been built for materials experiments in the PISCES-B facility. During the fast probe stroke, the probe tip voltage will be swept rapidly. This results in a number of Langmuir probe traces at different radii. These traces can be fitted automatically by the data acquisition system to produce a discrete spatial profile of electron temperature and density across the plasma column. Also, the use of the fast probe in PISCES-B material experiments will minimize sample contamination resulting from sputtered probe materials. This is important because under plasma bombardment the surface modification can readily be triggered by trace amount of impurities [2].

---

[1] R. Lehmer et. al., UCLA-Report# UCLA-PPG-1228 (1989).
[2] Y.Hirooka et. al., Nucl. Instr. & Methods-B 23(1987)458.

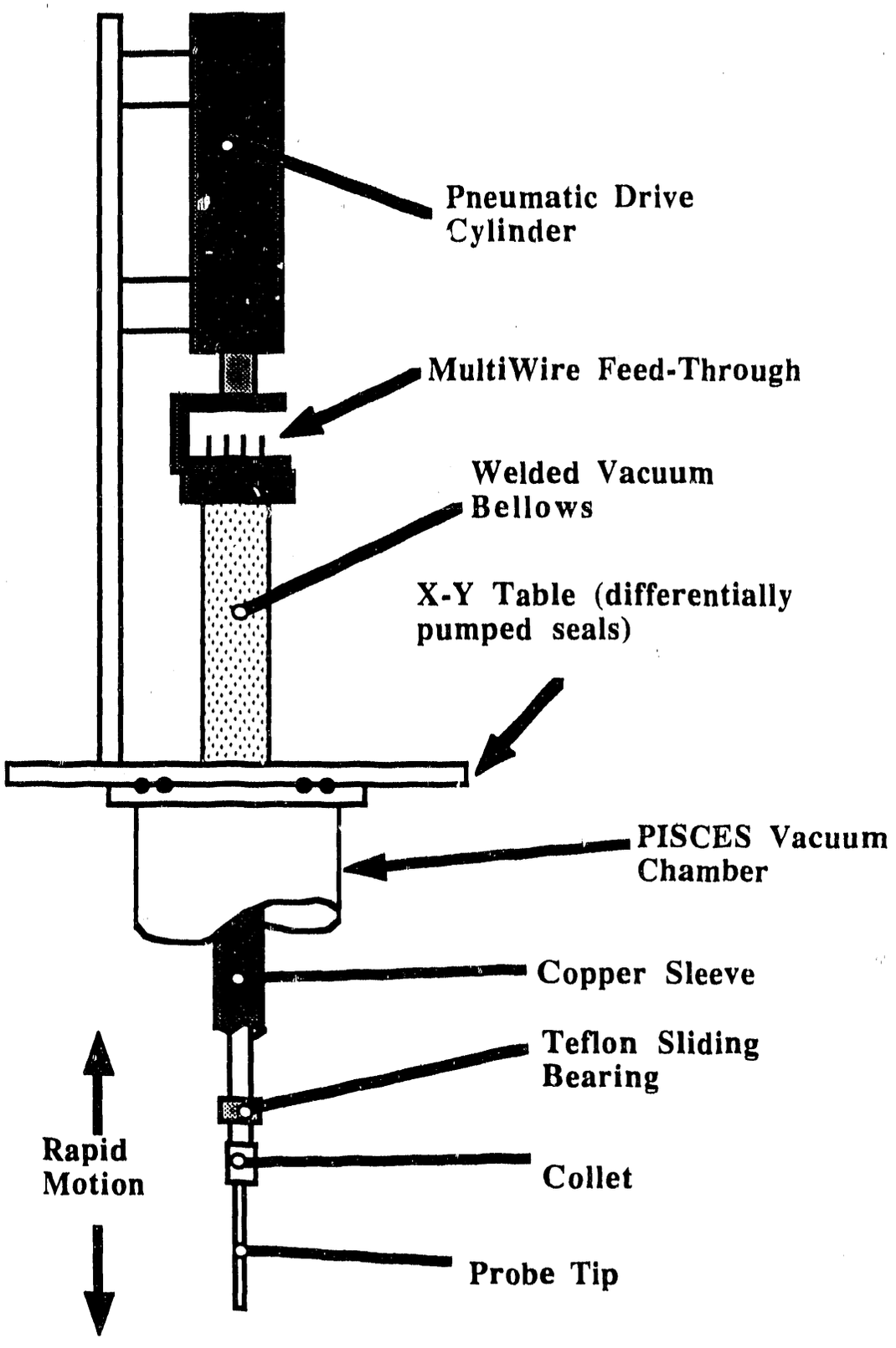

Figure 1: Schematic of the UCLA/PISCES-A Fast Scanning Probe Actuator

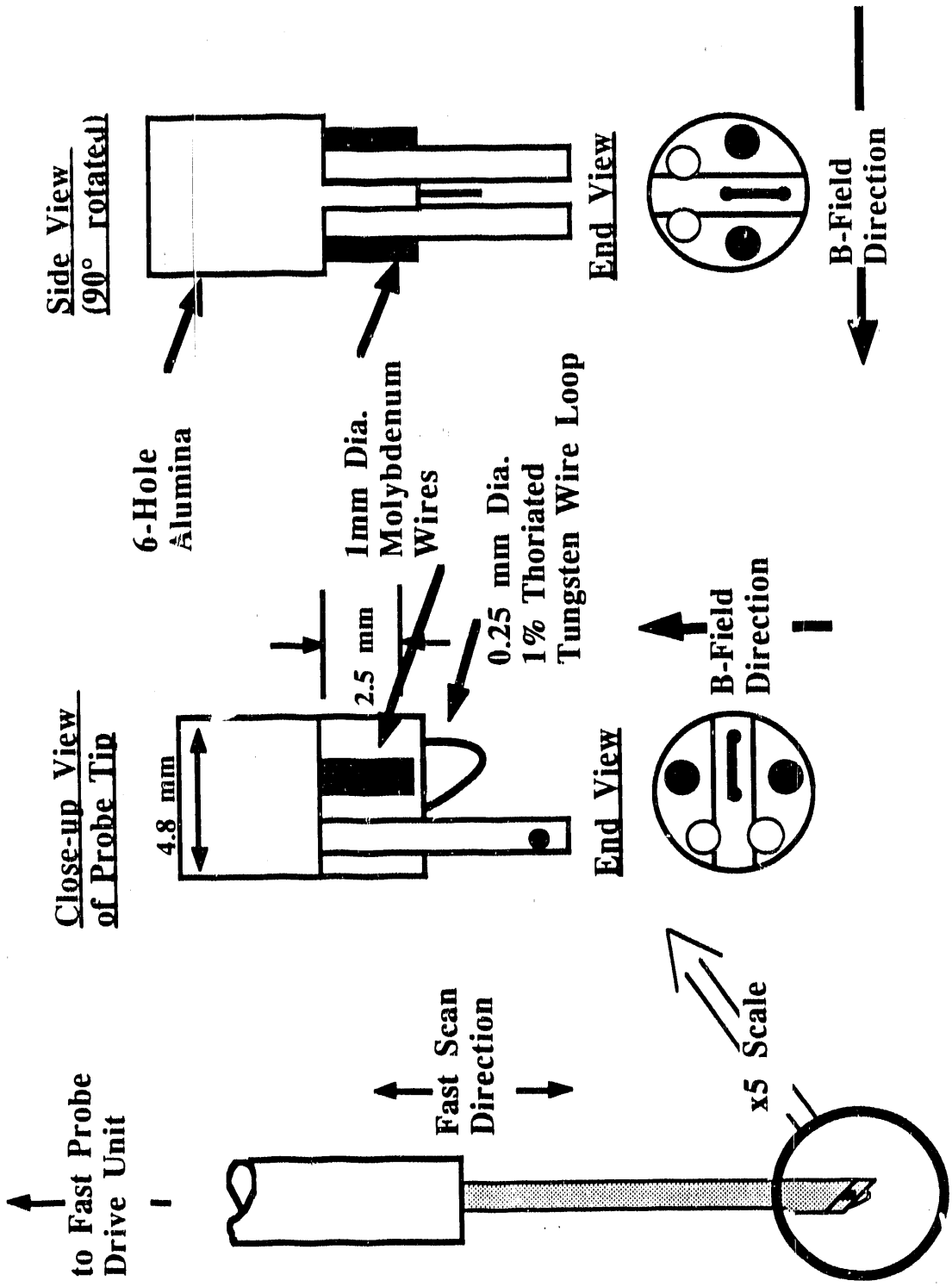

Figure 2: Geometry of the UCLA/PISCES-A Combination Emissive and Mach Probe Tip

Spectroscopic diagnostics facility for PISCES A and B

Spectroscopic techniques have been applied in PISCES A and B in diagnosis of erosion yields [1], ion temperature [2], impurities[2], density profile measurement [3] and RF plasma modifications [4]. Apart from its uniqueness in in-situ erosion yield measurement in material experiments, spectroscopy emerges as an integral part of many edge physics experiments in both PISCES A and B.

The spectroscopic diagnostic instruments in the PISCES Laboratory consist of a 1.3M Czerney-Turner spectrometer, a .5M Crossed Czerney-Turner spectrometer, an OMA system, a CID camera and a computer image-analysis system. The OMA can be integrated with the spectrometers to obtained both spectral and spatial information of the plasma.

The CID camera can be used to obtain spatial emission profiles or, when integrated with the spectrometers, can produce spectral and spatial profiles simultaneously. This is made possible with in-house development of interfacing the separate instruments and computer software.

A 0.3M Crossed Czerny-Turner VUV spectrometer has been installed recently on the PISCES-B machine. Because its wavelength range is between 105nm and 60 micrometers, it is well suited to study plasma-facing components containing carbon and/or boron elements such as boronized graphite and C-C composite.

The OMA system can be integrated with this spectrometer to obtain emission lines of carbon and boron on the same spectra allowing direct comparison between these elements (see Fig. 1).

Investigation of the behavior of boronized graphites as plasma-facing components using this new feature of PISCES-B is planned. Routine support is also provided for on-going material experiments (e.g. C-B and high temperature graphite experiments), and for physics experiments (e.g. impurity transport and gaseous divertor experiments).

---

1. W. K. Leung et. al., JVST A, 7 (1989) 21.
2. W. K. Leung et. al., Bull. Am. Phy. Soc., Baltimore , vol. 31 , October (1986).
3. W. K. Leung et. al., Bull. Am. Phy. Soc., San Diego , vol. 32 , October (1987).
4. T. Shoji and PISCES group, to be published.

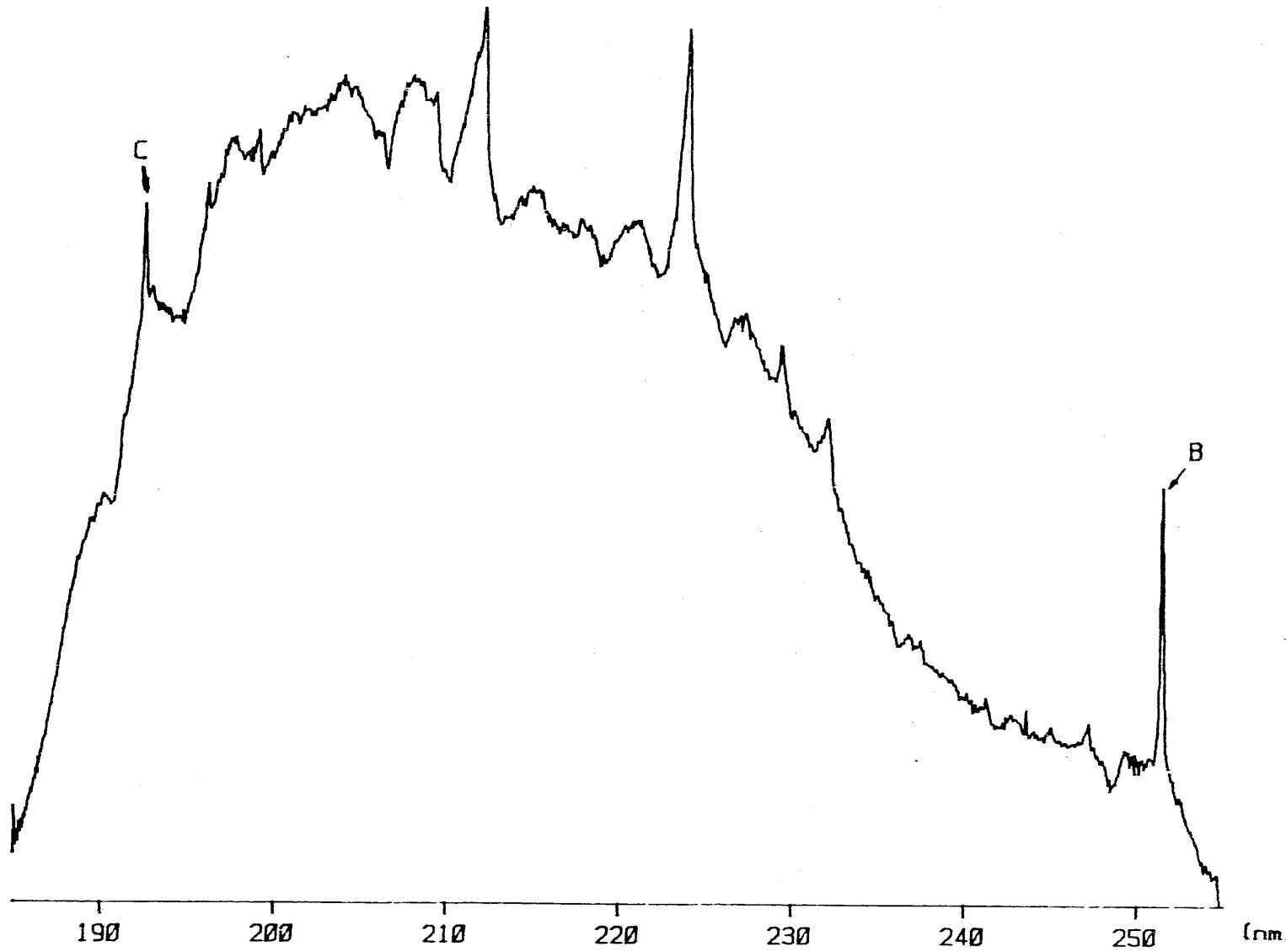

Fig. 1 Emission spectra from OMA

The PISCES Laboratory Data Acquisition System

The PISCES Data Acquisition System provides for the storage and manipulation of raw data from the PISCES-A, PISCES-B, and CCT Tokamak. The main components of this PISCES Data Acquistion System are the CAMAC (Computer Automated Measurement And Control) crates containing fast and slow data loggers and connected to a VAX cluster, consisting of a Micro Vax-II and three Vax-2000 workstations (Fig.1). A Serial Highway Driver is attached to the VAX cluster, communicates with the CAMAC crates through the Fiber Optics cables, which provide high voltage isolation from the PISCES and TOKAMAK machines.

The CAMAC crate connected to the PISCES-A machine contains two 32-Channel slow loggers and is capable of sampling data at a rate of up to 100 KHz. The number of active inputs is programmable. To achieve maximum sample rate fewer inputs are used depending upon the available memory in the crates. Individual channels have descriptive logical names assigned to them, which facilitates user access to raw data. ORNL CAMAC crate drivers are used for setting up the data loggers and retrieving raw data from CAMAC crates. The MIT MDS software manages the raw data storage and allows users to access the database. The CAMAC Crate connected to the PISCES-B machine contains one slow logger similar to the one used with PISCES-A.

PISCES-developed software DACPs (Data Acquisition Control Programs) control the continuous as well as post-triggered data samplimg on PISCES-A and PISCES-B machines. The DACPs provide the users, the users controlled data acquisition functions and also compute the process data from the recently retrieved raw data. The CAMAC crate used by the CCT Tokamak contains two fast loggers with each 4 channels capable of sampling data at 1 MHz and one slow logger with 32 channels.

The MIT MDS software as well as the DACPs executes on the Micro VAX Cluster environment. Apart from this, other USER CUSTOMIZED software using IDL, MCCOOL and DISSPLA graphic packages provide the realtime data analysis and manipulation capability. In addition, PISCES developed Fluctuation Analysis Software is executed for analyzing fluctuation induced transport in CCT. Further improvements and refinements have been included in this software so that it can be used at other (fusion research faclities) DIII-D, PBX-M and TEXTOR machines.

The VAX cluster is connected through an ETHERNET to a DecServer 200 terminal server connecting other variaties of peripherals (3 Macintoshes , 2 IBM PC/AT, XT 'S, Tek-4105 ,Tek-4696 for color graphic capabilities, modems for communications, and DEC Laser Printer for hard copies). Terminal emulation programs executing on the Macintoshes and IBM PC/AT's facilitate transfer of data to and from the VAX Cluster environment.

The above PISCES CLUSTER is also conneted to The Fusion Research Acadamic Network VAX-8350 (FRAN), which provides the network capability to other networks, such as MFENET (Magnetic Energy Fusion Network) and ESNET (Energy Science Network).

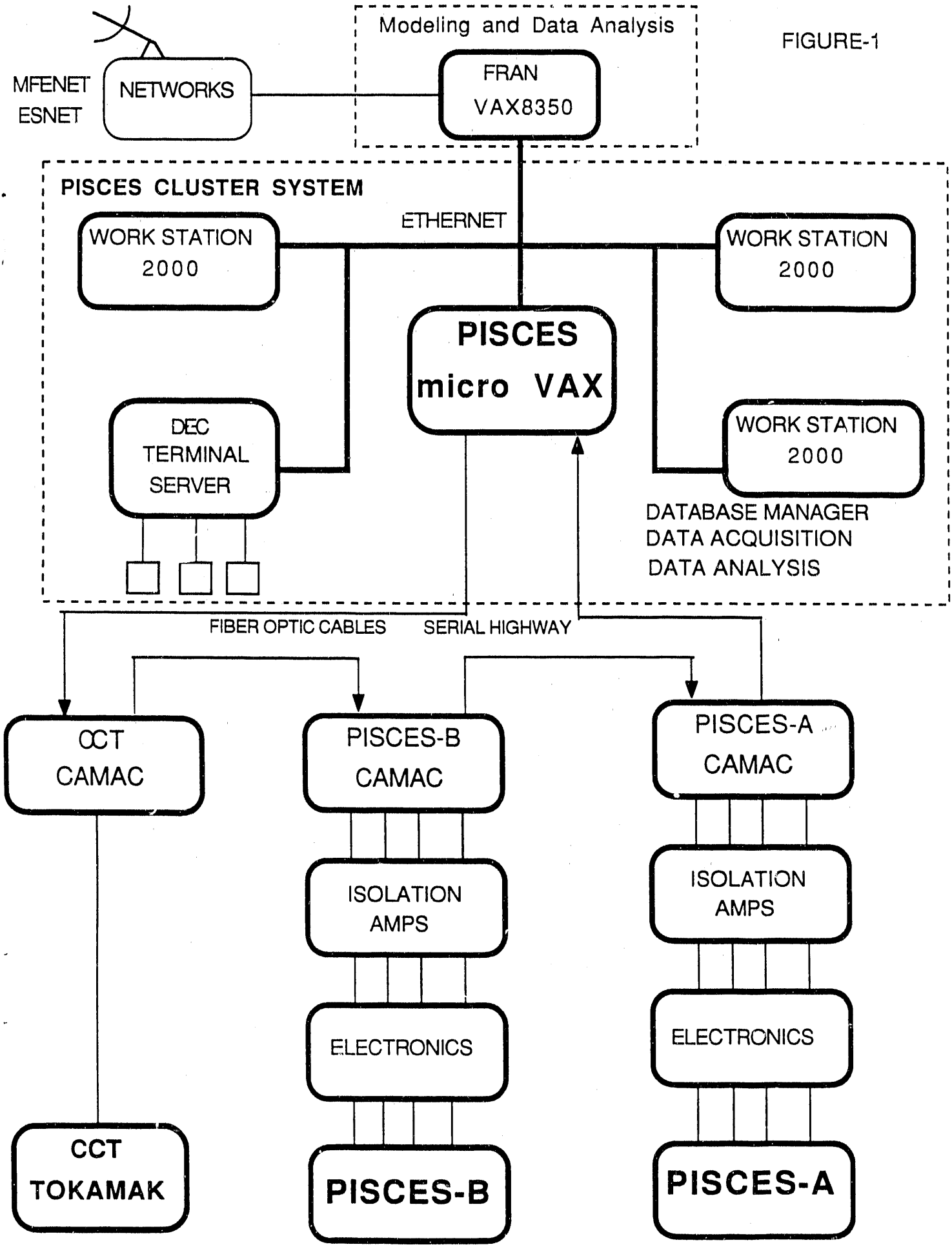
Modeling and Data Analysis
FIGURE-1
MFENET
ESNET
NETWORKS
FRAN
VAX8350
PISCES CLUSTER SYSTEM
ETHERNET
WORK STATION
2000
WORK STATION
2000
PISCES
micro VAX
DEC
TERMINAL
SERVER
WORK STATION
2000
DATABASE MANAGER
DATA ACQUISITION
DATA ANALYSIS
FIBER OPTIC CABLES
SERIAL HIGHWAY
CCT
CAMAC
PISCES-B
CAMAC
PISCES-A
CAMAC
ISOLATION
AMPS
ISOLATION
AMPS
ELECTRONICS
ELECTRONICS
CCT
TOKAMAK
PISCES-B
PISCES-A

SEM-EDX Facilities (UCLA-TRW Laboratory)

Materials tested in PISCES-B are routinely analyzed in the UCLA-TRW laboratory using Scanning Electron Microscopy (SEM, JEOL T-330), and Energy Dispersive X-ray Analysis (EDX, KEVEX DELTA CLASS IV). The EDX system is currently used for the analysis of boronized graphites.

The boron Kα line at 0.185 keV is generally difficult to detect. Also, the B Kα line lies at the edge of the electronic noise of the Kevex X-ray detector so that a part of the peak is lost in the noise. Further, for the boron-carbon system, the B Kα (0.185 keV) and C Kα (0.282 keV) peaks overlap since the FWHM for the Kevex system is 160 eV. With these limitations, the system has been optimized to detect boron from boronized graphite with a boron concentration above 3%.

The analysis of the boron-carbon system was done first semi-quantitatively, using the deconvolution technique [1]. Using pure boron (99.9%) and pure Graphite (POCO), along with B_4C with known concentration as a reference, the calibration curve has been obtained for B in boronized graphite as shown in figure 1. The offset seen for 0% B arises, presumably due to the B and C peak overlap.

For more quantitative, standard based analysis, a Faraday cup is used to measure the electron beam current. Analysis is done using deconvolution by reference[2] so as to account for the distortion of the B peak due to the electronic noise. The Kevex Quantex software is used to apply the ZAF corrections to the 'k' ratios* obtained using reference deconvolution, and determine the percent atomic as well as weight concentration of B in boronized graphite. Figure 2 shows the results for a number of samples. The data are in general agreement.

Another feature of the Kevex EDX system is the availability of X-ray mapping, ie. the areas of the sample where boron is concentrated can be determined. This feature is especially useful for a two phase material like boronized graphite. Figure 3 shows the X-ray maps acquired for the range of 3 to 30% B in boronized graphite. The B enriched areas have dimensions of the order of 7 microns for B concentration upto 20% and 25 microns for B concentration of 30%.

---

* 'k' ratio is the ratio of the peak intensity of the sample to the peak intensity of the reference standard.

[1] 'Kevex Quantex Software Reference Manual.' Kevex Instruments 1985.

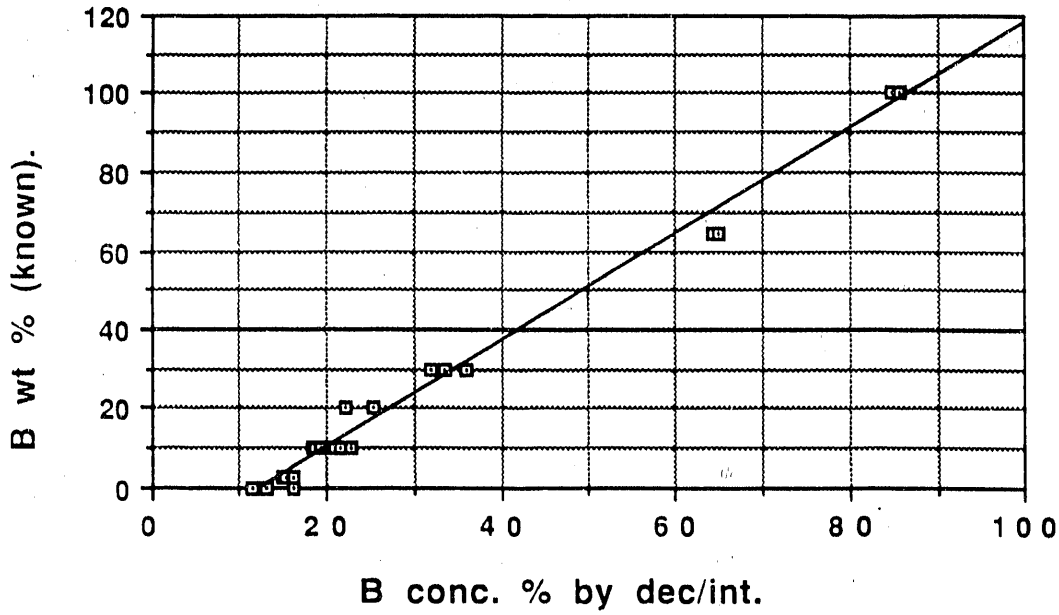

B (known) = - 16.662 + 1.3397 B (dec/int).

Figure 1: Calibration curve for Boron by dec/int.

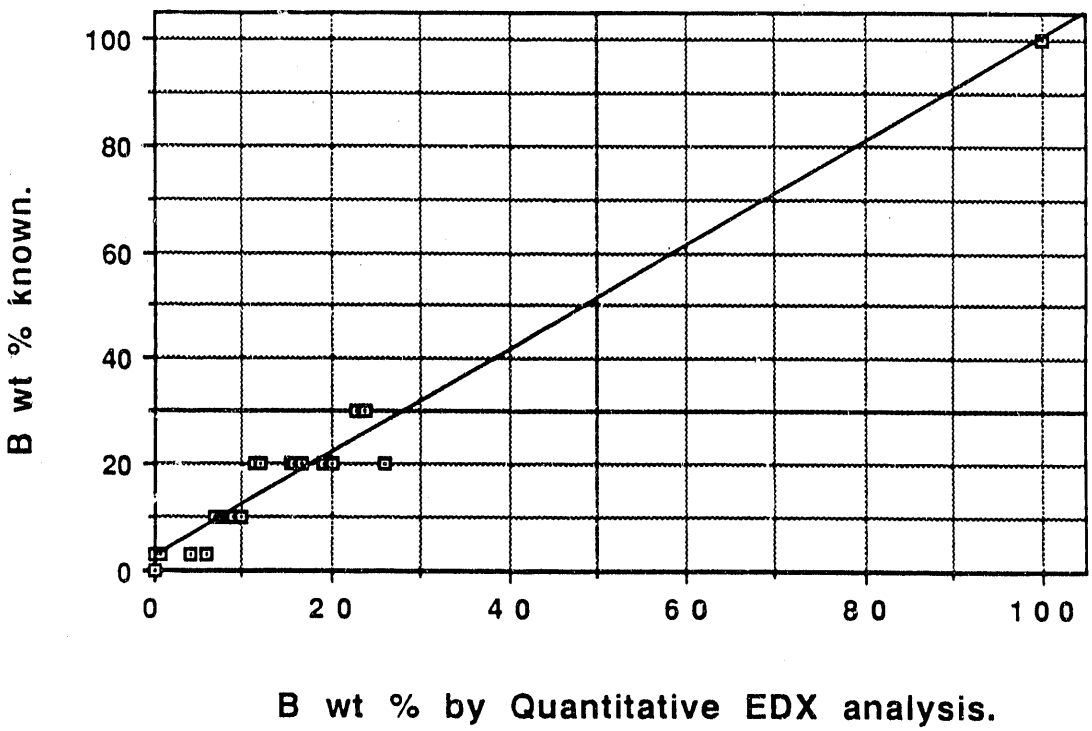

Figure 2: Results for B concentration by quantitative EDX analysis.

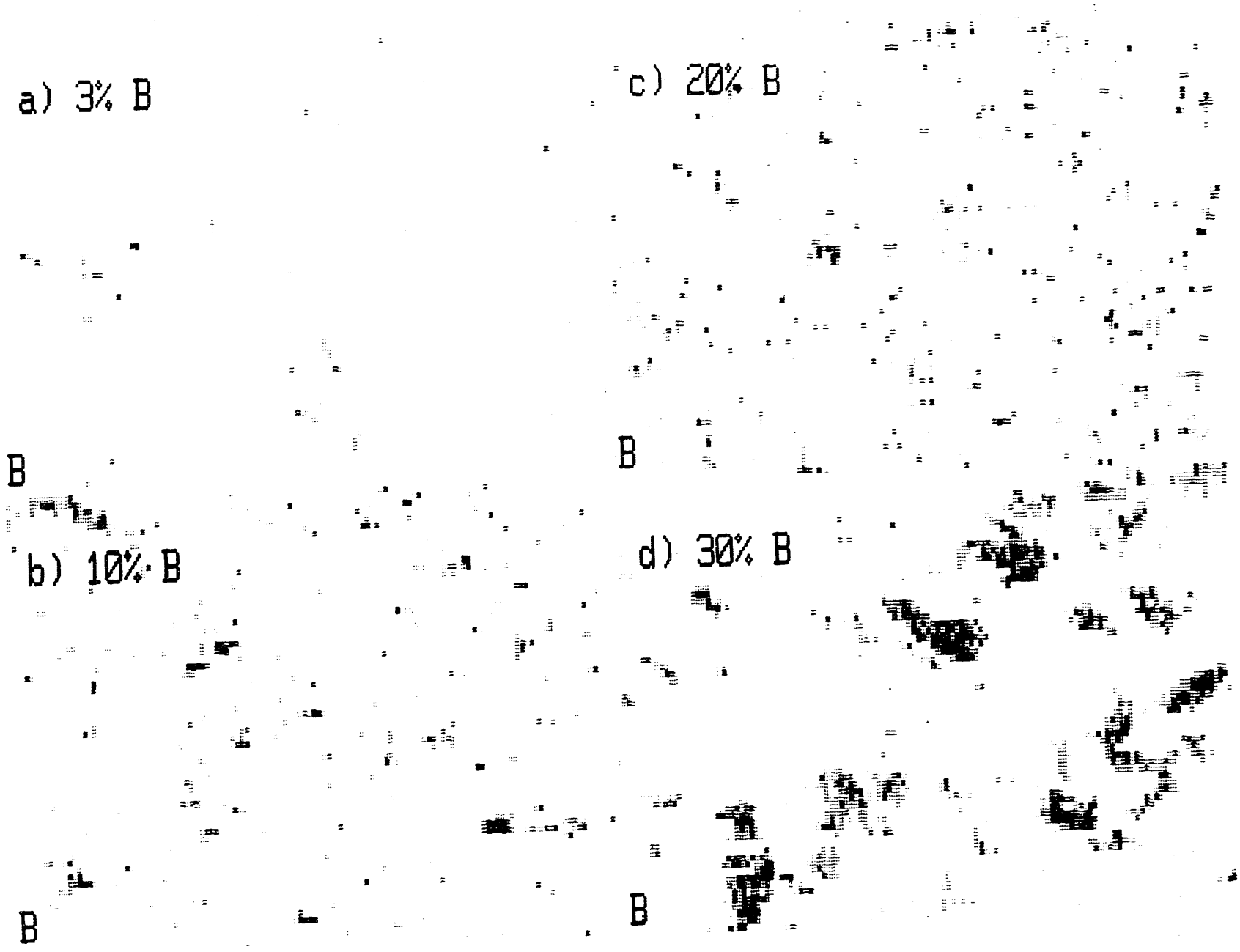

Figure 3: X-ray maps of Boron in Boronized Graphite, at 500X.

Vacuum Outgassing Facility for Thermal Desorption Spectrometry

It is widely recognized that outgassing from plasma-facing components in tokamaks can significantly affect the performance of plasma confinement. Therefore, it is important to study the outgassing behavior of materials using off-line facilities. The thermal desorption spectrometry (TDS) technique is generally used to measure the outgassing characteristics of materials.

Recently, a facility to perform outgassing measurements has been constructed in the PISCES-lab. A schematic diagram of this facility is shown in Fig. 1. The system consists of: (1) 6-way cross stainless steel chamber; (2) BA-gauge; (3) a turbomolecular pump with a pumping speed of 170 l/s; (4) a residual gas analyzer (RGA) with a PC-data acquisition system; and (5) a computer-controlled infrared (IR) furnace.

In this outgassing facility, a test sample can be heated by the IR-furnace from room temperature to temperatures around 1000°C typically at a rate of around 20 deg/min. During the course of thermal desorption measurement, partial pressures of desorbed gases are monitored with the RGA system.

As an example, the thermal desorption spectra from a bulk-titanized graphite sample are shown in Fig. 2. The total amount of desorbed gasses is calculated from the time-integration of their partial pressures. In this case, the total desorption is 2.64×10^{18} molecules/cm^2. Also, from these TDS data, the activation energy (E_d) for the desorption process can be estimated using the relation [2]:

$$(E_d/RT_m^2) = (\nu_d \, n \, \sigma^{n-1}/\beta) \exp(-E_d/RT_m)$$

where n is the order of the surface reaction, T is the peak temperature, ν_d is the frequency factor, σ is the concentration of the gas, β is the temperature ramp rate. The evaluation of the activation energy is under way for the desorption of deuterium from bulk-titanized graphites.

---

[1] P.A.Redhead Vacuum 12 (1962) 203

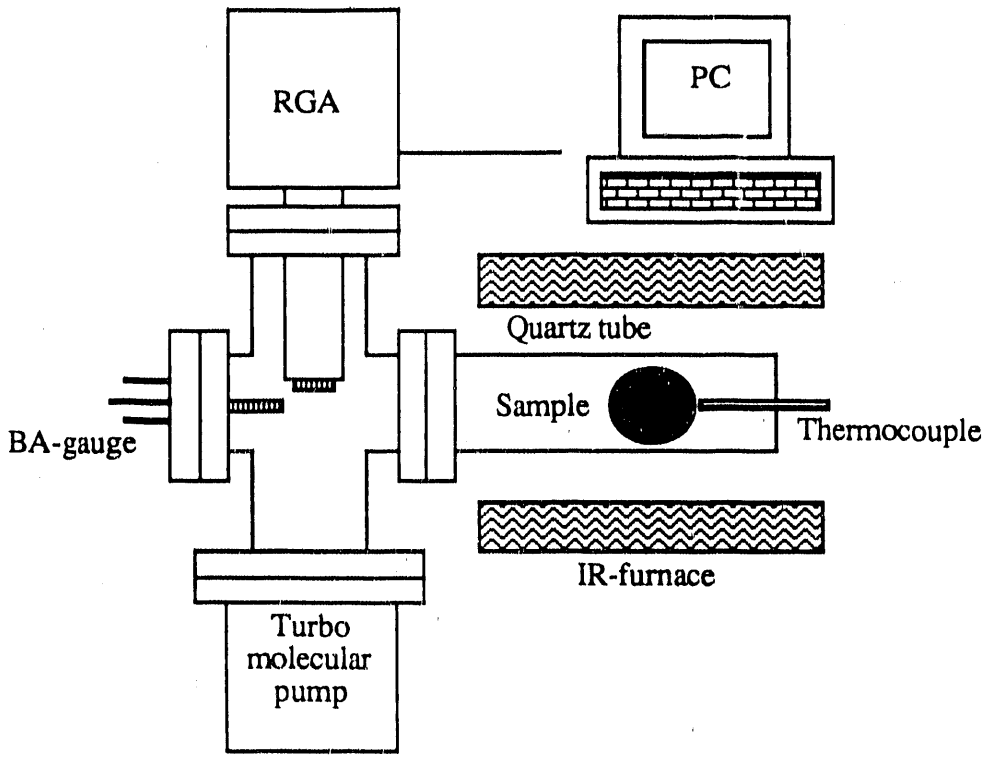

Fig. 1 A schematic diagram of the vacuum outgassing facility.

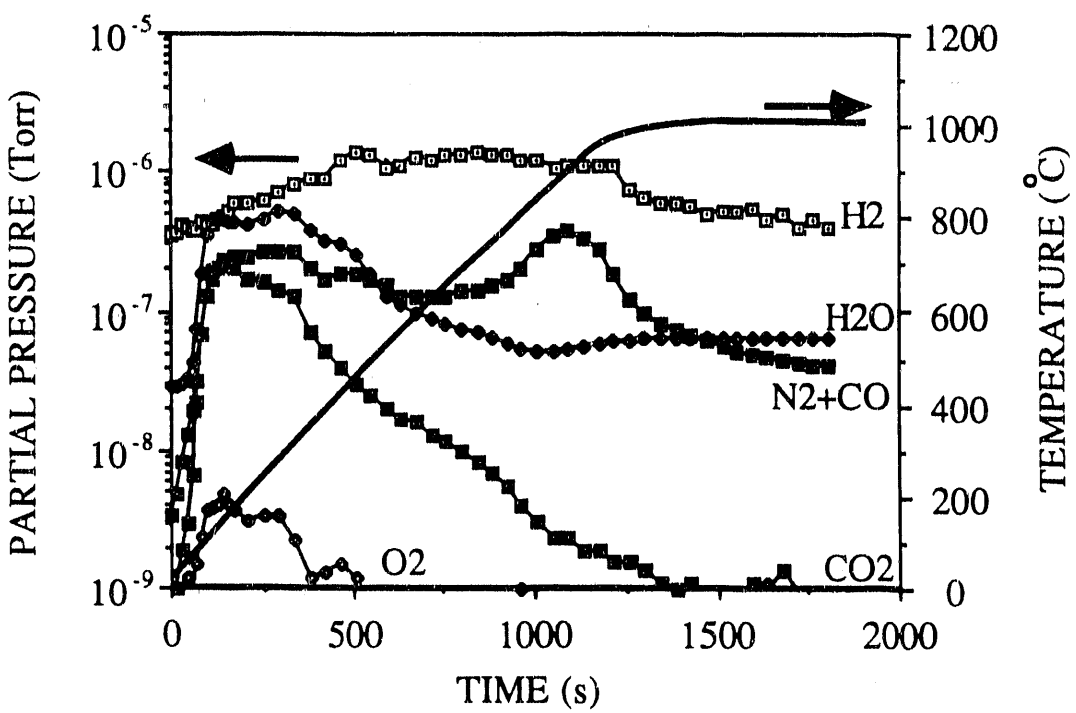

Fig. 2 Desorption from titanized C-C composite (CCTK-420).

PISCES-Exps.

- Materials Physics -

Evaluation of Bulk-Boronized Graphites as Plasma-Facing Materials

Graphites have been widely used as plasma-facing materials in major tokamaks including TFTR, DIII-D, JT-60, JET and TEXTOR. However, graphite generally suffers from chemical sputtering and radiation enhanced sublimation due to hydrogen plasma bombardment at elevated temperatures. In fact, graphite components in JET and TEXTOR have recently been modified with beryllium and boron coatings, respectively. The plasma confinement has been significantly improved in these tokamaks due to the surface modifications of plasma-facing components.

As such, coatings are effective in improving surface characteristics of graphite. However, by nature surface coatings cannot be used for plasma-facing components in steady-state fusion devices such as the International Thermonuclear Experimental Reactor (ITER). Clearly, graphite should be bulk-modified for use in ITER-type reactors. The PISCES-team at UCLA has been contributing the ITER R&D activity in the States.

From this point of view, 3 wt% bulk-boronized graphite was bombarded with steady-state hydrogen plasmas and showed an improved erosion resistance, relative to ordinary isotropic graphites in our recent work [1]. For more improved performance, Similar bulk-boronized graphites with higher boron concentration have been developed. These bulk-boronized graphites have been systematically evaluated as plasma-facing materials in aspects related to several critical issues pointed out in the ITER design study. These issues include: (1) thermal stability; (2) neutron radiation damage; (3) plasma erosion; (4) tritium inventory; (5) thermal shock cracking; (6) steam/air oxidation.

This materials evaluation has been done in collaboration with major national and foreign institutions. These institutions include:

(1) Toyo Tanso in Japan for materials production and air oxidation tests

(2) SNLL for tritium inventory measurements

(3) SNLA for thermal shock cracking tests

(4) INEL for steam-oxidation tests

(5) ORNL for neutron radiation tests (still under way)

(6) Tokamak de Varennes in Canada (to be done in Sep.-90).

The PISCES-team has organized this collaboration in the manner shown in Fig. 1 and has been in charge of the evaluation of these materials regarding surface characterization and measurements of the plasma erosion yield. Also, this activity is acknowledged as part of the US-Japan and US-Canada collaboration programs.

---

[1] Y.Hirooka et.al. J.Vac.Sci. & Technol. **A8** (1990) 1790.

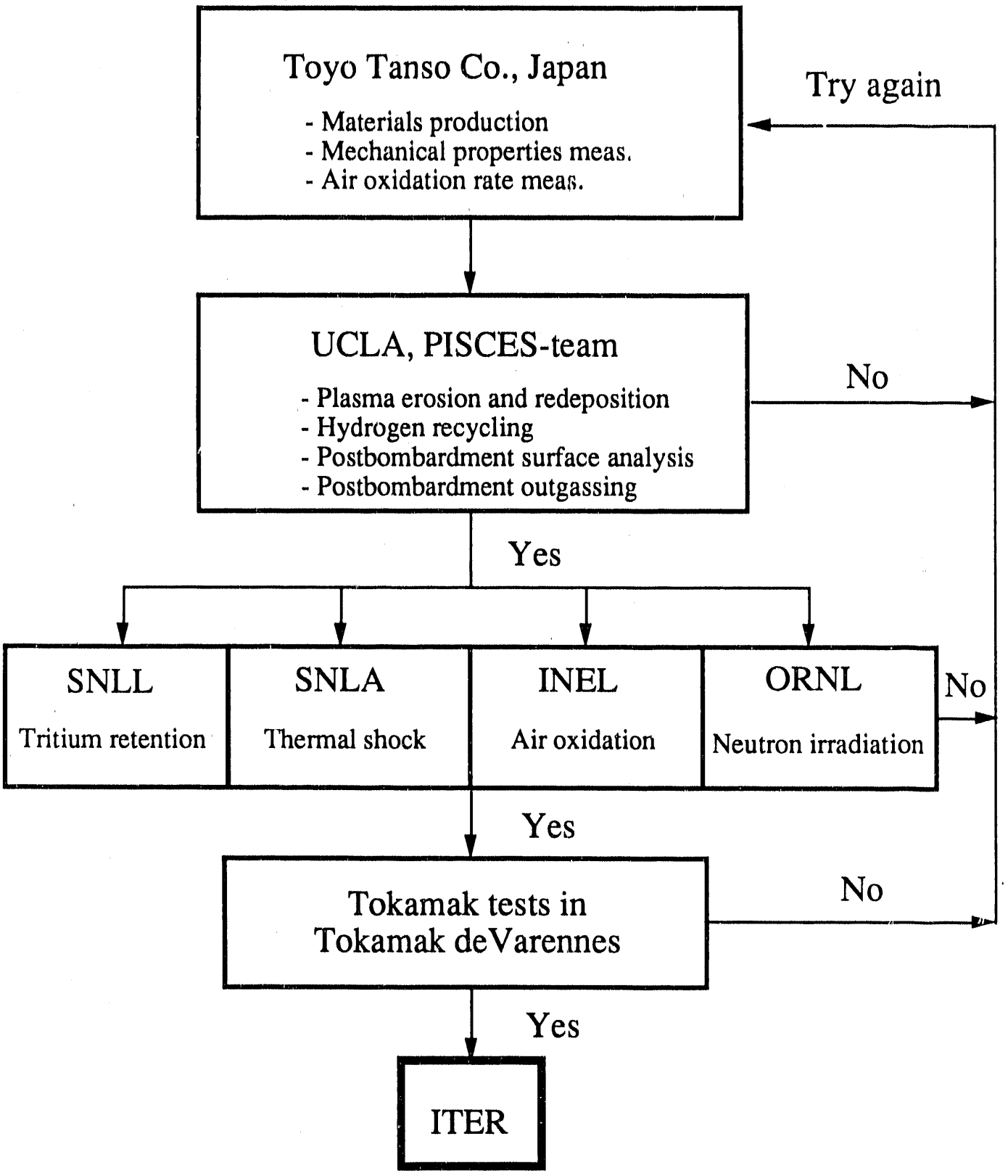

Fig. 1 A flowchart of the evaluation procedure of bulk-boronized graphite as a plasma-facing component material for ITER.

Bulk-Boronized Graphites: (1) Plasma Induced Erosion [1]

Perhaps the most critical issue in the current design of ITER is the erosion of the divertor plate due to high-flux plasma bombardment. The divertor plate will be subject to high-flux, steady-state plasma bombardment and the estimated rate of recession of a divertor plate, if made of graphite, can be as high as 27 cm/year even if the effect of redeposition is considered. Obviously, new materials need to be developed.

Using the PISCES-B facility, deuterium plasma bombardment was done in the erosion regime: an ion bombarding flux of 2.5 x 10^{17} ions cm^{-2} s^{-1}; an ion bombarding energy of 250 eV; an electron temperature of 10 eV. The sample temperature was controlled between 200 and 1600°C. The maximum temperature here is relevant to the temperature at which the "carbon bloom" starts in TFTR.

Shown in Fig. 1 are the plasma erosion data taken for bulk-boronized graphites and non-boronized isotropic and pyrolytic graphites for comparison. It is found that the erosion yield of bulk-boronized graphites is a factor of 2-3 smaller than that of non-boronized graphite. Using ion beams, a reduced chemical sputtering has been observed for graphites contaminated with impurities [2]. However, it is important to note here is that radiation enhanced sublimation (RES) as well as chemical sputtering is suppressed.

From the Arrhenius plots (see Fig.2) of the erosion yield data at temperatures above 1000°C, the activation energies for RES are evaluated to be 1.1 eV and 1.4 eV for pyrolytic graphite and bulk-boronized graphites, respectively. The difference in these activation energies clearly indicates the effect of boron on the kinetics of carbon migration. More interestingly, the activation energy obtained here for bulk-boronized graphites is in excellent agreement with the interaction potential between boron and interstitial carbon of 1.45 eV. This agreement strongly supports our interpretation of the RES data.

In earlier work [3], it was predicted that high-flux ion bombardment might result in a reduction of RES-erosion in the manner that $Y \propto \Gamma^{0.91}$ where Γ is the ion flux. This power law predicts that the RES-erosion yield at 10^{17} ions cm^{-2} s^{-1} is about 34% smaller than that at 10^{16} ions cm^{-2} s^{-1}. Contrary to this prediction, the erosion yield data obtained here at 1500°C for pyrolytic graphite agree well with those at an ion flux of about 1 x 10^{16} ions cm^{-2} s^{-1}[4]. From these observations, one concludes that the flux dependence prediction will not hold for high-flux plasma bombardment conditions to be seen in the divertor region of ITER.

[1] Y.Hirooka et.al., paper presented at 9th PSI-conference at Bournemouth, May, 1990.
[2] J.Roth, J.Nucl.Mater. **145-147**(1987)87.
[3] A.A.Haasz and J.W.Davis, J.Nucl.Mater. **151**(1987)77.
[4] J.Bohdansky and J.Roth, Proc.15th Symp. on Fusion Technol., Utrecht, Sep, 1988.

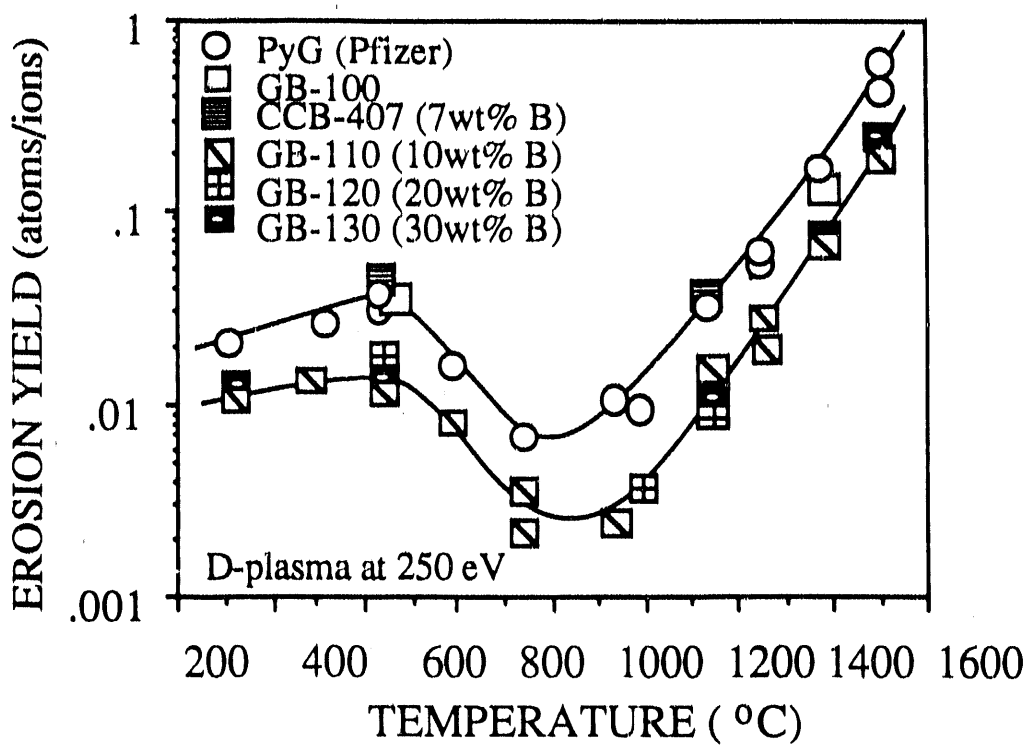

Fig. 1 Plasma-induced erosion of bulk-boronized graphites.

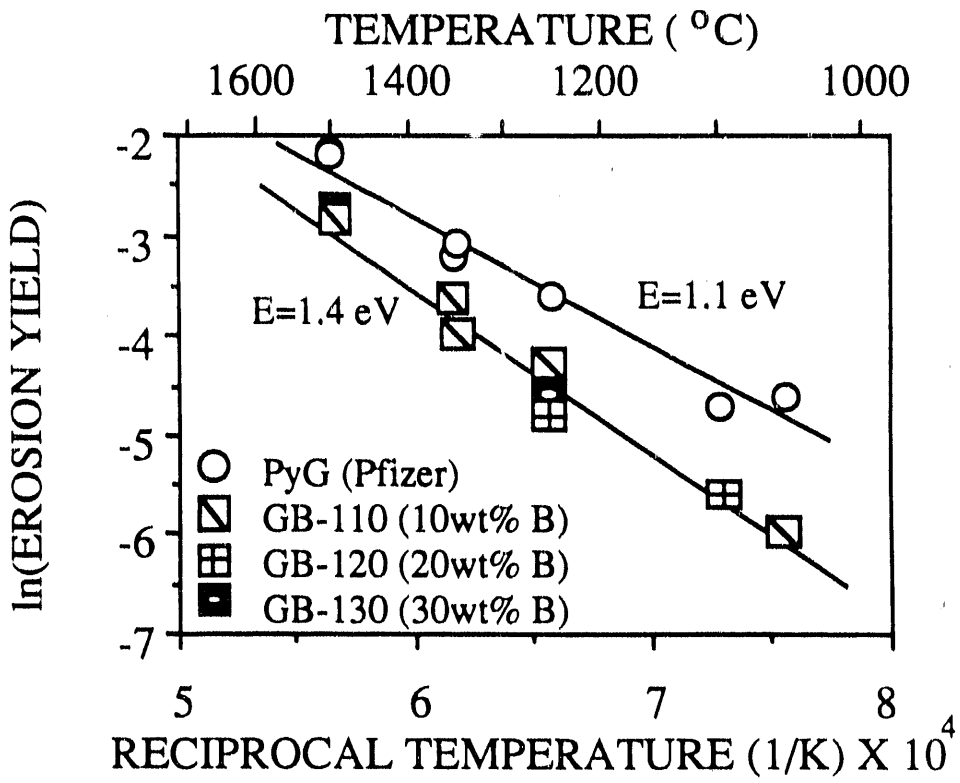

Fig. 2 Arrhenius plots of RES erosion yeilds.

Bulk-Boronized Graphites: (2) Surface characterization [1]

Bulk-boronized graphites are manufactured via high temperature baking of a carbon and boron carbide powders with a diameter of 3-5 μm. Naturally, the resultant material has two phases. According to the phase diagram data [2], bulk-boronized graphite is believed to consist of: (1) the solid-solution phase with dissolved boron substituting carbon at the lattice site; and (2) the boron carbide phase, presumably of B_4C. To characterize bulk-boronized graphites, energy dispersive X-ray (EDX) analysis has been done. Shown in Fig. 1 are the 2-dimensional mapping data for boron. One sees localized boron-rich areas, indicative of the boron carbide phase.

For the use of such compounds for plasma-facing components, it is important to investigate the effect of plasma bombardment on the surface composition. For example, 20 wt% bulk-boronized graphite, has been analyzed after deuterium plasma bombardment at 550 and 1350°C under similar conditions to those used for erosion measurements. At these temperatures, one can observe the concentrated effects of chemical sputtering and radiation enhanced sublimation. The total fluence was of the order of 10^{21} ions cm^{-2}, which is equivalent to the wall road for a few hundred confinement discharges in major tokamaks such as TFTR.

The EDX surface analysis data are shown in Fig. 2 as a function of fluence. At 550°C boron is observed to be slowly enriched to about 30 wt% as the fluence approaches the order of 10^{21} ions cm^{-2}. A simple explanation might attribute this finding to the preferential chemical sputtering of carbon. However, one must take into account that in this material boron carbide particles are dispersed. Given the statistical fluctuation due to the two phase structure, the observed boron enrichment should not be considered as a serious concern about bulk-boronized graphites.

However, deuterium plasma bombardment at 1350°C does not rapidly alter the surface composition. Even after plasma bombardment at 1600°C, no significant depletion of boron was observed. In earlier RES-data on TEXTOR-type boronized amorphous carbon films, no effect of boron was observed at temperatures above 1500°C [3]. One suspects that these a-C/B:H films might be largely depleted with boron. Therefore, it is possible to hypothesize that for bulk-boronized graphite, even if the solid solution phase is depleted with boron due to evaporation, the depletion may be compensated by the dissolution of boron from the carbide phase to maintain the equilibrium composition.

[1] Y.Hirooka et.al., paper presented at 5th Carbon Workshop at KFA, May, 1990.
[2] C.E.Lowell, J.Am.Ceram.Soc. 50(1967)142.
[3] V.Philipps et.al., Int.Conf.on Fusion Reactor Materials, Kyoto, Japan, 1989.

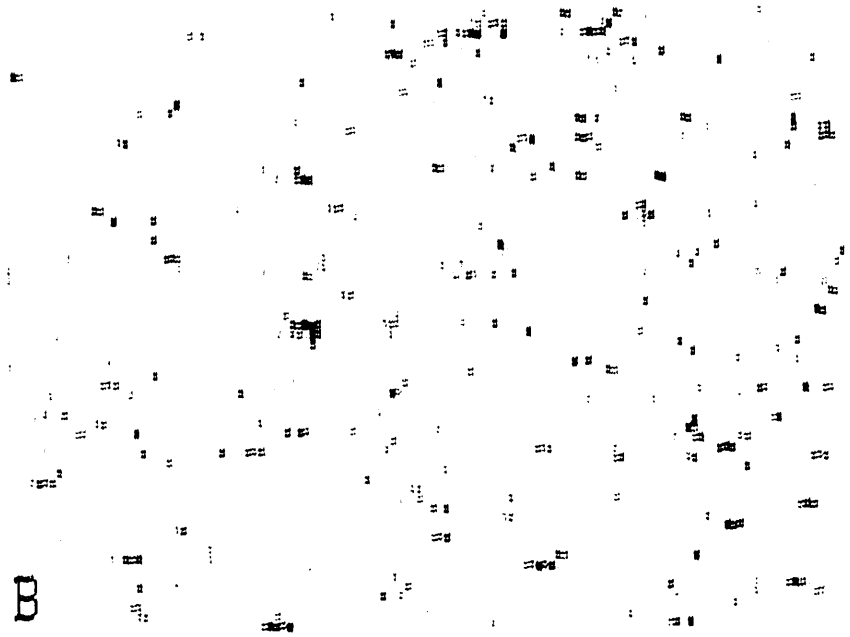

Fig. 1 2-D mapping of boronized spots on the surface.

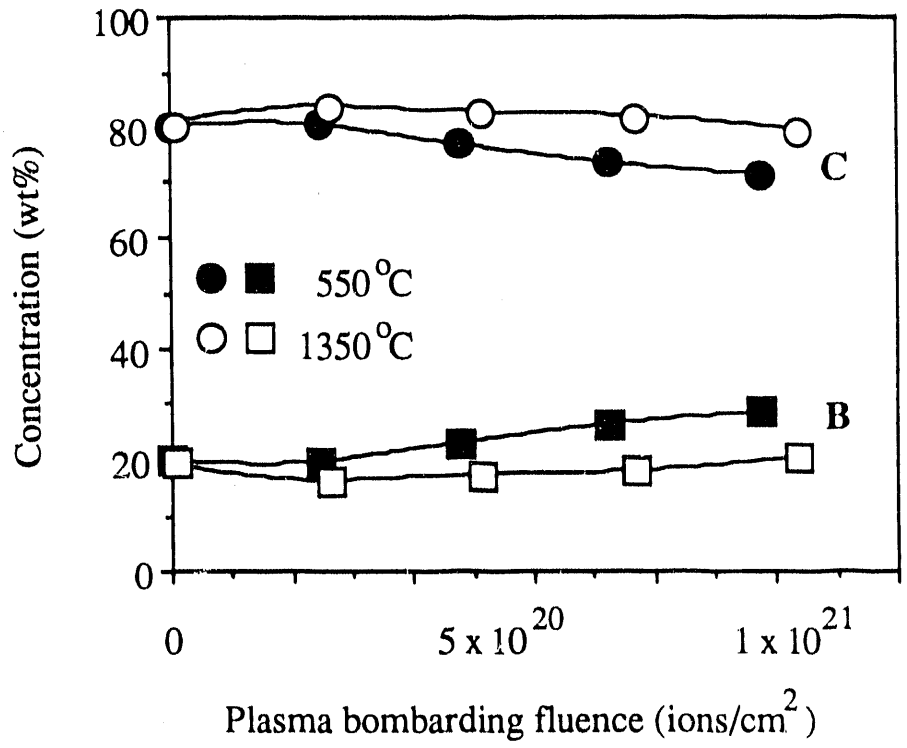

Fig. 2 Surface composition of 20% bulk-boronized graphite bombarded with deuterium plasmas to high fluences.

Bulk-Boronized Graphites: (3) Thermal desorption [1,2]

The behavior of postbombardment thermal desorption from bulk-boronized graphites is described here. For the preimplantation of deuterium, plasma bombardment was done in PISCES-B at an ion bombarding energy of 300 eV and at an ion bombarding flux of around 4 x 10^{17} ions cm^{-2} s^{-1}. The sample temperature was varied from room temperature to 800°C. The total ion bombarding fluence was around 3 x 10^{20} ions cm^{-2}, which well exceeds the minimum deuterium fluence to saturate the surface layer of isotropic graphites [3].

Thermal desorption spectroscopy measurements were carried out in the vacuum outgassing facility shown earlier in this report. The base pressure in this facility is of the order of 10^{-9} Torr using a turbo molecular pump with a pumping speed of 170 l/s (for nitrogen). The sample temperature was programmed to ramp from room temperature to 720°C at a rate of 20 degs/min.

Deuterium containing species detected with the RGA during thermal desorption are HD, D_2, CD_4 and C_2D_4. These species were not observed for non-bombarded samples. Shown in Fig. 1 are the thermal desorption spectra of deuterium (D_2) and deuteromethane (CD_4) from 3 wt% bulk-boronized graphite and POCO-graphite (AXF-5Q), both bombarded with a deuterium plasma at 320°C. Notice that the desorption of deuterium from boronized graphite is clearly enhanced, relative to that from POCO-graphite. The opposite is true for deuteromethane. A similar trend has been observed for HD and C_2D_4, the spectra of which are not shown here. An enhanced desorption of hydrogen and a suppressed desorption of methane has been observed also for graphite with metallic impurities such as Fe, Ni and Ti [4].

Importantly, the total deuterium retention for these materials has been found to be essentially the same. Consistent with this, as seen in Table 1, the amount of deuterium consumed due to the enhanced desorption of HD and D_2 is in excellent agreement with that saved from the reduced desorption of CD_4 and C_2D_4. These observations clearly indicate a catalytic effect of boron on the desorption kinetics of molecules containing deuterium. From these findings, one concludes that the enhanced recombinative desorption of deuterium is responsible for the reduced chemical sputtering observed here for bulk-boronized graphite.

[1] Y.Hirooka et.al., paper presented at 5th Carbon Workshop at KFA, May, 1990.
[2] Y.Hirooka et.al., paper presented at 9th PSI-conference at Bournemouth, May, 1990.
[3] B.L.Doyle et.al., J.Nucl.Mater. 93-94(1980)551.
[4] S.Fukuda et.al., J.Nucl.Mater. **162-164**(1989)997.

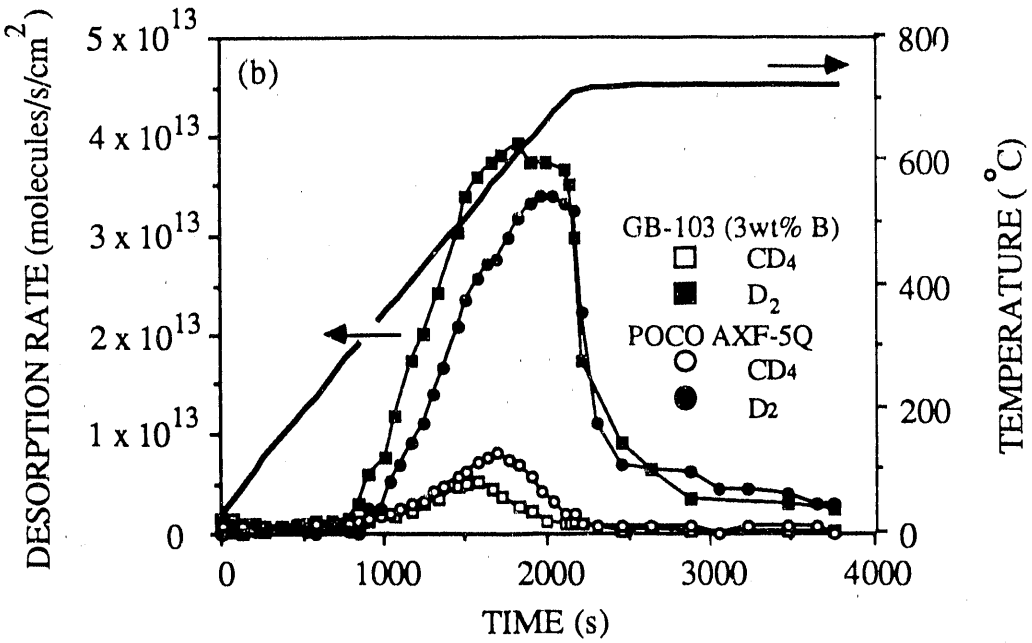

Fig. 1 Desorption of implanted deuterium from bulk-boronized graphite.

Table 1 Contribution of various gases to deuterium desorption.*

Gas species	POCO (D-atoms/cm^2)	GB-103	Effects of boron
D from HD	0.16 x 10^{17}	0.17 x 10^{17}	Enhanced
D from D_2	0.77 x 10^{17}	0.92 x 10^{17}	D-desorption
Sub-total	0.93 x 10^{17}	1.09 x 10^{17}	0.16 x 10^{17}
D from CD_4	0.29 x 10^{17}	0.19 x 10^{17}	Reduced
D from C_2D_4	0.09 x 10^{17}	0.04 x 10^{17}	CD-desorption
Sub-total	0.38 x 10^{17}	0.23x 10^{17}	0.15 x 10^{17}
Total D-atoms	1.31 x 10^{17}	1.32x 10^{17}	

*Deuterium plasma bombardment was done at 320°C.

Bulk-Boronized Graphites: (4) D-T Retention [1]

The total deuterium uptake due to plasma bombardment can be estimated by time-integrating partial pressures of deuterium containing species during thermal desorption in the manner that $Q=\int \Sigma s_i p_i(t)dt$ where Q is the total throughput, s_i is the pumping speed and $p_i(t)$ is the time-dependent partial pressure. The total deuterium retention is shown in Fig.1 as a function of surface temperature during plasma bombardment. One sees that the deuterium retention tends to maximize at around 300°C. This result contradicts earlier ion beam data taken at relatively high energies [2] but agrees well with recent measurements using thermal atomic hydrogen [3]. Pyrolytic graphite (Union Carbide) shows the smallest deuterium retention, indicating the effect of surface porosity.

Possible explanations for these findings are as follows. Low energy deuterium such as Frank-Condon neutrals is weakly bound to the surface and needs to be thermally activated to migrate deeper into the bulk via diffusion. However, above a certain temperature the thermal desorption becomes predominant, which then decreases deuterium retention. Also, such weakly bound deuterium atoms can be liberated upon the exposure to air, which also reduces deuterium retention. The air-exposure effect is important for the plasma exposure at room temperature for which the migration depth is relatively shallow.

The volumetric dissolution of tritium in grains of graphite becomes important in determining the total uptake at elevated temperatures. For tritium inventory measurements, 3 wt% and 10 wt% bulk-boronized graphites and non-boronized graphite (GB-100) have been exposed to deuterium+tritium plasmas (99% D and 1% T) at an ion bombarding energy of 100 eV at temperatures above 800°C, each for 1 hour in the TPX-facility at SNLL. Plasma-bombarded samples were first dissolved in a chromosulphuric acid solution at 160°C, then the tritium activity was measured with a liquid scintillation counter.

Shown in Fig. 2 are the resultant tritium retention data as a function of temperature. Notice at temperatures above 1100°C, the tritium retention in bulk-boronized graphites is considerably lower than that in non-boronized graphite. In fact, the tritium retention in bulk-boronized graphites at these high temperatures is close to that in pyrolytic graphite. Generally, tritium tends to be trapped by crystalline defects with unsaturated bonds if graphite is not well graphitized. One possible explanation for the reduced retention of tritium is that boron dissolved in the lattice (i.e. the solid-solution phase) might preoccupy these trapping sites or deactivate unsaturated bonds.

[1] Y.Hirooka et.al., paper presented at 9th PSI-conference at Bournemouth, May, 1990.
[2] B.L.Doyle et.al., J.Nucl.Mater. 103-104(1981)513.
[3] V.Philipps et.al., J.Nucl.Mater.145-147(1987)292.

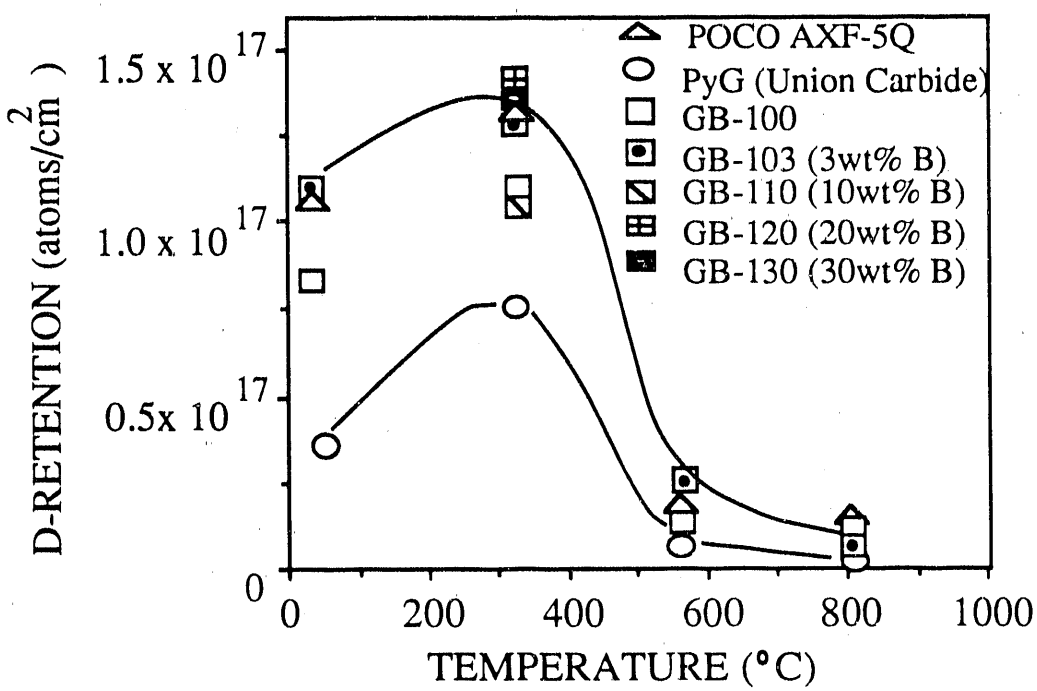

Fig. 1 Deuterium retention in various graphites at T < 800°C.

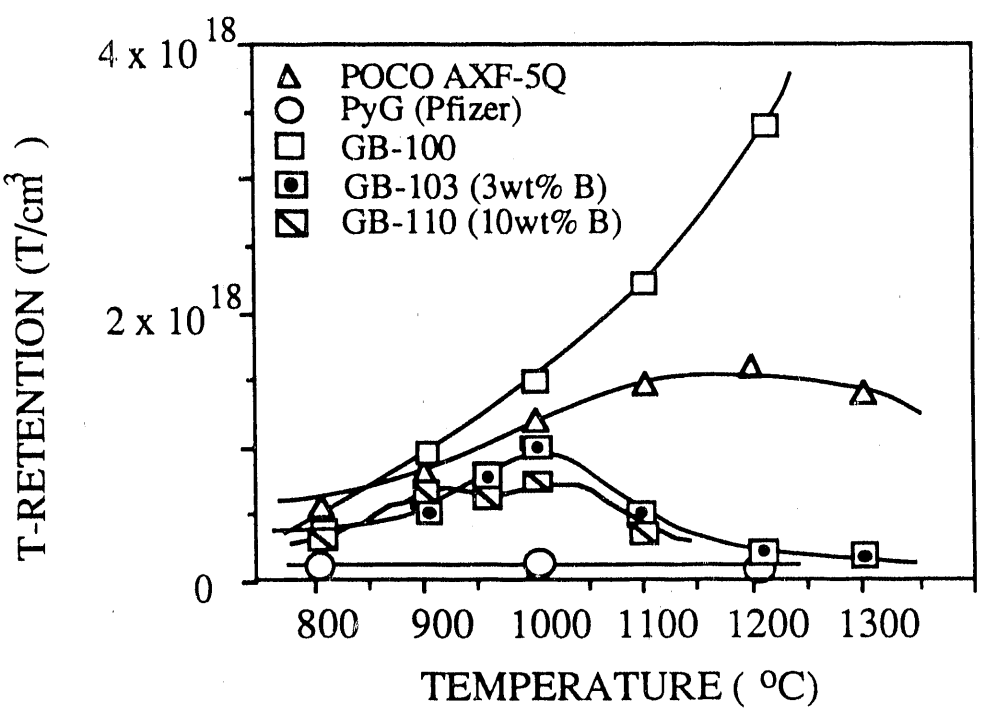

Fig. 2 Tritium retention in various graphites at T > 800°C.

Bulk-Boronized Graphites: (5) Air, steam oxidation [1]

Despite of its importance, little attention has been paid to safety concerns about accidental losses of vacuum of a fusion reactor. The reaction of surface components made of graphite with air-moisture at high temperatures results in a generation of hydrogen. Therefore, accidental vacuum losses can be followed by an explosion of hydrogen mixed with air. Also, hot graphite surfaces will react directly with air, leading to massive combustion. The oxidation behavior of bulk-boronized graphites is described here. Using the Toyo Tanso facility, the air oxidation reaction rates were measured at 800°C. At INEL, the steam oxidation reaction experiments were conducted at about 1100 and 1350°C.

The results are shown in Figs.1 and 2. Notice that in Fig. 1 the air-oxidation reaction appears to be inhibited almost completely for 10 wt% and 30 wt% bulk-boronized graphites. These surprising data were not only measured with weight loss but were also confirmed with gas analysis of reaction products such as CO. As shown in Fig. 2, bulk-boronized graphites (particularly GB-110) clearly exhibit suppressed reaction with steam, relative non-boronized graphite (GB-100).

The improved oxidation resistance in air is partly due to the formation of a passive protective surface layer of boron oxide (B_2O_3) [2]. Obviously, this protective layer argument does not completely explain the present data because the melting point of boron oxide is 450°C. One speculates that the molten oxide layer may be effective in reducing the oxidation rate until the temperature approaches its boiling point of 2250°C. Nevertheless, if bulk-boronized graphites are used in present-day fusion devices, the formation of surface oxides will be important in reducing the contamination due to oxygen. In fact, the oxygen gettering effect has been pointed as the key to the recent confinement improvement in JET [3] and TEXTOR [4].

On the other hand, boron is known to enhance graphitization during the final baking process [5]. The oxidation rate is generally expected to be lower for better graphitized structures. Consistent with this, in Fig. 2 pyrolytic graphite shows appreciably lower oxidation rates than other graphites. Therefore, the enhanced graphitization in bulk-boronized graphites is considered to play an important role in improving the oxidation resistance.

---

[1] Y.Hirooka et.al., paper presented at 9th PSI-conference at Bournemouth, May, 1990.
[2] T.Matsuda et.al., paper presented at 27th Summer Seminar on Carbon Materials, Aug.29-Sep.1, 1989, Nagano, Japan.
[3] JET-Report #JET-P(89)80, "JET-posters presented at the 31st APS Meeting, Anaheim, USA, Nov.13-17, 1989".
[4] J.Winter et.al. N.Nucl.Mater. 162-164(1989)713.
[5] A.Oya, Tanso 102(1980)118.

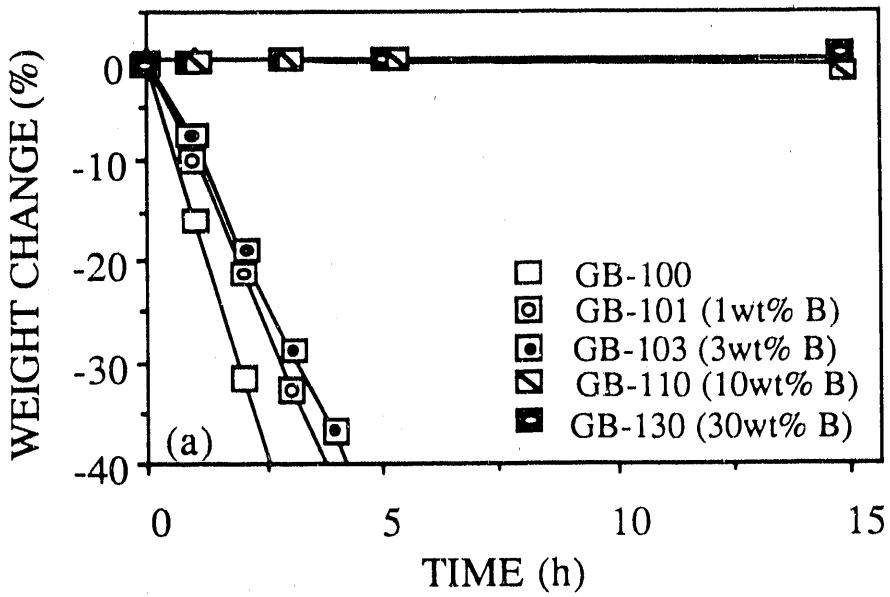

Fig. 1 Air-oxidation behavior of bulk-boronized graphites at 800 °C.

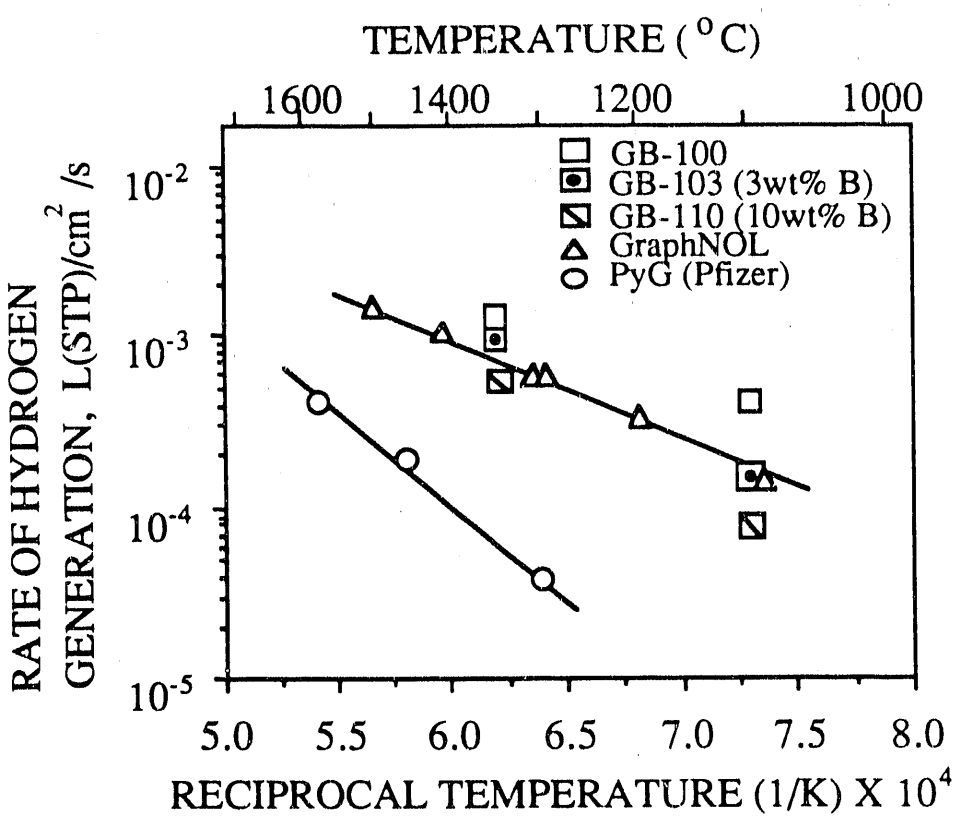

Fig. 2 Arrhenious plots of steam-oxidation rates of various graphites at T > 1000°C.

Chemical Erosion of Selected Carbon-Carbon Composites*[1]

Because of their improved thermo-mechanical properties, carbon-carbon (C-C) composites have recently drawn considerable attention from the fusion engineering community. In fact, some of these C-C composites are already used in major tokamaks including TFTR and JET for plasma-facing components. However, it is also true that there is no established data base on chemical sputtering for these C-C composites to allow us to select suitable materials for future fusion devices such as ITER and LHD**.

Using the PISCES-B facility, 3D-weave, unidirectional and random felt-type C-C composites and POCO (AXF-5Q) graphite have been bombarded with hydrogen plasmas. The plasma bombardment conditions are: an ion bombarding flux of 2.6×10^{18} ions cm^{-2} s^{-1}; an ion bombarding energy of 200 eV. These conditions are believed to be relevant to those predicted for the divertor regions in ITER and LHD. The resultant heat flux is about 0.8 MW/m^2, which heats the sample naturally from room temperature to temperatures around 900°C. Along with the temperature excursion, the erosion yield due to chemical sputtering was monitored in-situ with optical spectroscopy using the CH-band and a differentially pumped residual gas analyzer simultaneously. Similar to our previous work [2], the spectroscopic data were calibrated by the weight loss method separately.

The calibrated erosion yield data indicate:

(1) for POCO graphite and unidirectional felt-type composites, the chemical erosion yield clearly exhibits two maxima at 500 and 700°C, consistent with our earlier observations [2];
(2) for other materials, the erosion yield appears to maximize only at around 700°C; and
(3) the maximum erosion yields for these materials are different from one another by about 80%. These findings are presumably due to the structural effects of materials. For plasma bombarded materials, strong surface modifications have been observed with SEM. Also, from the in-situ RGA data, C-, C_2-, and C_3-hydrocarbons are identified at 600 °C for all the materials tested in this work.

---

*This work has been done as part of the US-Japan collaboration for 1990. In particular, materials tested here are candidates for plasma-facing components to be used in LHD**.
**LHD is a Large Helical Device which is being designed at NIFS, Japan. Currently, LHD is planned to start operation sometime in 1997.

[1] A.Sagara, to be presented at 16th SOFT conf. in UK, Sep, 1990.
[2] Y.Hirooka et.al., J.Vac.Sci. & Technol. A7(1989)1070.

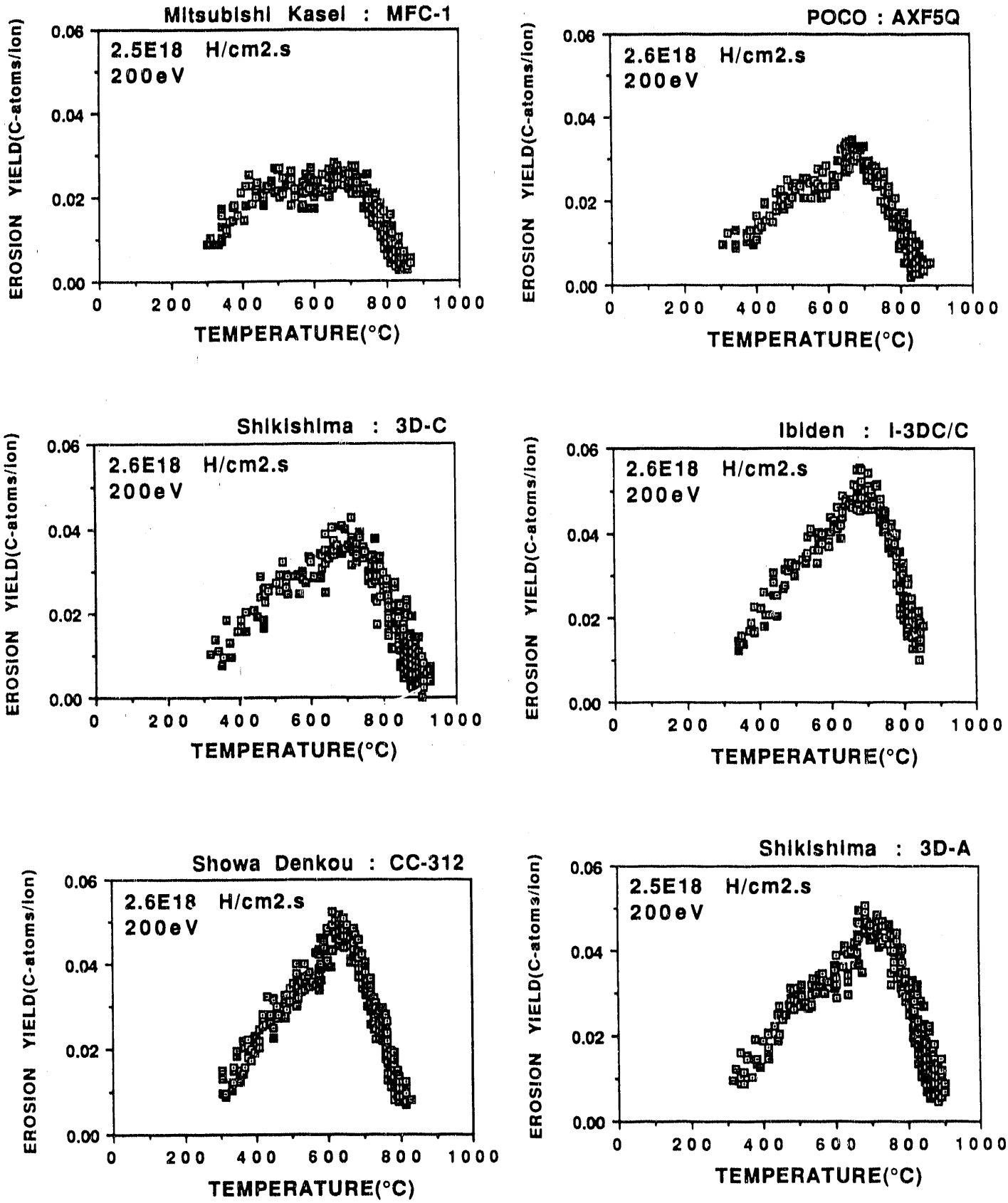

Fig. 1 Chemical erosion of various C-C composites due to hydrogen plasma bombardment in the PISCES-B facility.

ITER: Characterization of Plasma-Redeposited Carbon Materials

It is well known that plasma-facing materials eroded due to plasma bombardment will eventually be redeposited elsewhere in a torus. However, only limited information about redeposited materials is available. One of the critical issues pointed out in the ITER R&D activity is the behavior of hydrogen retention in plasma-redeposited carbon materials. In this work, the total deuterium retention in the redeposited carbon has been investigated using the postdeposition thermal desorption technique.

Used here as substrates are POCO AXF-5Q graphite and molybdenum disks. The substrate is set at one end of a carbon cylinder crucible with the other end open to the plasma flow, parallel with the magnetic field. Deuterium plasmas are used for these redeposition experiments. The plasma diminishes as it flows deeper in the crucible because of its interactions with the carbon wall. Due to these plasma-carbon interactions, deuterocarbons are formed and re-ionized in the plasma. Therefore, the substrate is subjected to plasmas of deuterocarbons as well as deuterium. The plasma conditions are: a plasma inflow flux of 1.5×10^{18} ions cm^{-2} s^{-1}, an ion bombarding energy of about 110 eV, and deposition time about 40 min.

Generally, redeposited carbon films on molybdenum substrates are uniform and smooth, whereas those on graphite substrates are not so, presumably due to the porous surface morphology of graphite. The quantity of redeposited carbon is evaluated by weight gain measurements after redeposition. From the weight gain measurements, the thickness of redeposited carbon is estimated to be about 1 mm for molybdenum substrates. However, the corresponding weight gain for graphite substrates is reproducibly 20-30% less, which is indicative of the effect of sputter erosion of the substrate. This may not directly mean that the thickness of redeposited carbon is less. Details are still unclear.

The thermal desorption behavior of these plasma-redeposited carbon films has been investigated and the desorption spectra are shown in Fig. 1. The desorption of deuterium exhibits two peaks, similarly to earlier data [1], indicating trapping sites with two different binding energies. The desorption of deuterocarbons appears consistent with chemical sputtering data in that the maximum rises at around 500°C. From these thermal desorption spectra, the total quantity of co-deposited deuterium in terms of the D/C ratio for molybdenum substrates is evaluated to be about 0.4 and that for graphite substrates is about 0.3. These D/C numbers are in good agreement with reported values for hydrogen-saturated surface layers of graphite [2].

[1] K.Ashida et.al. J.Nucl.Mater. **128-129**(1984)792.
[2] K.L.Wilson and W.L.Hsu, J.Nucl.Mater. **145-147**(1987)121.

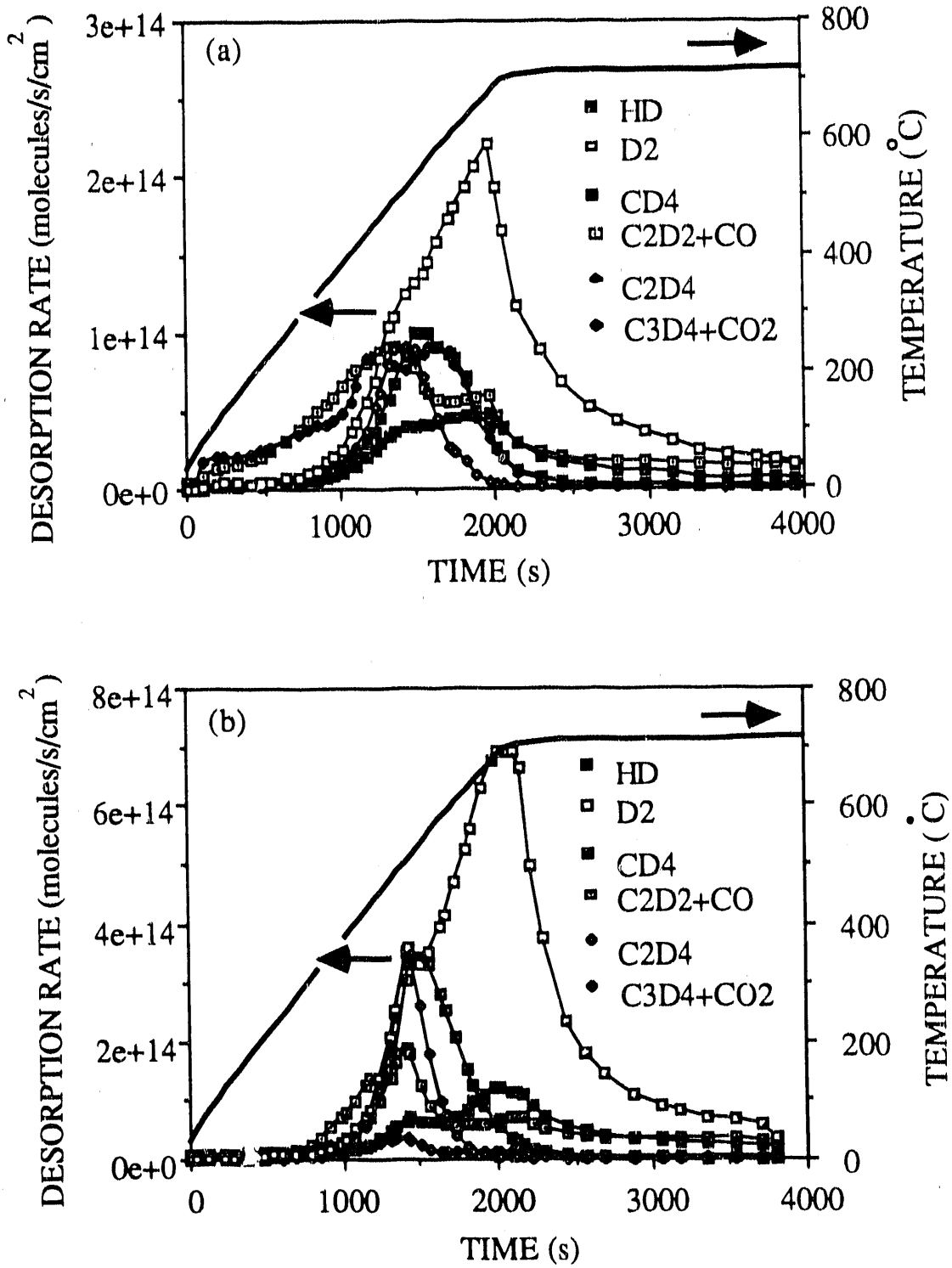

Fig.1 Thermal desorption from redeposited carbon on (a) POCO-graphite; and (b) molybdenum.

Materials Analysis of TEXTOR Limiter Tiles [1]

Plasma confinement and edge plasma characteristics are strongly influenced by the interaction of the plasma with the first material it contacts. In the TEXTOR tokamak, this is either the full toroidal belt pump limiter (ALT-II) or an inner bumper limiter (IBL). 26 graphite tiles (16 ALT-II tiles and 10 IBL tiles) have been removed from TEXTOR and subjected to materials analysis. The analysis has taken place collaboratively at several institutions located around the world. Macrophotography, scanning-electron microscopy and energy dispersive X-ray analysis were performed at the KFA-IRW. Deuterium profiling using nuclear reaction analysis and surface impurity distribution using the nuclear microbeam probe were performed at SNLA. The erosion and hydrogen recycling of the tiles, while subjected to hydrogen plasma bombardment, were measured spectroscopically in the PISCES-B facility at UCLA. In addition, in-situ analysis of the IBL tiles were performed by SNLL using beta backscattering.

The analysis results indicate low metallic impurity concentration (consistent with Inconel) on the surfaces of both types of tiles. This level of metallic contamination does not vary systematically around the device. Regions of increased metallic concentration coincides with regions of increased plasma flux to the surface. The ALT-II tiles exhibit a fairly uniform eroded surface, whereas the IBL shows both eroded and redeposited regions. These regions agree with power deposition measurements to the tiles using IR cameras in TEXTOR. The red posited regions of the IBL tiles exhibit increased erosion and recycling when exposed to a controlled plasma environment in PISCES-B, while the ALT-II tiles behave similar to a clean graphite surface as is shown in the accompanying figure.

---

[1] R.Doerner et.al., paper presented at 9th PSI-conference at Bournemouth, May, 1990.

a)

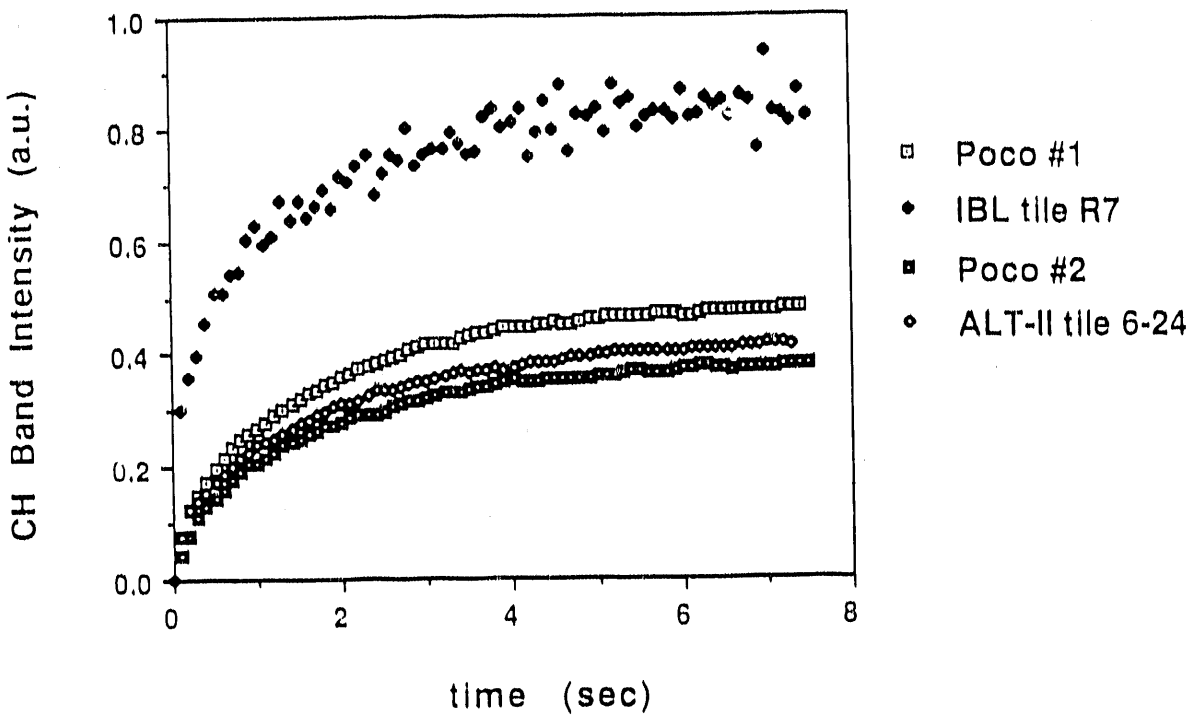

b)

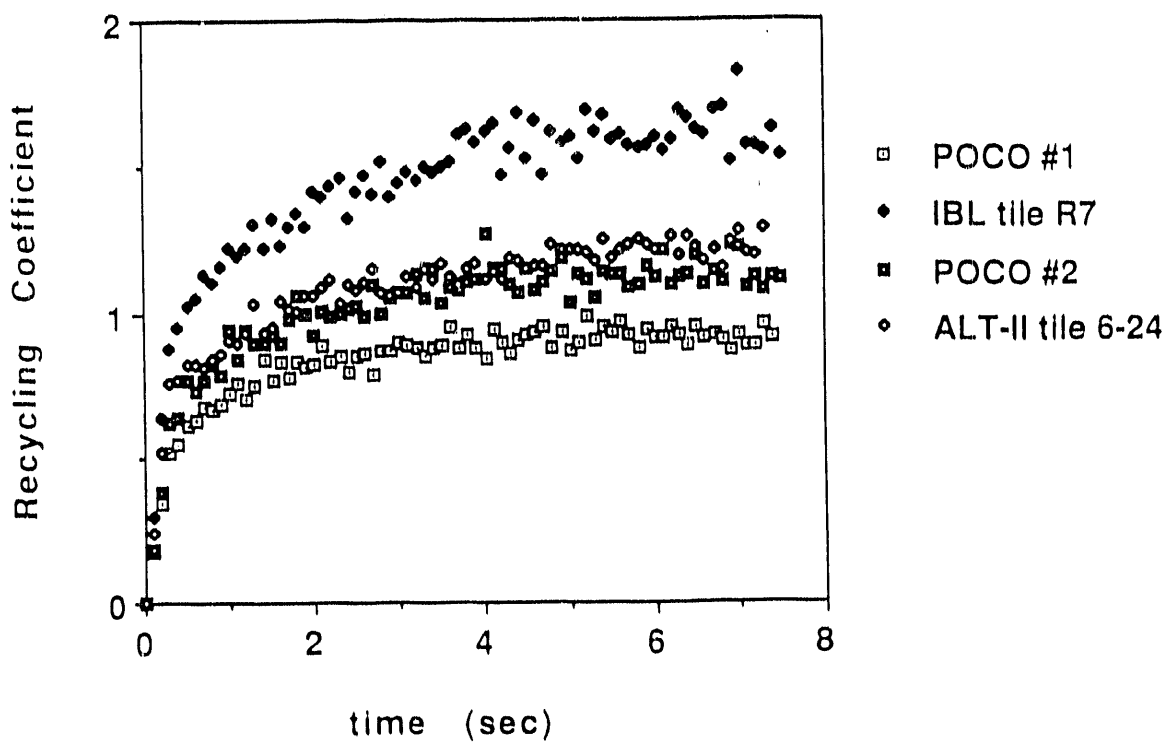

Measurements of a) the chemical erosion and b) the hydrogen recycling (normalized to unity for POCO graphite) from limiter tiles exposed to identical plasma conditions, in this case 200 eV hydrogen ions and a surface temperature of 200° C.

Chemical Sputtering of Graphite due to Oxygen Plasma Bombardment

Oxygen has recently been found to be a deep-penetrating impurity affecting the core plasma confinement in tokamaks. This is particularly true if graphite is used for plasma-facing components. However, the behavior of interaction of oxygen plasmas with graphite has not been well investigated to date. Virtually no data have been published under tokamak-boundary-like conditions.

Using the PISCES-C facility, the interaction of oxygen plasmas with graphite under high flux and low energy conditions has been studied. The oxygen plasma with a flux of 10^{17} $O_2^+cm^{-2}$ s^{-1} is inductively generated by a 13.56 MHz rf plasma source. Since the discharge is made at a high neutral pressure (1 mTorr) and a low power (600 Watt), most of ions are presumably oxygen molecules. (The OII line has been found to disappear at high neutral pressures.) A graphite sample is placed in the plasma using the high-temperature holder. The optical emission spectroscopy is used to observe the carbon-monoxide resulting from the chemical sputtering of graphite. Due to the strong interference of oxygen band systems, not too many bands have been identified successfully. Fig. 1 shows the Angstrom system of CO band at 5198 Å which is found most useful. An optical multichannel analyzer (OMA) is used to monitor radiation intensity.

POCO graphite is irradiated with an oxygen plasma. The sample floats with the potential of 20 eV with respect to the plasma. The temperature dependence of CO band intensity is shown in Fig. 2. O_2^+ band system at 5200 Å is simultaneously observed and the CO band intensity is calibrated with respect to this. The CO band intensity is strongly localized within a couple of cm from the sample. Thus, the contribution of residual carbon-monoxides is negligible. Since carbon-monoxide is the dominant product of chemical sputtering, Fig. 2. can serve as the temperature dependence of the chemical sputtering of graphite. Interestingly, the chemical sputtering yield minimizes at temperatures around 300 ^oC. Obviously, this finding contradicts earlier data from ion beam experiments in which no temperature dependence was observed [1]. This is presumably due to the fact that oxygen generated in PISCES-C is mostly in the molecular form whereas the ion beam experiments are using atomic oxygen ions. However, details of the surface reaction chemistry are still unknown. The minimum of chemical sputtering yield is currently considered to be caused by the concomitant reaction of oxygen to CO_2. CI line intensity shows similar behavior. This is because physically sputtered carbons can escape from the plasma without radiation.

[1] E. Hechtl and J. Bonhdansky, J.Nucl.Mater.154 (1988) 201

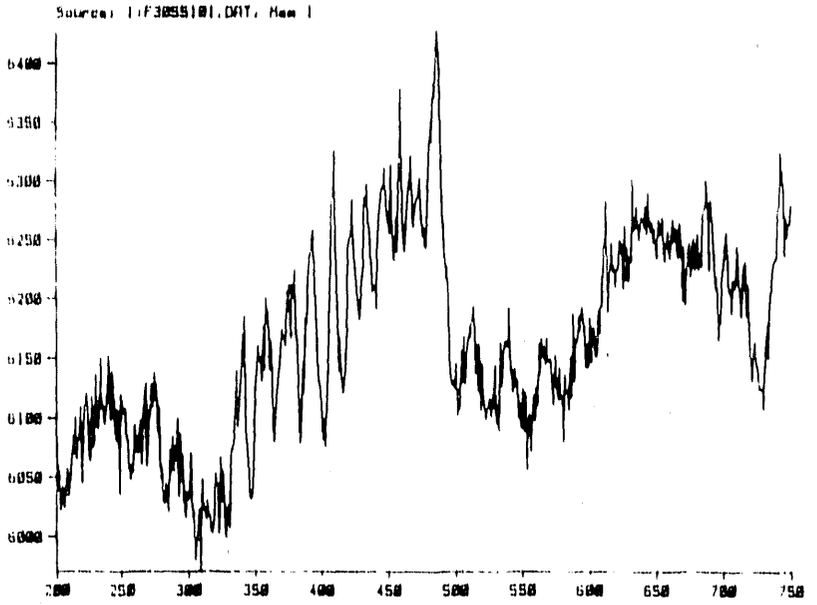

Fig. 1. The Angstrom system of CO band at 5198 Å

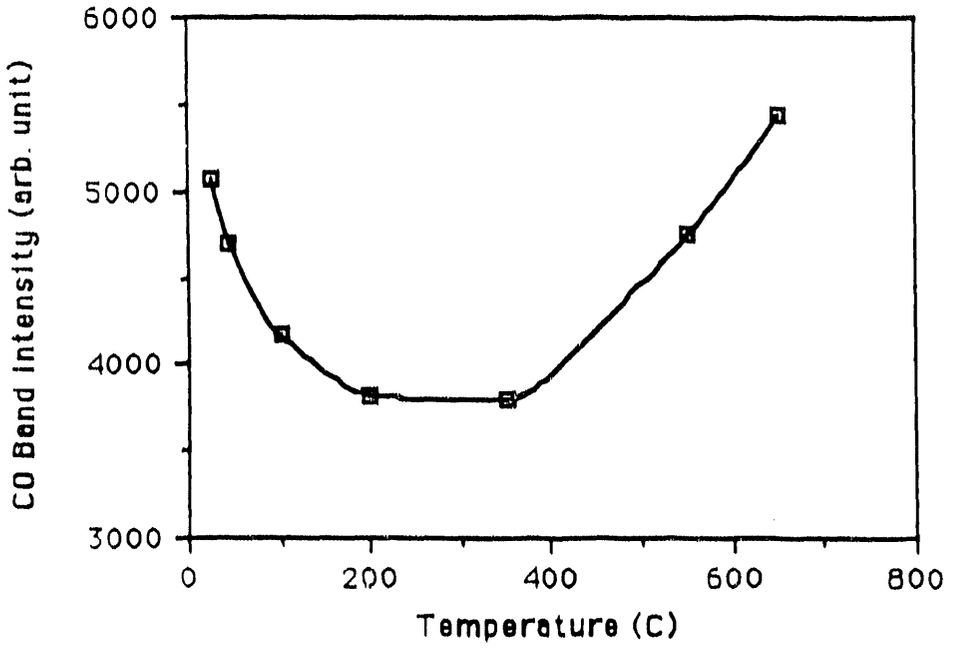

Fig. 2. The temperature dependence of the chemical sputtering of graphite with oxygen.

PISCES-Exps.

- Edge Plasma Physics -

Experimental Simulation of the Gaseous Divertor Concept in PISCES-A

Management of the divertor heat-load deposition is a critical issue for the design of next generation fusion devices such as ITER and CIT. The heat load to the outer divertor region is estimated to reach values of up to 50 MW/cm^2 in ITER during the technology phase. The severe erosion and impurity control problems at these power levels have stimulated research on alternative divertor concepts. The idea of the reentrant divertor is to redistribute the divertor heat flux over a large surface area by radiation and/or elastic and inelastic collisions with neutral particles. An annular slot with a transverse dimension close to the width of the scrape-off layer has been proposed to confine the required neutral gas. The poloidal depth of the slot can be quite small since the magnetic field is primarily in the toroidal direction. Simulation experiments are performed in the PISCES-A linear plasma device to test the basic concept and to evaluate the axial and radial particle and heat transport. To date, data have been obtained in steady state hydrogen and argon plasmas at densities of up to $2x10^{13}$ cm^{-3} and electron temperatures of 5-30 eV. In contrast to previous experiments the neutral gas is confined in a cylindrical neutralizer tube and multiple collisions between neutrals and plasma ions are likely to increase the neutral energy and penetration depth. Simultaneously, high neutral pressure can be maintained inside the tube while the leakage of neutrals towards the plasma source is greatly reduced.With moderate gas feed (7 mtorr averaged pressure) to a simulated divertor slot (length 90 cm, diameter 4.5 cm) we have observed the electron temperature to decrease axially from 25 eV to 3 eV. At higher neutral pressure (>13 mtorr) a "neutralizer" regime is found, where the plasma density at the simulated divertor target can be reduced by more than two orders of magnitude. Radial plasma loss is proportional to the neutral pressure and greatly enhanced as compared to the Bohm rate and the classical diffusion rate, which is very beneficial for the reduction of the parallel particle and heat flux.

The basic set-up of the gaseous divertor simulation experiment in PISCES is shown in Fig. 1. Downstream at a distance of about 1 m from the source, the flowing plasma is accepted in a water-cooled circular neutralizer tube. The axial magnetic field can be varied from 0.4 - 1.7 kG. The simulated divertor target is located at the downstream side of the tube (z=0). The tube is made of anodized aluminum and is electrically floating. Neutral gas (H_2, D_2, He, Ar) can be fed from the end of the divertor tube. The neutral pressure in the plasma source can be kept well below 1 mtorr even at high secondary gas feed rates. An axially moveable Langmuir probe provides measurements of the electron temperature, plasma density and floating potential profiles along the length of the divertor tube. The chamber neutral pressure is measured with an ionization gauge, and the neutral pressure at two axial positions inside the tube (at distances z =1.5 cm and z = 41 cm from the divertor target) is recorded with ionization

and baratron gauges. A CID camera as well as a 1.3 m Czerny Turner spectrometer with a photomultiplier tube is used to analyze plasma and neutral line radiation. A fast scanning, pneumatic Langmuir probe is used to obtain radial profiles of the plasma density and the space potential at select axial positions. A multitip radial probe is used to obtain the density and potential fluctuations $\tilde{N}$ and $\tilde{\phi}$ as a function of plasma radius. The radial particle flux driven by fluctuating electric fields is evaluated from the probe signals.

Fig. 2 shows the normalized ionization mean free path (ionization mean free path divided by the plasma radius) for H and Ar neutrals for a typical electron temperature of 15 eV. The shaded areas indicate the parameter ranges covered in the PISCES-A experiments. In the recent argon experiments reported here, the plasma density is $N_e > 10^{13}$ cm^{-3} and the plasma is opaque to cold Ar neutrals, but partially transparent to energetic (>1 eV) neutrals.

Typical axial profiles of the electron temperature, the plasma density and the neutral pressure P_n in the "neutralizer" regime are presented in Fig. 3 for a high density argon plasma. The magnetic field is 1.7 kG. Here, the average Ar neutral pressure is about 14 mtorr, maintained by a secondary gas feed at the end of the neutralizer tube (z=0). For reference, the neutral pressure measured with the plasma shut off, P_{n0}, is also shown. The pressure difference (about 40%) is due to plasma pumping effects. The electron temperature is observed to decay from kT_e=15 eV close to the tube entrance (z=90 cm) to kT_e =3 eV at the divertor target. The electron energy loss is primarily caused by inelastic collisions (ionization and excitation) with Ar neutrals. Ionization is less important for z < 35 cm and the density decreases rapidly towards the target as a result of strong anomalous radial transport.

At low neutral pressure, the density at the divertor target $N_{e\ target}$ is increased as compared to the density N_{es} at the tube entrance as a result of the additional particle source. Fig. 4 shows the density ratio as a function of neutral pressure. The "neutralizer" regime is reached for $P_n > 5$ mtorr. In this regime the target density can be decreased by more than two orders of magnitude. Fig. 5 shows the parallel plasma heat flux transmitted to the divertor target as a function of the neutral pressure (averaged over the length of the tube). The heat flux through the sheath is given by $Q = N_e c_s \gamma kT_e$, where N_e is the plasma density, c_s is the ion acoustic speed, and γ =7 is the sheath heat transmission factor. Shown is the normalized heat flux Q_{target}/ Q_s, where Q_{target} is the heat flux transmitted to the divertor target and Q_s is the equivalent heat flux at the tube entrance. A dramatic reduction is observed if the average neutral pressure exceeds 5 mtorr. The largest reduction factor observed so far in the experiment is $2x10^3$. Future work will attempt to identify the underlying mechanism for the strong anomalous radial particle transport. We will also directly determine the axial and radial heat flux, including the contribution from energetic neutrals, with a calorimetric technique.

PISCES Gaseous Divertor Experiment

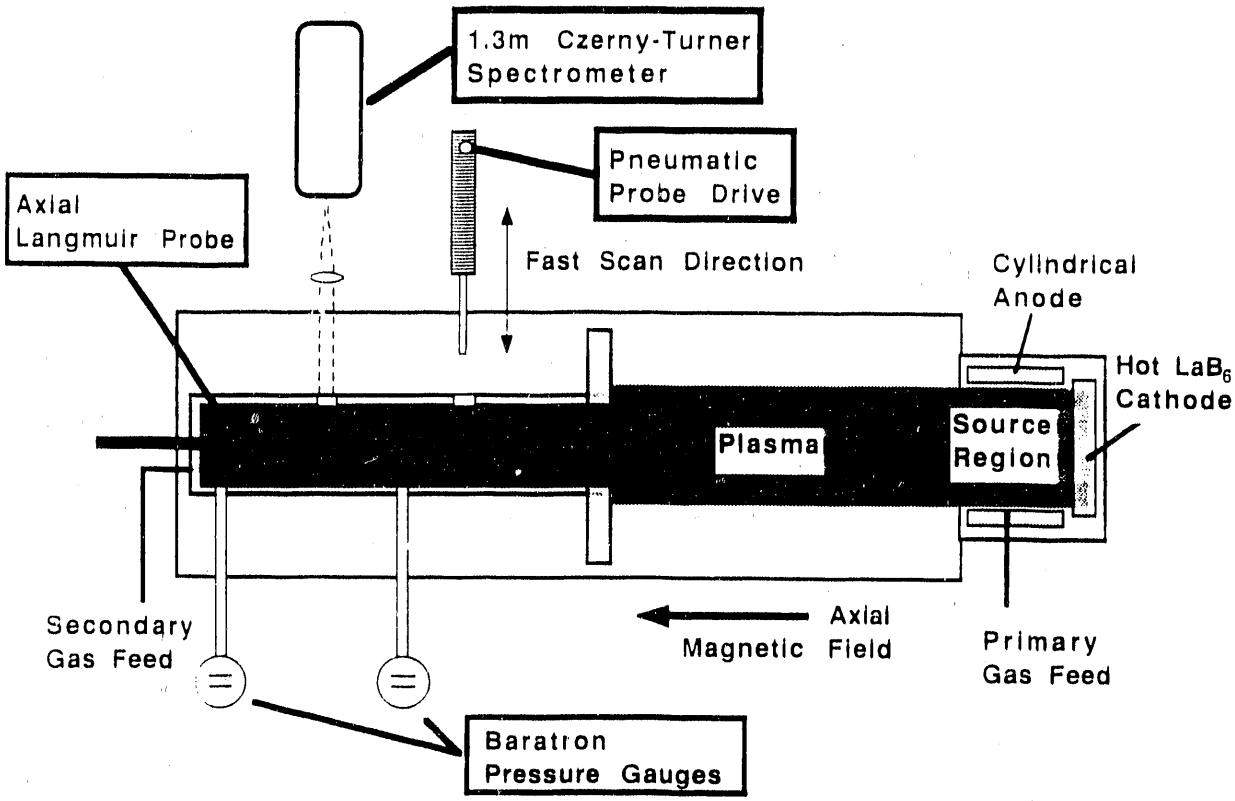

Fig. 1. Schematic of the gaseous divertor simulation set-up in PISCES-A, showing the plasma source, the neutralizer tube and various diagnostics.

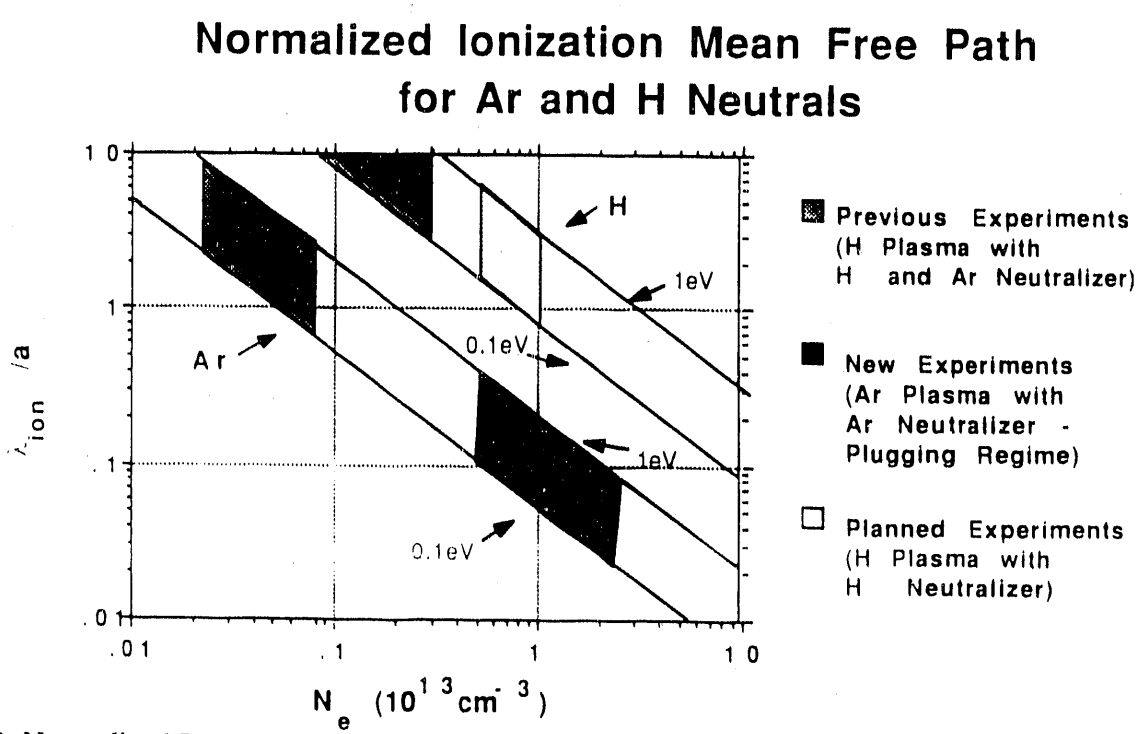

Fig. 2. Normalized Ionization mean free path (ionization mean free path λ_{ion} divided by the plasma radius a) for atomic hydrogen and argon neutrals with $kT_n = 0.1$-1 eV vs. plasma density N_e. The electron energy is 15 eV. The regimes accessed in different PISCES experiments are indicated.

Axial Profiles - Neutralizer Regime (Ar)

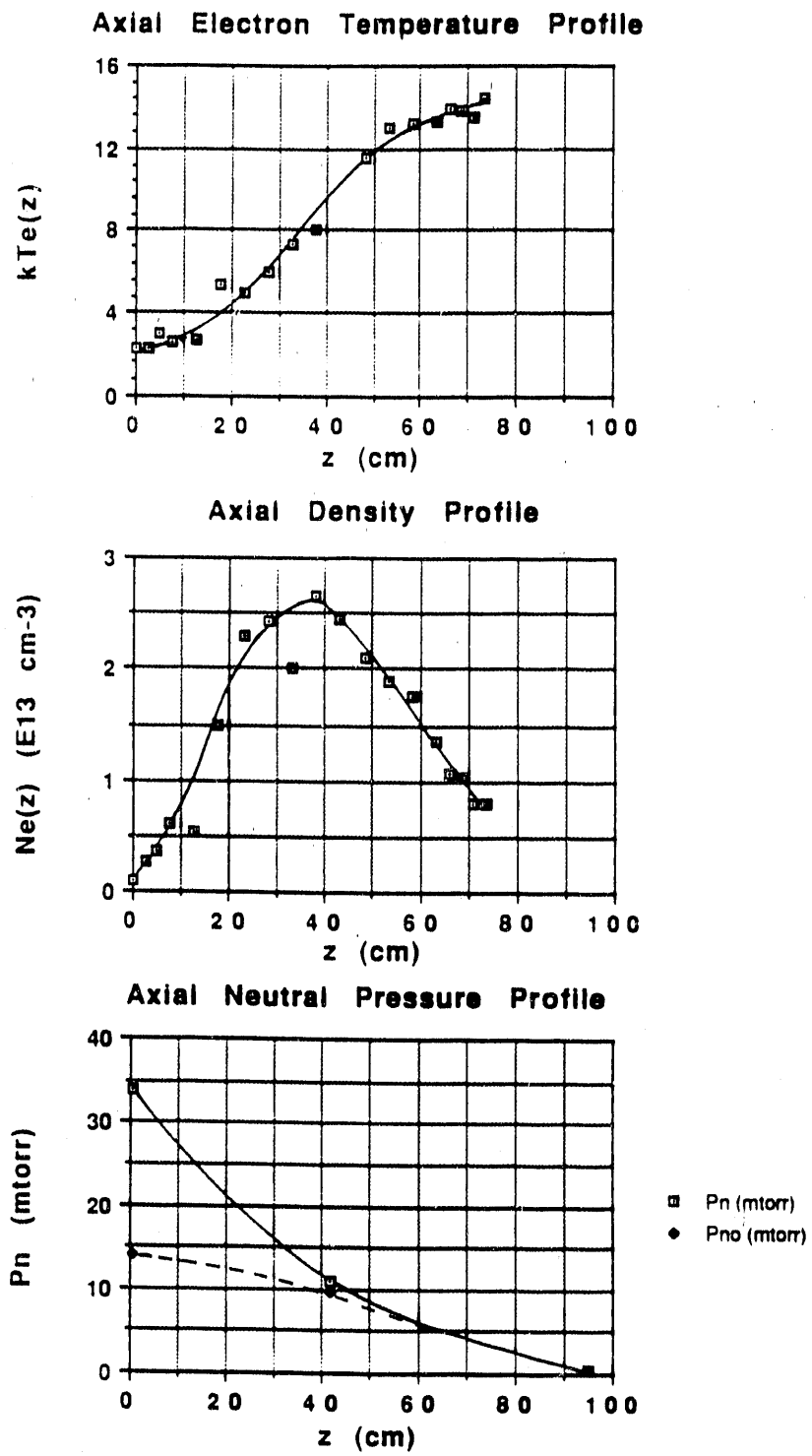

Fig. 3. Axial profiles of electron temperature, plasma density, and neutral pressure in the "neutralizer" regime (Ar plasma; B=1.7 kG). The simulated divertor target in located at z=0; the tube entrance is at z = 90 cm.

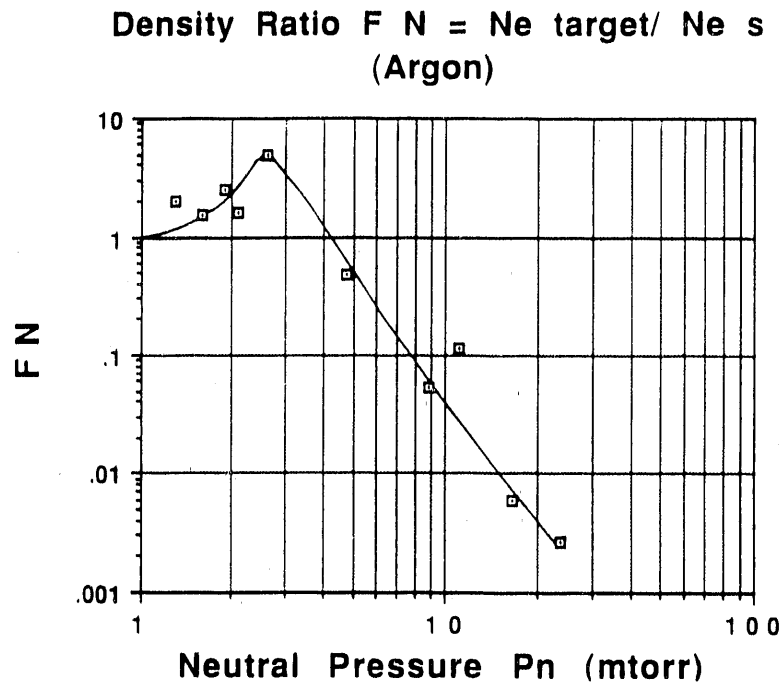

Fig. 4. Density ratio $F_N = N_{e\ target}/N_{es}$ as a function of the averaged neutral pressure in the neutralizer tube (Ar plasma; B=1.7 kG, kT_{es} = 15 eV).

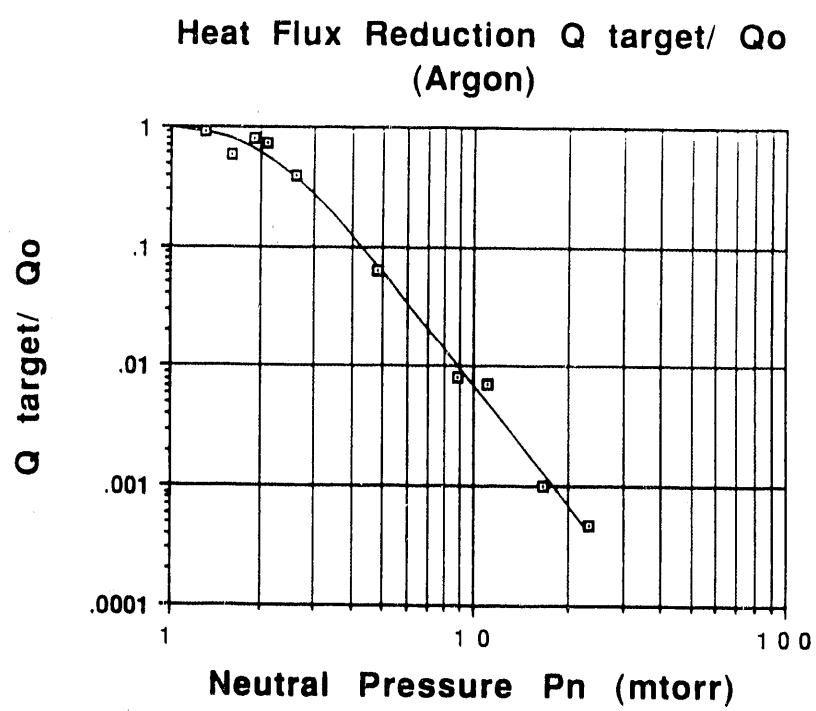

Fig. 5. Heat flux reduction Q_{target}/Q_s as a function of the averaged neutral pressure in the tube (Ar plasma; B=1.7 kG, kT_{es} = 15 eV).

Novel Technique for Edge Plasma Control By RF Ponderomotive Forces

We have developed a new method to reduce the plasma heat flow to a limiter head or divertor plate using RF ponderomotive potential barriers which are set up by driving an RF current in an antenna embedded in a limiter or in a free standing antenna at the plasma edge*. In contrast to the DC biasing method, both ions and electrons are reflected away from the RF source†. The electrons are reflected directly by the ponderomotive potential, and the ions by the resulting positive ambipolar potential, reducing net flow to the RF source. Drifts arising from the ponderomotive force cross product with the magnetic field can also be formed to modify drift surfaces and divert plasma around the antenna, Fig. [1a,b], as shown by numerical solution, Fig. [1c], of the dynamical equations of motion for an electron in the measured RF field distribution. Experimental proof, Fig. [2] of the RF limiter concept was carried out using the PISCES-A facility with plasma parameters comparable to the edge plasma of typical tokamaks. In addition, a remarkable suppression of low frequency fluctuations was observed, Fig. [3a,b], at the plasma periphery during application of the RF ponderomotive force, even at powers as low as 100W, which can be expected to reduce plasma transport at the boundary layer. Production of the RF potential ($\approx$ 20 eV) was confirmed by the reflection of an electron beam injected in vacuum with an RF power below 1KW, Fig. [3c,d]. Experimental tests of these concepts in toroidal geometry is planned for TEXTOR, Compact Helical System (Nagoya), and JFT=2M.

The concept of plasma boundary control by RF ponderomotive forces is made quantitative by use of the expression for the ponderomotive potential, Ψ_{rf} given by

$$\Psi_{rf} = \frac{1}{4m}\frac{e^2 E_\perp^2}{\omega^2 - \omega_c^2} + \frac{1}{4m}\frac{e^2 E_\parallel^2}{\omega^2}$$

where ω_c, $E_\perp$, and $E_\parallel$ are the angular cyclotron frequency, perpendicular RF electric field and parallel RF electric field respectively. For electrons, this potential is made to be of the order of the temperature of the plasma near the limiter head in the frequency range, $\omega_{ci} < \omega << \omega_{ce}$. In this frequency range the first term in the expression for the ponderomotive potential, which is used for plugging the leakage of the plasma flow in the open magnetic system, is negligible relative to the second term, which does not have the resonant denominator. This is preferable, because the ion heating and wave excitation which occur for frequencies near ω_{ci} are not desirable for the purpose of boundary control. The second term is larger for electrons because of the $\frac{1}{m}$ dependence. To produce this $E_\parallel$ field an RF current is drawn on the limiter parallel to the magnetic field. Near the limiter head, the ponderomotive potential repels most of the electrons from the head, so that as a result, a positive ambipolar potential is formed to reflect ions from the limiter and the plasma particle flow is reduced.

---

* T. Shoji, A.Grossman, et al., to be published, J. Nucl. Mater. (1990).

† A. Grossman, L. Schmitz, et al., PSI Satellite Workshop, Cadarache, France 1990.

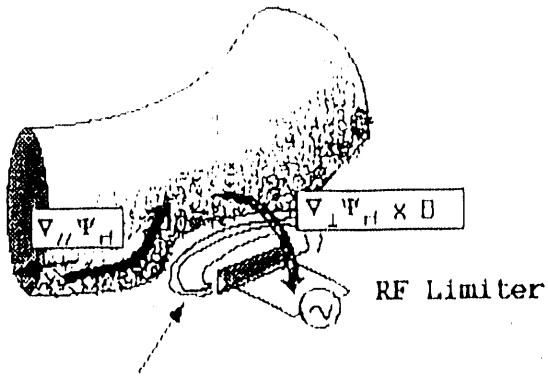

(a)

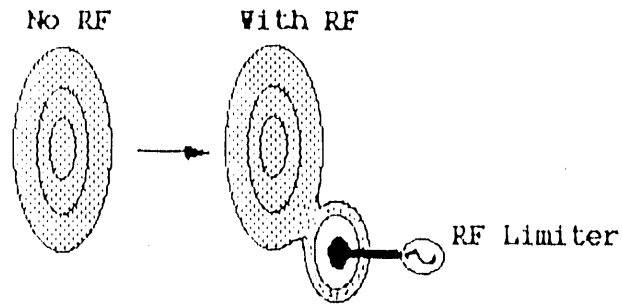

Drift Orbit Modification
(RF ponderomotive divertor)

(b)

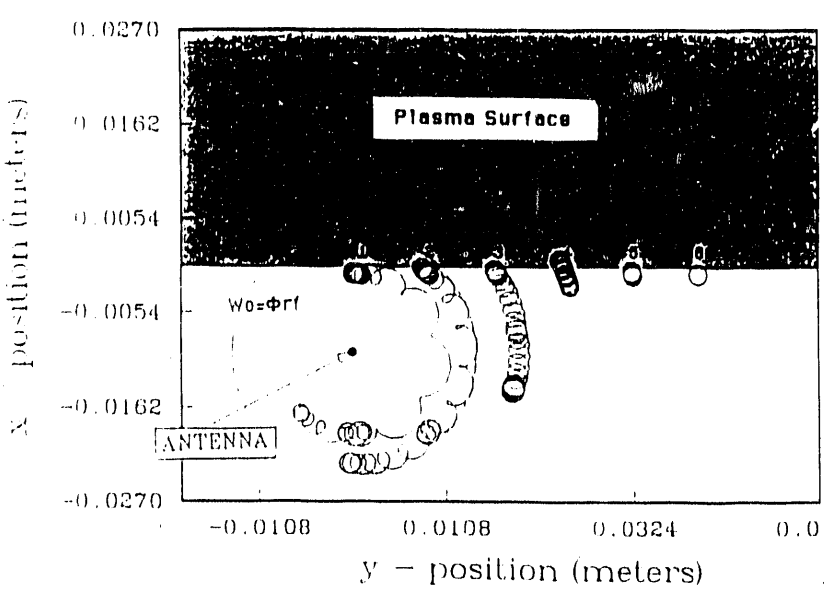

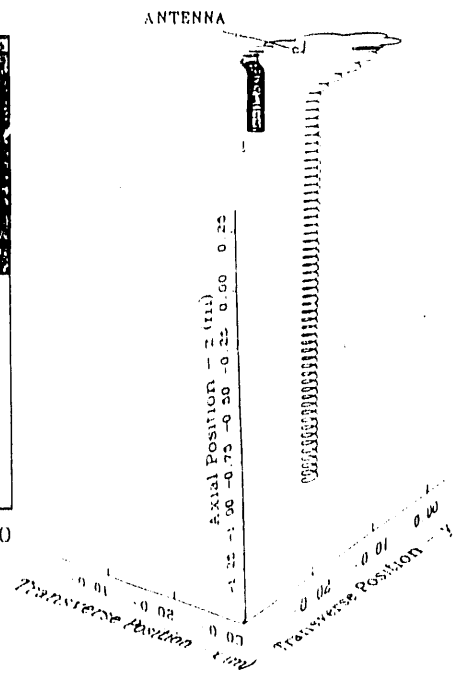

(c)

Fig. 1a RF Ponderomotive Limiter.

1b. Modification of Drift Surfaces by RF Ponderomotive Force.

1c. Numerical solution for electron trajectory in the measured RF field distribution.

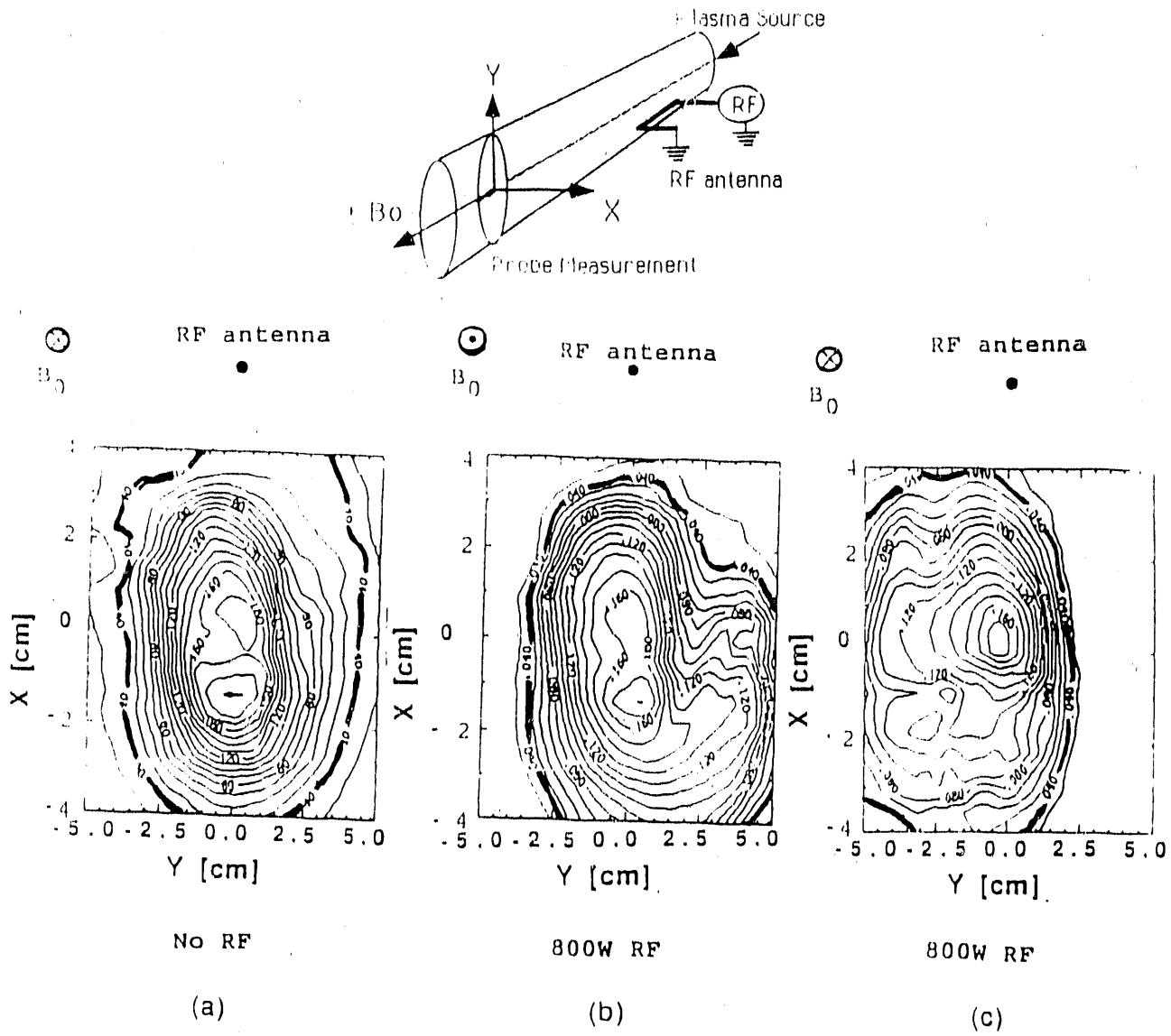

Fig. 2. Two dimensional ion flux profiles measured 40cm downstream from the antenna.
(a) No RF, (b), (c) Prf=800W, B= +/- 500G. Thick lines show the same intensity of the ion flux.

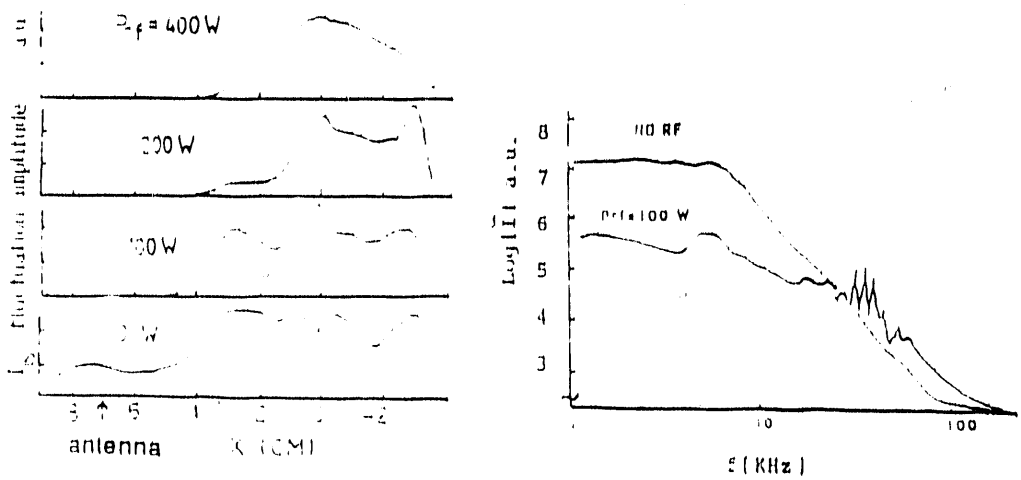

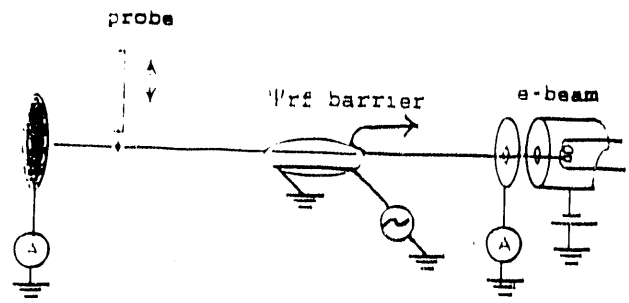

(c)

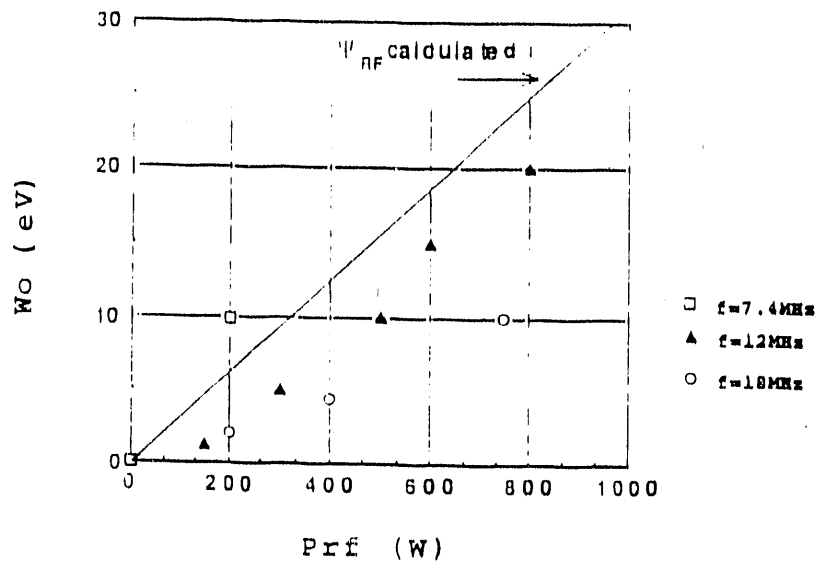

(d)

Fig. 3a. Radial profile of electrostatic fluctuation intensity integrated in the frequency range 1-100KHz. The RF antenna is placed 80cm upstream (x=7cm) from the probe.

3b. Change in the power spectrum of fluctuation at X=6cm.

3c. Schematic of electron beam experiment for ponderomotive potential measurement.

3d. Ponderomotive potential height as a function of the RF power.

H-Mode Transition Physics

Research on the L to H mode transition in tokamaks has centered on the radial electric field as being the controlling factor in the transition. The strength of the electric field, or the shear in the field, can dramatically influence the nature of the electrostatic turbulence in the edge plasma. Furthermore, it has been conjectured that the turbulent nature of the plasma controls the cross field heat and particle fluxes. Thus, the radial electric field can have a significant bearing on the rate of anomalous cross field diffusion.

While PISCES is not a tokamak experiment, it does provide a unique environment for studying the effects of radial electric fields on tokamak like edge plasmas. Steady state discharges are studied with probes, including a pneumatic fast scanning probe for recording profile information, and spectroscopic means. Because of the operation of the reflex arc source, an inwardly pointing radial electric field is present even without applying any bias to the plasma periphery. Using an annular electrode mounted on a limiting aperture plate (figure 1), the existing electric field can be modified and the peak electric field strength has been observed in excess of 100 V/cm. The radial electric field is increased by drawing a large electron current to an annular electrode, and when this occurs, the central density of the discharge increases (figure 2) and the density scrape-off lengths decrease significantly. When the bias is applied in the opposite direction, only the ion saturation current can be drawn through the inner electrode and the density scrape-off lengths and the radial electric field strengths are changed less than 20%. Additionally, when no bias is applied, a single shear layer can be inferred from the measured potential profile in plasma (figure 3). When the annular electrode draws an electron current, two closely spaced shear layers form. The changes in the density profiles could not be simply explained by an ion mobility term in the particle flux equation. Rather, we have observed that the fluctuation induced particle transport is decreased by 30 to 90% when a bias is applied to the electrode and a double shear layer forms.

In order to measure the fluctuation induced transport, as well as other turbulent properties of the plasma, a probe diagnostic similar to ones used on CCT and TEXT has been used in PISCES. The probe has an array of four tips and can measure both floating potential and density fluctuations simultaneously. The fluctuation induced particle transport can be inferred from the density and potential fluctuation levels through the formula

$$\Gamma = -\left(\frac{2}{B}\right)\mathrm{Re}\left[\int_0^\infty ik(\omega)P_{n\phi}(\omega)d\omega\right]$$

where $k(\omega)$ is the dispersion function of turbulence and the $P_{n\phi}(\omega)$ is the cross power spectrum between the density and potential fluctuations. When the radial electric field is increased, the levels of both the density and potential fluctuations decrease and fluctuation induced particle transport is reduced up to 90% at the radius which coincides with both the strongest density gradient and the inner electrode position (figure 4). In addition, in the double shear layer case, both the radial and poloidal correlation lengths decrease by a factor of two.

Future work will include a detailed study of the differences in the turbulence between the single and double shear layer cases. A two dimensional mapping of the turbulence will be conducted using both probes and spectroscopic techniques in both shearing cases. Scalings of the particle transport rates, correlation lengths, and other properties of the fluctuations with neutral pressure, magnetic field, and electric field strength and shear. Data from PISCES also provides a database of information to compare to an ongoing modelling effort at UCLA.

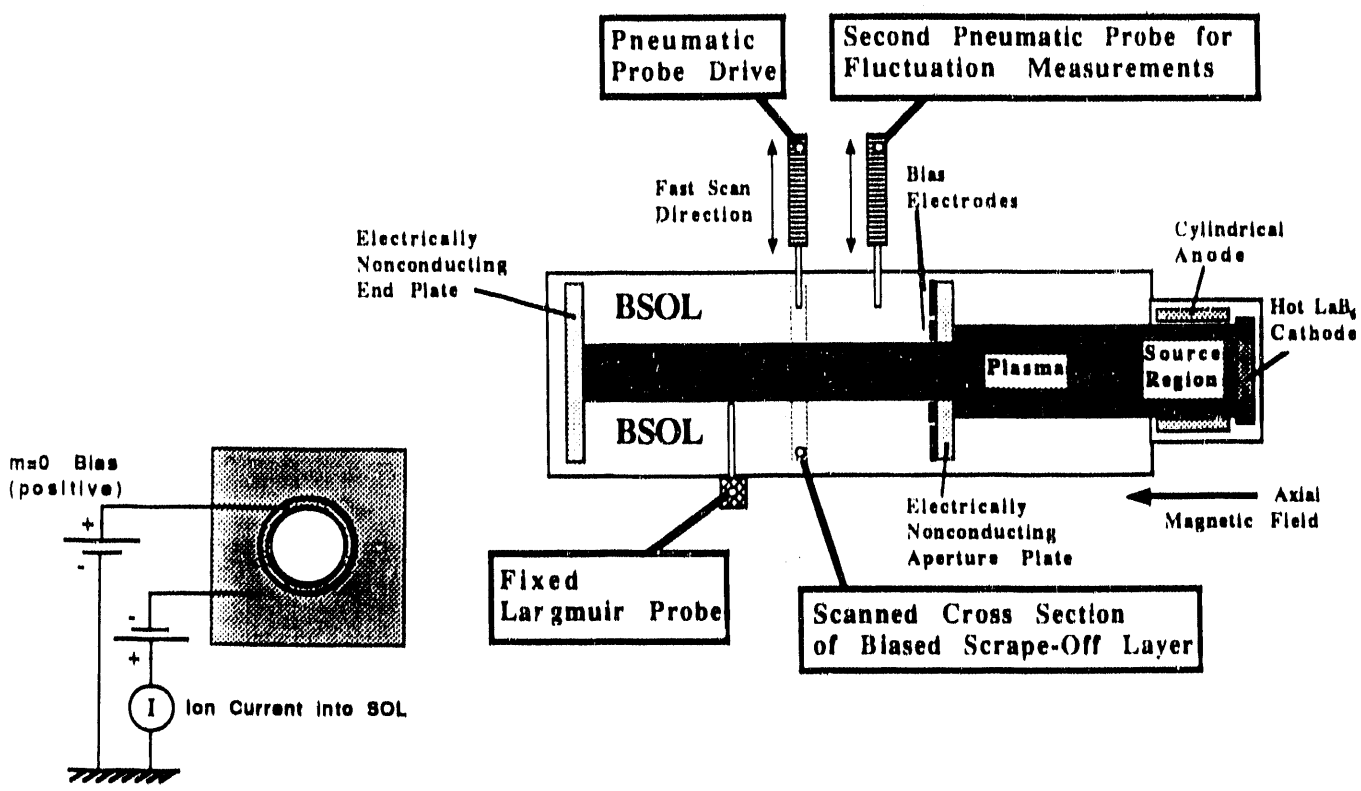

Figure 1 - Schematic diagram of the experimental setup for the bias experiments in PISCES-A.

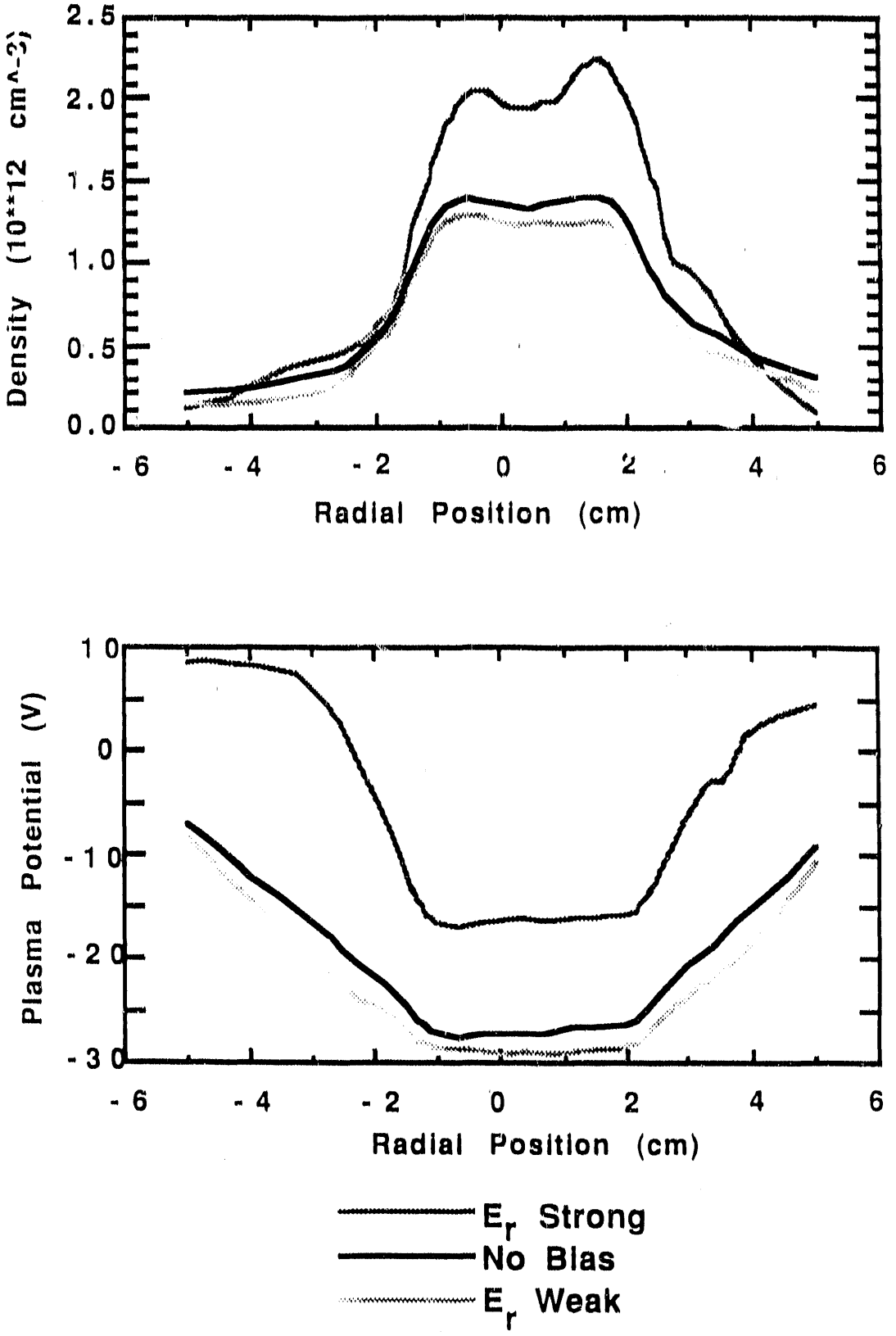

Figure 2 - Representative density and potential profiles in PISCES-A for strong and weak radial electric field.

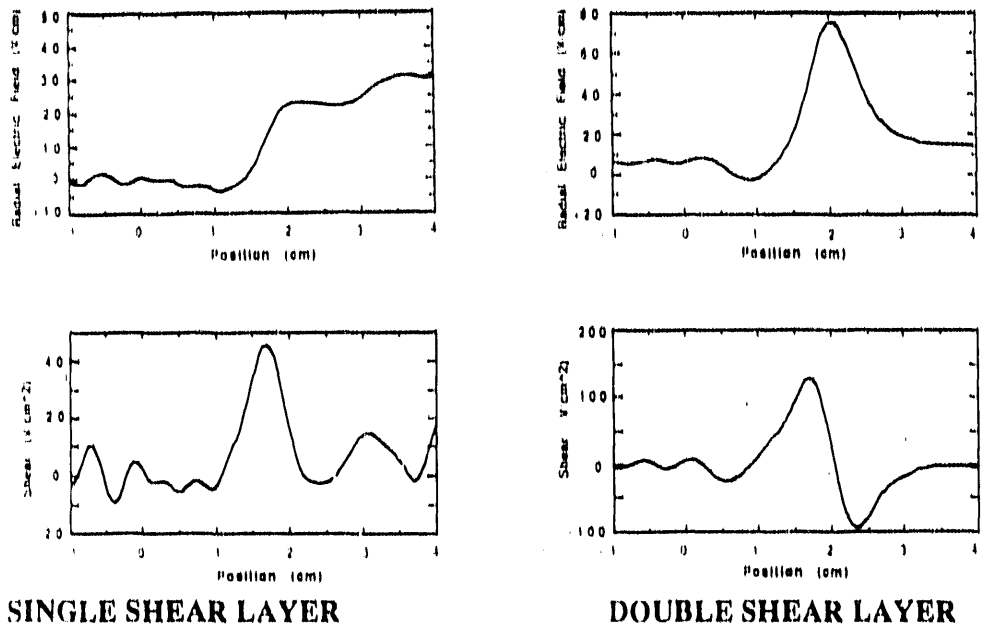

Figure 3 - Radial electric field and shear for single and double shear layer cases.

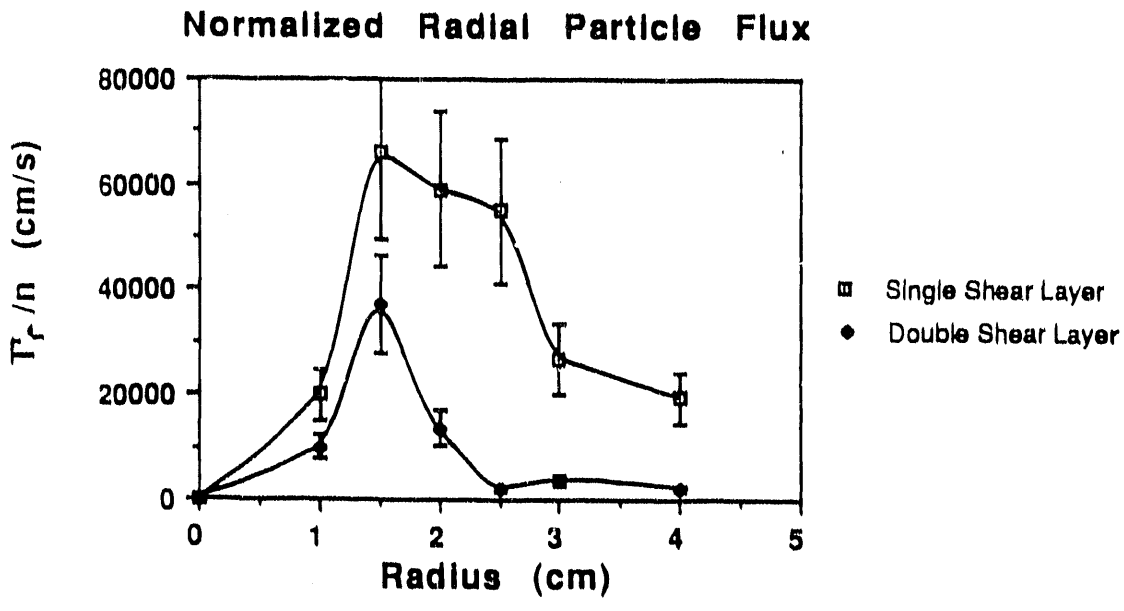

Figure 4 - Fluctuation induced radial particle flux in PISCES-A, normalized to the local plasma density for the single and double shear layer cases.

Edge-Plasma Physics Experiments in the CCT-tokamak

During the previous year, the PISCES-CCT edge physics collaboration has yielded a number of experimental observations related to tokamak transport physics. These results include: 1) detailed radial profiles of electrostatic fluctuation-induced particle transport across the confining magnetic field consistent with globally measured particle confinement times in both diverted and limiter discharges; 2) indications that edge turbulence and the associated transport are highly asymmetric in the poloidal direction, with transport peaking on the low-field, outside midplane region; 3) measurements of turbulence levels and statistics in the CCT induced H-mode suggesting a reduction in global transport.

A full poloidal array of Langmuir probes was installed on the CCT tokamak in 1989; each probe assembly has four small Langmuir probe tips arranged so that equilibrium quantities as well as fluctuating quantities can be measured. A view of the probe array and details of the tip geometry are shown in figure 1. The turbulence-induced particle transport $\Gamma_\perp$ is inferred from the second order correlation between density and electric field fluctuations, e.g. $\Gamma_\perp = \langle \tilde{n}_e \tilde{E}_\theta \rangle = \frac{2}{B} \int_0^\infty k\, |P_{n\phi}| \sin\alpha_{n\phi} df$, where <> denotes a time-averaged process and k is the poloidal wavenumber of potential fluctuations, $P_{n\phi}$ denotes the fluctuation level, and $\alpha_{n\phi}$ is the phase angle between density and potential fluctuations at a frequency f. To-date the probe array has been used to measure equilibrium and fluctuating quantities at a few poloidal positions; work in the upcoming report period will employ the full 2D capabilities of the probe array.

The rms density and potential fluctuation levels measured at the outside midplane and normalized by the local equilibrium value of the density and electron temperature respectively are shown in figure 2 as a function of minor radius. The density fluctuation level is typically 20-30% of the equilibrium value while the potential fluctuation levels are 50-60% of the electron temperature with a typical poloidal wavenumbers of 0.5-1.0 cm^{-1}. The phase angle between the density and potential fluctuations is 90 degrees in the scrape off layer and far edge region while at smaller minor radii, the phase angle is reduced to 20-30 degrees. The resulting cross-field particle flux due to the electrostatic fluctuations is shown in figure 3 and is sharply peaked at the last closed flux surface. In the scrape-off layer, the particle flux decreases rapidly due to rapid parallel flow into the limiter surface. Assuming that this particle flux is toroidally and poloidally symmetric, the global particle confinement time τ_p^{ES} expected if electrostatic turbulence was the dominant particle transport mechanism is 5 (+/- 2) msec. The particle confinement time measured by interrupting the neutral gas source momentarily during the Ohmic discharge, τ_p^*, was 8-10

msec. Fueling effects due to recycling are minimized by using a Titanium gettering surface on the vessel liner; hence the degree of similarity between τ_p^{ES} and τ_p^* suggests that electrostatic turbulence plays an important role in edge particle transport in tokamaks.

Similar measurements on the inside midplane, high-field side of the tokamak suggest that the electrostatic fluctuation-induced particle transport is significantly lower than at the outside midplane. Figure 4 shows the density fluctuation levels from the inside midplane compared with those from the outside midplane region. A limited amount of results for the particle flux $\Gamma_\perp = \langle \tilde{n}_e \tilde{E}_\theta \rangle$ suggests that the inside midplane cross-field particle transport is reduced by 5-10 times over that at the outside midplane. Work is presently underway to study this difference in detail and is expected to show that turbulent-driven particle transport occurs predominantly through the outside midplane region of the tokamak.driven particle transport occurs predominantly through the outside midplane region of the tokamak.

In the CCT tokamak, an H-Mode like transition is induced by injecting electrons on closed magnetic surfaces. A description of the technique and a summary of the changes in global parameters during the H-mode has been discussed in an earlier publication [1]. Probe measurements indicate that in the region r/a ≈ .95-1.0, the H-mode discharges develop strong radial electric fields and highly sheared near-sonic poloidal flows. The H-mode discharge is clearly seen to have a highly localized radial electric field. The radial variation of the electric field causes the plasma to develop a near-sonic poloidal flow $V_\theta \approx E_r/B$ at r/a ≈.97 with two strongly sheared flow regions of opposite signs centered at r/a ≈.95 and r/a ≈1.0. When the strong flow and shear is present, the density fluctuation levels are significantly reduced as seen in fig. 5, suggesting that edge turbulence-driven transport has been reduced. A narrowing of the poloidal wavenumber power spectra is also observed. These ongoing measurements in the CCT H-mode plasma are forming a basis for comparison with published theories of the H-mode transition [2,3].

Physics questions to be addressed in the upcoming research period include a continuation of detailed studies of poloidal asymmetries in edge turbulence and particle transport and continued characterization of edge turbulence and transport modifications at the transition to the CCT induced H-mode. New work aimed at searching for low-frequency convective cell-like structures and exploring the role of electrostatic turbulence in core transport and edge heat transport will be initiated towards the end of the next reporting period.

[1] R.J. Taylor et al., Physical Review Letters 63,2365 (1989)
[2] K.C. Shaing, E.C. Crume, Physical Review Letters 63,2365(1989)
[3] H. Biglari et al., Physics of Fluids B 2,1(1990)

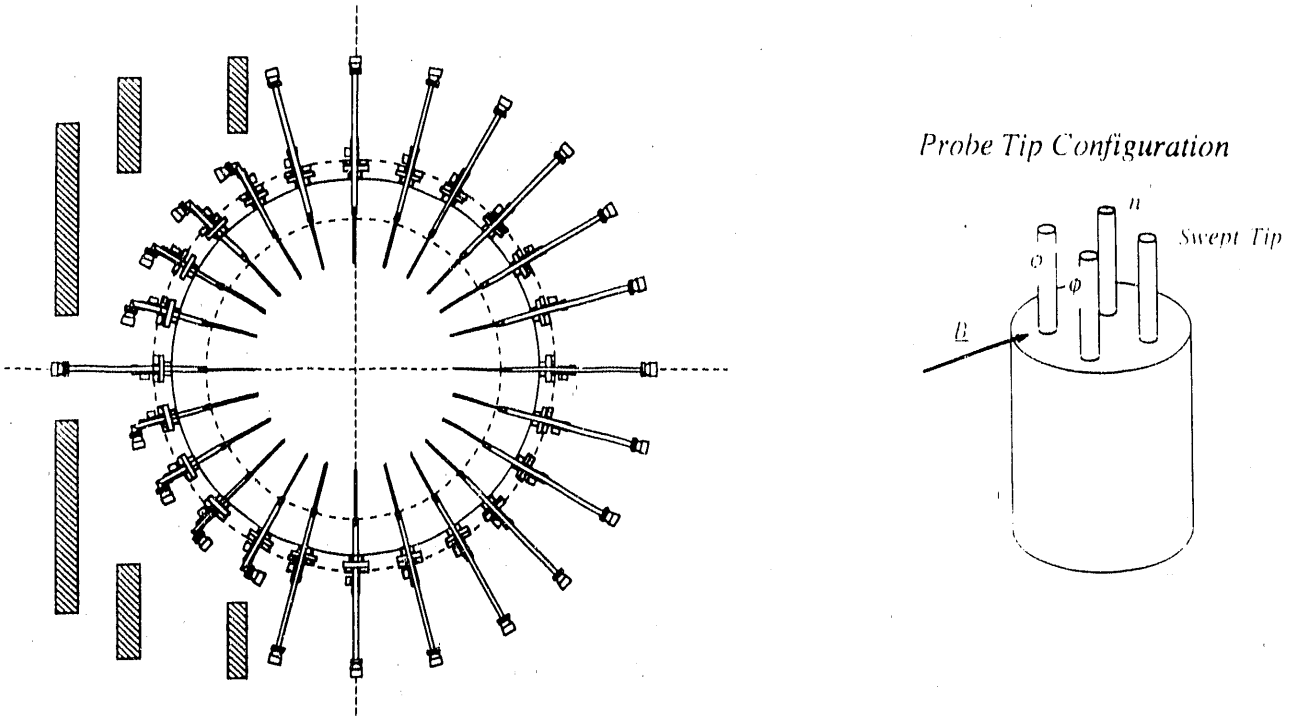

Figure 1: CCT Poloidal Probe Array and Probe Tip Details

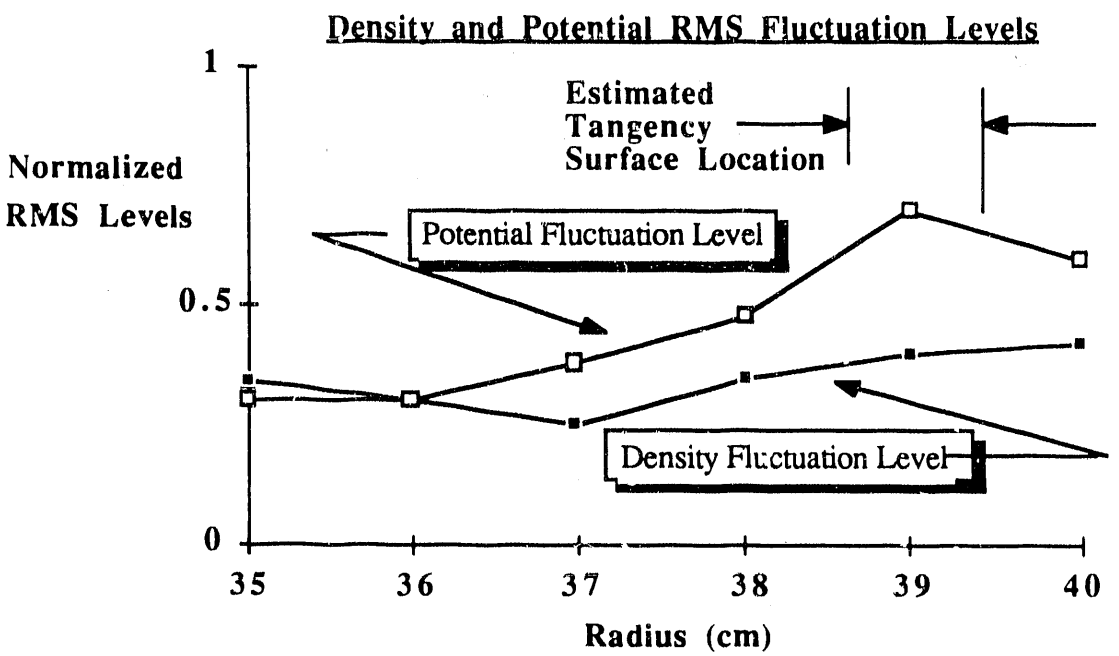

Figure 2: Normalized density and potential fluctuation levels v. minor radius. Data from outside midplane limiter Ohmic discharge. 38 kA, 1.4 x 10^{12} cm^{-3} R=148 cm, a=36 cm.

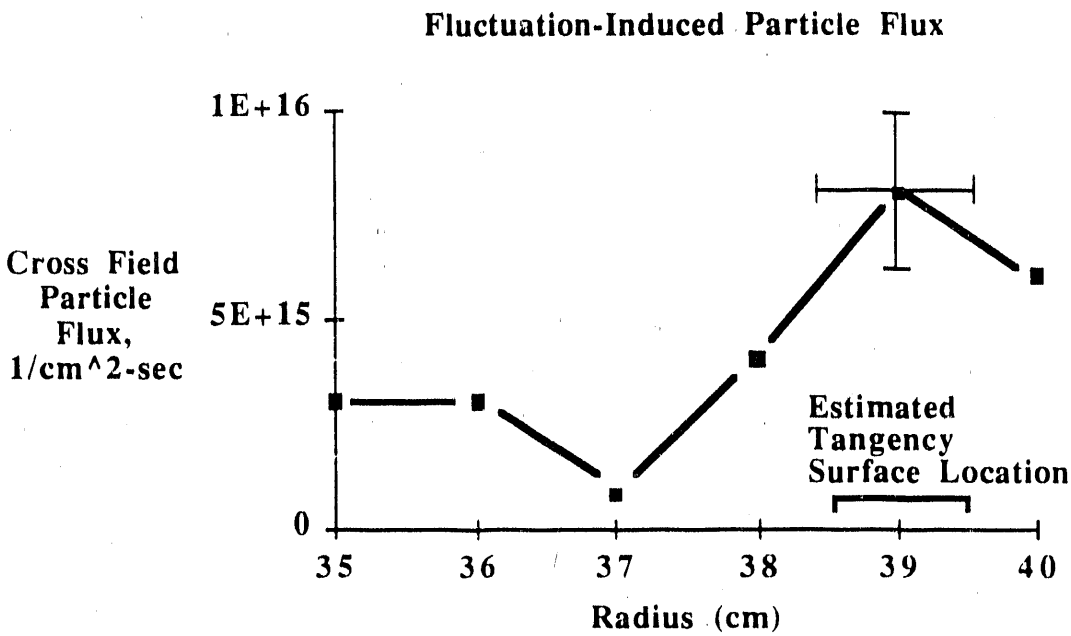

Figure 3: Cross field ion particle flux due to electrostatic turbulence v. minor radius. Data from outside midplane limiter Ohmic discharge. 38 kA, 1.4 x 10^{12} cm^{-3} R=148 cm, a=36 cm.

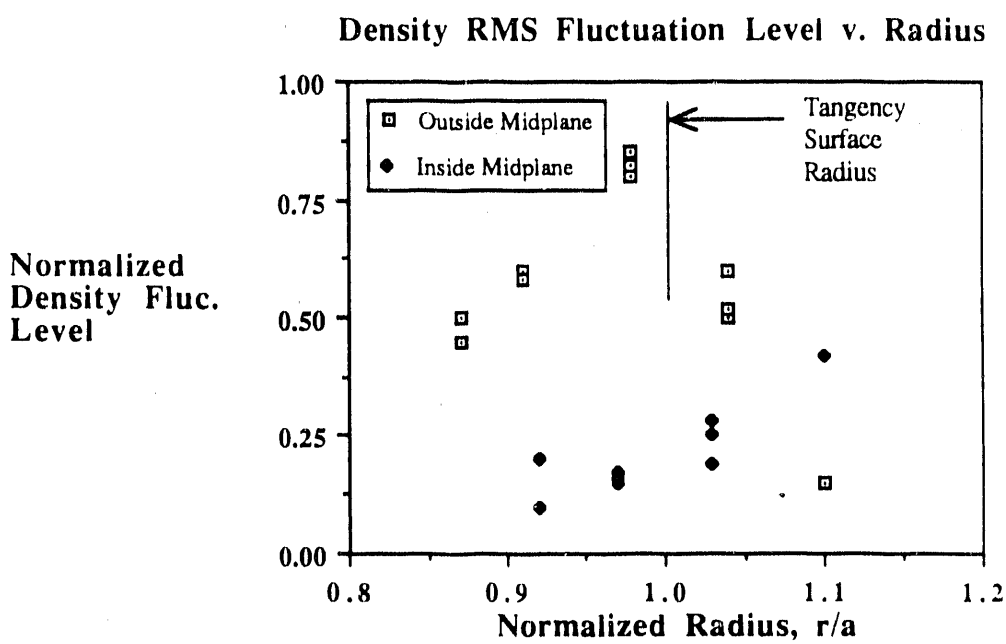

Figure 4: Density fluctuation levels from inside/outside midplane v. minor radius.

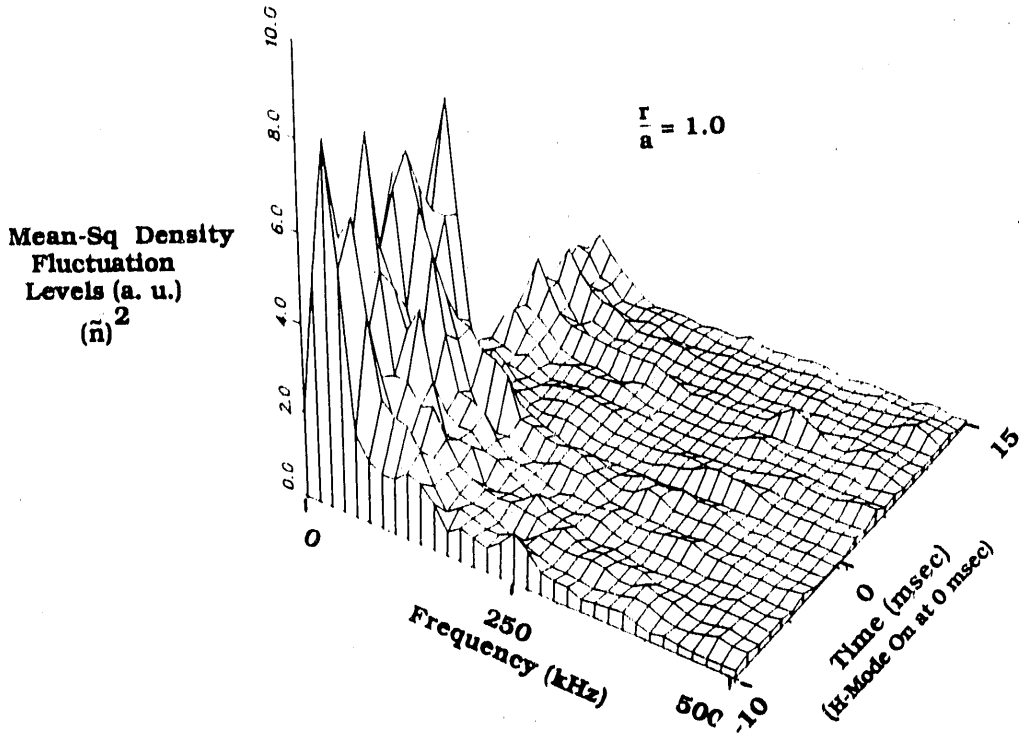

Figure 5: Density fluctuation power spectra evolution during CCT H-mode discharge. Data from last closed flux surface.

Helium Radiation Spectroscopy for Edge Plasma Diagnosis

The radiation spectroscopy using thermal Li-beams is widely used as one of the most useful edge-plasma diagnostic methods. However, the weakness of this method is that the penetration of lithium is not always deep enough to reach the point of interest in the edge plasma region. In contrast with lithium, because of its relatively small cross section for ionization, helium is expected to penetrate the plasma more deeply. In this work, thermal helium has been examined as an alternative edge-diagnostic probe beam, using the PISCES-B facility. Therefore, the purpose of this experiment is to investigate if there is one-to-one relation between the electron temperature and the ratio of radiation intensities at particular wave lengths. Using this relation, one can uniquely determine the electron temperature.

Pressure-regulated helium was introduced into steady-state argon plasmas through a similar gas injection system to the one used in our previous work [1]. The excitation of helium was monitored using a monochromator and an OMA system in front of the gas inlet in order that the attenuation effect due to expansion of the gas cloud can be minimized. The electron temperature and density of the host plasma were in the range from 5 to 30 eV and from 1×10^{12} to 1×10^{13} cm^{-3}, respectively and were not significantly modified by the injection of helium.

In these measurements, six triplet lines and six singlet lines were examined. Shown in Fig. 1 are several examples of the data in terms of the ratio of these line intensities. Also, theoretical values are shown for comparison. (Only the excitation from the ground state is considered for these theoretical values.) The disagreement between the theory and the data is presumably due to the secondary effect that the individual radiation intensity depends not only on the electron temperature but on the plasma density. Nevertheless, it is obvious that there is one-to-one relation between the electron temperature and the ratio of lines at 3888Å/5015Å, for example. Therefore, in principle, it is possible to use these data for estimating the electron temperature roughly. More data and detailed analysis may be needed using an off-line facility before this technique is applied for tokamaks.

---

[1] Y.Ra et.al., J.Vac.Sci. & Technol.-A8 (1990) 1783.

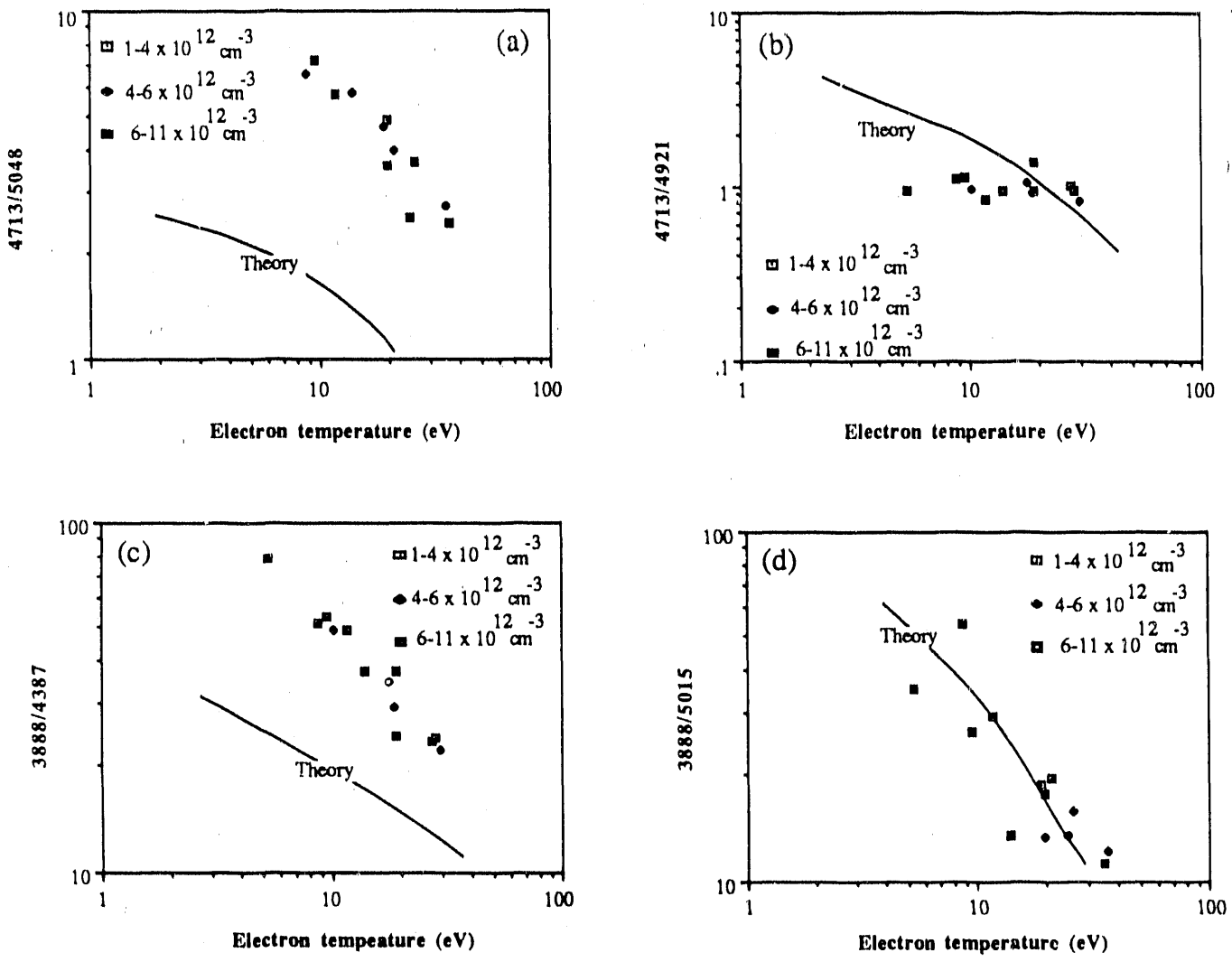

Fig. 1 He line intensity ratios of: (a) 4713Å/5048Å; (b) 4713Å/4921Å; (c) 3888Å/4387Å; and (d) 3888Å/5015Å.

END

DATE FILMED

12 / 10 / 90